Mountain, G.S., Miller, K.G., Blum, P., et al., 1994
Proceedings of the Ocean Drilling Program, Initial Reports, Vol. 150

10. SITE 906[1]

Shipboard Scientific Party[2]

HOLE 906A

Date occupied: 14 July 1993

Date departed: 18 July 1993

Time on hole: 4 days, 8 hr

Position: 38°57.896′N, 72°45.997′W

Bottom felt (rig floor; m, drill-pipe measurement): 924.5

Distance between rig floor and sea level (m): 11.6

Water depth (drill-pipe measurement from sea level, m): 912.9

Total depth (rig floor; m): 1526.9

Penetration (m): 602.4

Number of cores (including cores with no recovery): 68

Total length of cored section (m): 602.4

Total core recovered (m): 511.69

Core recovery (%): 85.0

Oldest sediment cored:
Depth (mbsf): 602.4
Nature: nannofossil clayey chalk
Age: upper Eocene
Measured velocity (km/s): 1.77

Principal results: Site 906 was drilled in 923 m of water on the middle continental slope offshore New Jersey, 3.3 km (1.8 nmi) north of Site 902. This site was selected after drilling at Site 905 ended because of safety concerns. We located Site 906 in the thalweg of modern Berkeley Canyon to minimize upper Neogene sediments and to penetrate a buried Miocene canyon. This buried canyon is strikingly revealed on an oblique crossing by *Maurice Ewing* Cruise 9009 MCS Line 1027. We conducted a detailed seismic survey of the buried canyon structure on approach to map its geometry. Scientific objectives at Site 906 were to (1) to compare the depositional history of a site on an interfluve of an extinct middle Miocene canyon (Site 902) with that of a site in the thalweg of the buried canyon (906); (2) evaluate the timing and mechanism of sediment deposition in both environments; and (3) determine the timing of canyon cutting and sedimentation changes with respect to global sea-level change.

Site 906 was spudded on 14 July 1993, and coring with the advanced hydraulic piston corer (APC) proceeded with 107% recovery to 62.5 m below seafloor (mbsf). Difficulties in drilling down the shoulder of the previous APC indicated refusal at this depth. Coring resumed with the extended core barrel (XCB) to a total depth of 602 mbsf with 83% recovery. A chalk unit was penetrated at 552 mbsf; the rate of penetration (ROP) slowed considerably and recovery fell off with increasing depth into this lithologic unit. Scientific objectives had been met and coring was terminated in the upper Eocene on 16 July. Four logging runs comprising the sonic-induction (84–590 mbsf), porosity (103–583 mbsf), FMS (119–577 mbsf), and geochemical (146–569 mbsf) tools were completed with the side-entry sub (SES). The hole was plugged and abandoned on 17 July.

Several of the lithologic units penetrated at slope Sites 902 through 904 are represented at Site 906 as well, and we maintained the same lithologic unit designations among all of the slope sites. Units II and III are not represented at Site 906. Gravity flow deposits divide Unit IV into two subunits as they do at sites 902 and 904. The canyon fill penetrated at Site 906 between 361.8 and 478.2 mbsf contains lithologies that are very different from coeval Unit V at Sites 902 through 904, and we designated three subunits of Unit V for these canyon-fill deposits at Site 906. As in the other slope sites, the deepest unit that we recovered is predominantly carbonate; the overlying units are all predominantly siliciclastic.

Unit I (0–55.4 mbsf), Holocene to upper Miocene silty clay with mud clasts. Subunit IA is silty clay with abundant mud clasts and rare quartz sand; Subunit IB is glauconitic sandy clay with possible mud clasts.

Unit IV (55.4–279.2 mbsf), upper and middle Miocene diatomaceous silty clay to clayey silts with siderite and pyrite nodules. Gravity-flow deposits occur in the middle and base of the unit. Subunit IVA is silty clay with nodules and glauconitic sandy interbeds; Subunit IVB is uniform slightly glauconitic silty clay.

Unit V (279.2–478.2 mbsf), middle Miocene canyon fill divided into three subunits: Subunit VA is predominantly laminated silty clay; Subunit VB is thinly bedded fine quartz sand; and Subunit VC comprises mainly silty clay interbedded with mud-clast conglomerates.

Unit VI (478.2–555.3 mbsf), upper Oligocene silty claystone and clayey siltstone with abundant glauconite, common nannofossils, clastic sills, and microfaults.

Unit VII (555.3–602.4 mbsf), upper to middle Eocene clayey nannofossil chalk.

The Pleistocene section at Site 906 is thin (43 m) and younger than the *Pseudoemiliania lacunosa* LAD (<474 ka). The upper Miocene section at Site 906 contains Zones NN9–NN10 and N16–N17 and thus is lower upper Miocene in age (8.2–10.4 Ma). The boundary between the upper and middle Miocene is not recognizable using biostratigraphic criteria.

Stratigraphic interpretation of the middle Miocene section recovered at Hole 906A is the least constrained of any of the slope sites because of a thick interval (~90–420 mbsf) barren of calcareous fossils and an interval of wide-ranging zonations in the mass-flow deposits below this interval. The only stratigraphic control currently available for the interval between 90 and 420 mbsf is provided by diatoms of the middle Miocene *R. barboi* Zone.

All of the canyon fill at Hole 906A is assigned to the *R. barboi* Zone (older than about 11.0 ± 0.5 Ma). High sedimentation rates for this section (minimum rate of 14 cm/k.y.) may be indicated by integration of diatom and magnetostratigraphic data. The mud-clast conglomerate found at the base of the canyon fill (421.1–478.2 mbsf) contains lower Miocene (Zone N6) and middle Miocene (*R. barboi* Zone) fossils. We assume that the older ages are the result of reworking of older clasts, and that the canyon fill is middle middle Miocene and younger (less than about 15 Ma).

The Oligocene section is assigned to Zones NP25 and P22 (upper part) and undifferentiated Zones NP24/NP25 (lower part). Calcareous plankton indicate that an ~66-m section of upper Oligocene glauconitic silty clay (Zones NP24–NP25 and P22) overlies an upper Eocene nannofossil clayey chalk (Zones NP19–20 and P15–P17).

As at Sites 902–904, magnetization intensities in sediments at Site 906 are generally below the detection limit of 1 mA/m for shipboard analyses.

[1] Mountain, G.S., Miller, K.G., Blum, P., et al., 1994. *Proc. ODP, Init. Repts.*, 150: College Station, TX (Ocean Drilling Program).
[2] Shipboard Scientific Party is as given in the list of participants preceding the Table of Contents.

Values are strongest in the section above 107 mbsf, including a representation of the Brunhes polarity chron, but they diminish downhole. A zone of very strong magnetization, containing a thick reversed magnetozone (282 and 393 mbsf), occurs between about 282 and 465 mbsf. This may reflect secondary magnetization caused by diagenesis. However, it is also possible to correlate this thick magnetozone with Chron C5Ar. This section and samples will be re-examined in a more detailed shore-based study that will include evaluating the effects of diagenesis on the rock magnetic record.

Headspace gas at Hole 906A consisted predominantly of methane, with minor amounts of ethane and traces of propane. The gases are of biogenic, rather than thermogenic, origin. Headspace methane concentrations ranged from 586 to 83,019 ppm in two maxima. An upper maximum occurs between 32.5 and 317.0 mbsf below the zone of sulfate reduction; C_1/C_2 ratios in excess of 1000 indicate biogenic origin. A gas-lean interval, associated with lower total organic-carbon (TOC) contents, occurs between 317.0 and 433.3 mbsf. A deeper gas-enriched sediment zone lies between 443.3 and 567.5 mbsf. Within this interval ethane generally increases with depth, from 1 ppm at 420.8 mbsf up to a maximum of 432 ppm at 555.1 mbsf; propane appears occasionally up to concentrations of 5 ppm. C_1/C_2 values drop dramatically across the Miocene/Oligocene unconformity (~478.2 mbsf) and remain below 500 down to 539.3 mbsf. However, TOC values are high in this section; C_1/C_2 values rise in the Eocene. The irregularity of the C_1/C_2 ratio with depth and the high organic-carbon content suggest that bacterial degradation of organic material is the source of the gas in the Oligocene sediments of this site.

TOC values in Hole 906A range from 0.29% in Pleistocene sediments to as high as 3.27% in the Oligocene. Middle Miocene laminated lithologic Subunit VA exhibits slightly lower than average values (1.4%), and it is surprising to see lower TOC contents in the presence of such thinly bedded, burrow-free silty clays.

Pore-water studies reveal patterns similar to Sites 902–904, although the interstitial water profiles differ above the upper Miocene because of the thin Pleistocene section at Site 906. As at the other sites, bacterial degradation of organic matter reduces sulfate concentrations to 0 by ~30 mbsf; below this, degradation proceeds by means of methanogenesis. Salinity increases abruptly at the top of the Miocene section and continues to increase with depth, suggesting underlying evaporite deposits. There is a corresponding downward decrease in pH to 6.7 at 135 mbsf, with values as low as 6.4 at 539 mbsf; these low pH values explain the disappearance of calcareous microfossils. Local ammonium maxima associated with organic-rich intervals are sites of reprecipitated carbonate minerals.

Eight physical properties units are recognized at Site 906 based on trends in GRAPE bulk-density and index properties. Many of these boundaries coincide with the lithostratigraphic unit boundaries. Good velocity measurements were obtained, and post-cruise studies will generate synthetic seismograms from the borehole velocities and densities. Velocities increase gradually to 1800 m/s at 380 mbsf, attain a general maximum of 2000 m/s at 500 mbsf, and decrease to ~1565 m/s below this. Downhole shifts in porosity, thermal conductivity, and penetrometer values generally occur at the same level as changes in wet-bulk density. Natural-gamma-ray emissions, which were measured routinely on the multisensor track, show close parallels to values measured in the downhole log.

Good hole conditions, plus our use of the logging heave compensator and the side-entry sub, resulted in an excellent suite of logs at Site 906. Four log units are recognized, with several boundaries or log character in close agreement with lithologic features. Gamma-ray values in log Unit 1 (100-384 mbsf) suggest several upward-fining cycles 10 to 40 cm thick; this unit contains a very large peak in both density and velocity caused by a 1-m cemented bed at 252 mbsf. Velocities and densities at most other levels throughout log Unit 1 vary within a narrow range. Significantly increased densities and slightly lower velocities define log Unit 2 (384-425 mbsf), and much of this unit corresponds to the fine quartz sand of lithologic Subunit VB. Log Unit 3 (425-approximately 561 mbsf) shows the greatest variations in log signatures of all units at Site 906. The largest of these divide the interval into three log subunits with boundaries at 478.5, 520 and 561 mbsf. The first of these depths corresponds to the base of lithologic Subunit VC, the second to the top of an interval of downward decreasing velocities and densities, and the third with the top of the Eocene chalks of lithologic Unit VII. Log Unit 4 (561-deepest log at 588 mbsf) exhibits the highest velocities and densities at this site other than the few measurements within the cemented bed at 252 mbsf.

The principal result from Site 906 is that it provides the basic history of the oldest "Icehouse" slope canyon along the New Jersey Sea level Transect. We confirmed that the oldest surface incised by the canyon matches reflector m3 (Blue; middle middle Miocene); the oldest surface filling the canyon and traced across our seismic grid correlates to reflector m2 (Yellow-2; upper middle Miocene). This brackets the canyon formation to between 13.5 and ~12.4 Ma and correlates with a glaucioeustatic lowering inferred by a major shift in the marine $\delta^{18}O$ record. Additional mapping is required to identify the upslope extent of this canyon and evaluate similarities to modern slope canyons, many of which were clearly incised during Pleistocene glacioeustatic lowerings. The Miocene canyon at Site 906 filled initially with debris shed from the continental slope, probably derived from its own walls. Remarkably fresh sand turbidites comprise younger fill not found at other slope sites. Laminated silty clays constitute the third and youngest stratigraphic unit within this canyon, indicating low oxygen bottom-water conditions (suggested by similar evidence at Site 903). The stratigraphic succession above reflector m2 and below m6 is similar to that found at the other Leg 150 slope sites.

BACKGROUND AND OBJECTIVES

Site 906 was selected, surveyed, and approved in the aftermath of curtailed operations at Site 905. Core recovery had been generally excellent at the previous three slope sites (Sites 902–904), with the exception of the lower Miocene and upper Oligocene at Site 903. It was evident that little more would be gained by returning to drill the same facies at a similar location. Sites 902 and 904 had been located on Cruise Ew9009 MCS Line 1027 (Fig. 1), and a buried Miocene canyon, channel, or slump scar is visible 3 km updip from Site 902. This was recognized by the Shipboard Scientific Party as a unique opportunity to sample and date sediments that record a significant mass-wasting event from the time of the "Icehouse world." The feature had been crossed once during the water-gun single-channel seismic (SCS) survey between our drilling Sites 903 and 904 (see Chapter 4, this volume). An additional SCS survey was conducted in the Site 906 area to define the geometry of this buried feature (Fig. 2).

According to the widely accepted model of sequence stratigraphy (Posamentier et al., 1988), relative falls in sea level are recorded in siliciclastic sediment by a downward shift in depositional base level. Downward shifts are of two types: those in which base level passes seaward of the former clinoform inflection point and valleys become deeply incised, and those in which base level remains landward of this critical position and there is little or no incision as far seaward as the clinoform inflection point. In either case, a sequence boundary is formed during the relative fall; the former example is referred to as a "Type 1" sequence boundary, the latter as a "Type 2" sequence boundary. For times in the "Icehouse" older than sequence boundary Blue (ca. 13.5 Ma; Greenlee et al., 1992), all clinoform inflection points along the New Jersey Margin are on or landward of the modern middle continental shelf. Consequently, even at times when Type 1 sequence boundaries may have formed beneath the modern shelf, valleys were not incised as far seaward as the modern continental slope. However, this pattern did not persist. During the middle Miocene to Pleistocene, sediment supply greatly exceeded the available accumulation space ("accommodation"), and clinoforms prograded seaward across the continental shelf and eventually reached the modern slope.

Reflector m3 (Blue) marks the first major "Icehouse world" incision of submarine channels seaward of a clinoform inflection point. The buried channels we observe are beneath the modern outer shelf (G.S. Mountain, K.G. Miller, and N. Christie-Blick, unpubl. data, 1990) and can be traced to the slope where they are often overlain by more recent canyons. The age and origin of these overlying canyons

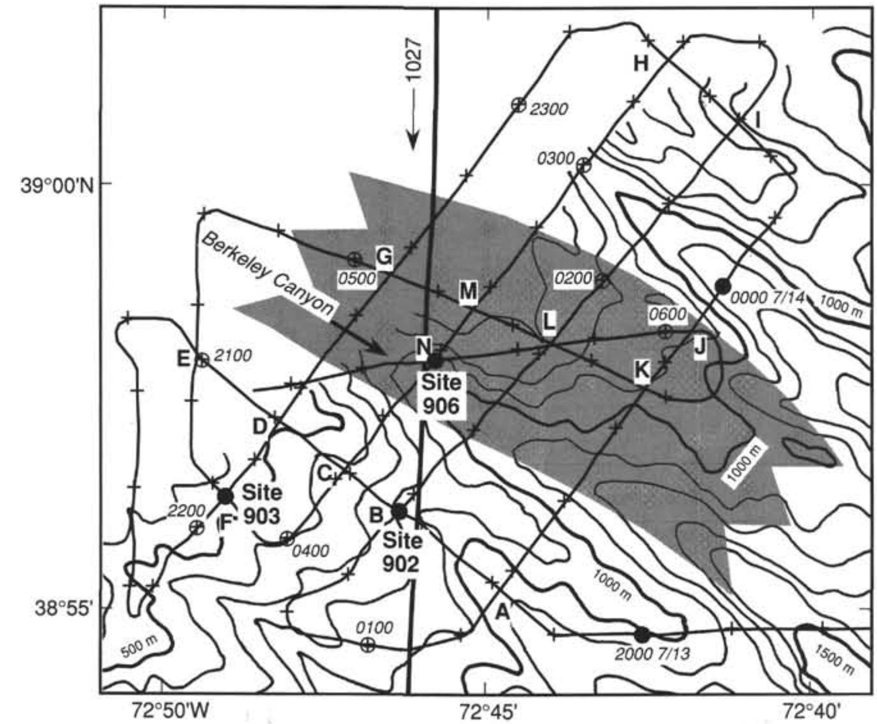

Figure 1. SeaBeam bathymetry with survey tracks near Sites 902, 903, 904, and 906. The locations of the COST B-3 and AMCOR 6021 wells are shown. A portion of *Maurice Ewing* Cruise 9009 (Ew9009) MCS Line 1027 is shown in Figure 2. Canyons are indicated by arrows. The outcrop indicated near DSDP Site 612 was sampled using the *Alvin* in 1989.

is controversial. Reflection geometry suggests they are younger than reflector p5 (orange; middle Pleistocene). This age supports the argument that they are related to sea-level changes, being inactive today but active during glacioeustatic lowerings. At Site 906, we want to determine if one of these Miocene channels buried beneath the modern slope is genetically related to the modern canyons and if it formed in response to relative sea-level changes or to other processes.

Several of these "other processes" provide alternative explanations for the origin of this and similar discontinuities beneath the continental slope. The incision model presumes that, during lowstands, rivers deliver more sediment to the slope than there is space to accumulate. Turbidity currents and mass flows become agents that carry this excess sediment down the slope, and in the process carve steep-walled slope canyons that remain entrenched for long periods of time. Alternative models do not involve changes in either sea level or base level. These models all presume that sediment failure of various types can occur as a result of processes taking place on the slope itself. These processes include (1) seismicity (Heezen and Ewing, 1952); (2) the activity of bottom-dwelling fauna (Shepard and Dill, 1966); (3) undercutting by erosive bottom currents (Paull and Dillon, 1980); (4) groundwater sapping caused by changing in situ pore pressure (Robb et al. 1981); (5) along-shelf transport and sediment buildup at the shelf edge (May et al., 1983); and (6) diagenesis leading to jointing and collapse (McHugh et al., 1993).

The pre-site survey conducted during Leg 150 (Fig. 2; see also Chapter 4, this volume) provided details on the dimensions of the slope channel cut into sediment of m3 (Blue) age reflector (~13.5 Ma); this erosion predates reflector 2 (Yellow-2; ~12.4 Ma). In contrast to Pleistocene-age canyons cut into the modern slope, this buried feature is wide, moderately deep, and relatively flat-floored (Fig. 1); furthermore, it trends more west to east than do modern analogues. We recognized several issues to be resolved by drilling. The most outstanding objective will be to determine the time when the buried canyon was formed and by what process. This requires a drill site at the deepest part of the structure where the oldest fill can be dated. An equally important objective will be to evaluate the facies of the infilling sediment and compare it with that of the surrounding channel walls. With this information we will (1) compare the time of origin to other unconformities on the slope, (2) determine the length of time that this channel could have been a conduit for sediment to by-pass the slope, and (3) examine the process by which this channel was filled in, and its relationship to deposition on the slope.

OPERATIONS

Site MAT18a was proposed in the field as an alternate to proposed Site MAT13 after the early termination of Site 905 and because some of the Site MAT13 objectives had been accomplished at other sites. The drilling location was on the continental slope less than 2 nmi north of Site 902 and in the thalweg of Berkeley Canyon. Site objectives were based on a comparison of timing and nature of formation and infill of a buried valley with sedimentation on an interfluve between canyons (Site 902) over the same time period. The particular location was chosen because seismic records and PDR showed that the axis of the buried valley could be drilled with minimal overburden if drilled in the deepest part of the modern Berkeley Canyon.

An 11-hr arrival survey was conducted to pinpoint the drilling location and to relate the new site to nearby Sites 902 and 903 (see Chapter 4, this volume). After the positioning beacon was dropped at 0630 hr (Universal Time Coordinated [UTC]), 14 July 1993, the vessel continued 2 nmi past the drop point, recovered gear, and returned to the beacon.

Hole 906A

An APC/XCB bottom-hole assembly (BHA) was assembled and run to spud depth. Problems in deploying the APC cost 1 hr of operating time when the old, oversized aft coring line became fouled

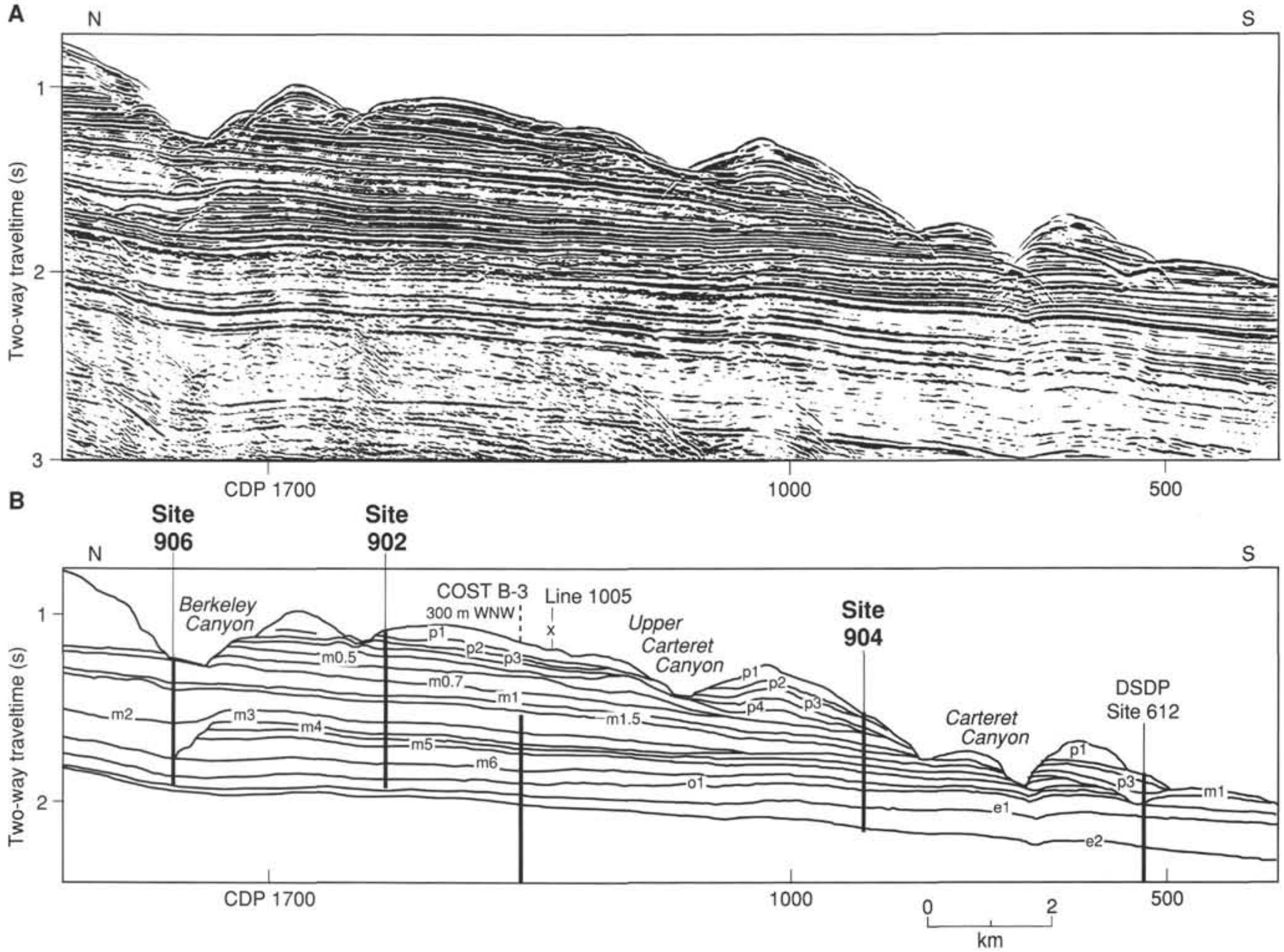

Figure 2. Cruise Ew9009 MCS Line 1027, an oblique dip profile. **A.** Uninterpreted seismic section. **B.** Line drawing interpretation connecting Sites 906, 902, and 904, the COST B-3 well (projected from ~300 m west-northwest), and DSDP Site 612. Vertical axes are two-way traveltime (s). Reflectors (e.g., p1, p2) are described in the "Seismic Stratigraphy" section (this chapter). CDP = common depth point. Location of crossing with Line 1005 (Fig. 1) is shown (x). See also Plate 1 (in back-pocket foldout).

in the oilsaver. The wire finally was removed from service, and the new forward coring line (which had been installed during the move from Site 905) was used for the remainder of Leg 150 operations.

Seafloor depth was determined by the initial APC core to be 924.5 m from driller's datum. Continuous APC cores were taken through the Pleistocene section. Incomplete stroke was attained on Core 150-906A-5H at about 45 mbsf, a few meters into stiff Miocene clay (Table 1). Difficulty in drilling down the shoulder for Core 150-906A-7H indicated firm sediment and a probable clay ball on the bit, so coring was switched to the XCB mode.

Core recovery was excellent from the beginning in silty clay with minor sands. A sandy interval from about 380 to 420 mbsf was the exception, producing poor to fair recovery (Table 1). Coring proceeded without incident to about 552 mbsf, just above the contact with Eocene chalk. The marly chalk repeatedly jammed the XCB shoes, despite all measures that could be taken, and both ROP and core recovery fell sharply. Because of the lack of satisfactory progress, coring ended at 602.4 mbsf. This was short of a secondary drilling objective, but primary goals had been achieved.

The hole was then conditioned for logging with a wiper trip and a mud sweep. Logging sheaves and the SES were rigged with the bit at 84 mbsf and the sonic-induction tool string was assembled.

A failure in the telemetry cartridge forced interruption of the first logging run. After the tool string had been recovered and the cartridge replaced, a successful log was recorded from 590 to 84 mbsf. A good run with the porosity tool followed, with logging data obtained from 583 to 103 mbsf.

The Formation MicroScanner (FMS) tool was the third tool string to be run. After an SES-assisted first pass, a bridge prevented lowering the tool for a second pass. When logging personnel attempted to pull the tool inside the pipe for a return to the bottom of the hole, the top of the tool would not enter the pipe. They surmised that the float valve flapper had closed on the wire, but using pump circulation succeeded in opening the flapper to permit entry. Logging personnel decided to retrieve the tool and check for damage before attempting a second FMS pass. A severe kink was found in the cable about 30 m above the tool and marks on the "torpedo" connection near the cable head confirmed contact with the float valve. A rehead of the cable was required and plans for a second FMS pass were canceled because of time constraints. A final logging run was then made with the geochemical combination tool string from 569 to 146 mbsf.

When the logging equipment had been rigged down, the hole was plugged, the bit pulled clear of the seafloor, the two positioning beacons recalled, and the ship offset toward Hole 903D in dynamic positioning (DP) mode.

LITHOSTRATIGRAPHY

Site 906 was positioned to explore the sedimentary fill of canyon-like structures observed in seismic reflection profiles (see "Background and Objectives" section, this chapter). Despite the unusual paleotopographic setting, the succession recovered at Site 906 can be described in the context of the lithostratigraphic scheme derived from Sites 902 to 904 (Figs. 3–4). The principal contrasts with the normal slope successions are in Units I and V as outlined below (Table 2).

Unit I, recovered from below the floor of a modern submarine canyon, belongs to the Pleistocene and upper Miocene and is composed predominantly of mud-clast conglomerates. The lithofacies are appreciably different from those that make up the bulk of Unit I at Sites 902 and 903 in which lithoclasts are much less abundant. Units II and III of Site 903 were not encountered at Site 906; however, an interval of reworked glauconitic sand at the base of Unit I is consistent with erosional truncation and partial redeposition of these units within the thalweg of the existing canyon.

Unit V, developed within the older, target canyon, was very different from the glauconitic silty clays that characterize middle to lower Miocene of Unit V at Sites 902 through 904. The unit at Site 906 comprises an upper interval of laminated and thinly-bedded silty clay, a middle interval of thinly bedded, quartz sand, and a basal interval of silty clay interbedded with mud-clast conglomerate.

As determined in each of the other Leg 150 slope sites, the deepest lithostratigraphic unit (VII) is nannofossil chalk. All of the overlying units are siliciclastic.

Unit I

Interval: Sections 150-906A-1H-1, 0 cm, to -7H-2, 90 cm
Depth: 0–55.4 mbsf
Age: Pleistocene (? upper Miocene)

Subunit IA

Interval: Sections 150-906A-1H-1, 0 cm, to -5H-4, 130 cm
Depth: 0-43.3 mbsf

Subunit IB

Interval: Sections 150-906A-5H-4, 130 cm, to -7H-2, 90 cm
Depth: 43.3-55.4 mbsf

Unit I comprises an assortment of lithofacies (Fig. 4). The unit can be divided into two subunits. Subunit IA (0–43.3 mbsf; Sections 150-906A-1H-1, 0 cm, to -5H-4, 130 cm) consists of bioturbated and color-banded greenish gray silty clay, silty clay with abundant mud clasts, diatomaceous silty clay, and rare quartz-rich sand. The occurrence of lithified and unlithified clasts and rare convoluted bedding, suggests that much of this unit was deposited by mass-flow processes. Subunit IB (43.3–55.4 mbsf; Sections 150-906A-5H-4, 130 cm, to -7H-2, 90 cm) is composed of dark olive gray, glauconitic sandy clay and greenish gray clay with possible mud clasts.

The dominant lithology of Unit I is silty clay with abundant mud clasts. Individual beds commonly are difficult to distinguish; internally, they are largely homogeneous, with rare slump-folded color banding. In some cases, intervals of horizontal color banding separate these deformed beds and sharp basal contacts are observed. A heterogeneous mixture of mud clasts and lithoclasts is present. The lithology of these mixed beds includes dark gray and greenish gray unlithified silty clay, dark gray sandy silt, olive gray glauconitic silty clay, and coarsely crystalline, white quartz ("vein quartz"). Bioclasts, such as complete and fragmented gastropod and bivalve shells, are also common in these beds. The matrix between the clasts is predominantly greenish gray silty clay. Between 37.3 and 39.2 mbsf, a bed of olive gray diatomaceous silty clay with clasts of gray silty clay (pebble to boulder sized) is present. The margins of these clasts have irregular fractures, filled with the diatomaceous matrix. These beds appear to be matrix-supported debris flows.

The upper part of Subunit IB comprises dark green-gray silty clay with abundant, very fine- to fine-grained glauconitic sand as the burrow fill. These sharply defined burrows range in size up to ~2 cm and the fill is well sorted, a style of bioturbation that is typical of Pleistocene sediments at the other slope sites. Woody debris occurs sparsely. The glauconitic sandy clays sit with an abrupt contact on light greenish gray, homogeneous clay, and sediment is piped down across the junction in large (~2–3 cm) burrows (48.3 mbsf; Section 150-906A-6H-1, 130 cm). Patches of dark gray clay occur for 3 m below this contact; these may be either burrow fills or mud clasts. The basal contact between Units I and IV is taken at an uneven but sharp boundary; brown-gray to green-gray glauconitic silty clay, with glau-

Table 1. Coring summary, Site 906.

Core no.	Date (July 1993)	Time (UTC)	Depth (mbsf)	Length cored (m)	Length recovered (m)	Recovery (%)
150-906A-						
1H	14	1205	0.0–9.5	9.5	8.72	91.8
2H	14	1230	9.5–18.5	9.0	9.90	110.0
3H	14	1250	18.5–28.0	9.5	9.93	104.0
4H	14	1315	28.0–37.5	9.5	9.87	104.0
5H	14	1340	37.5–47.0	9.5	9.97	105.0
6H	14	1410	47.0–53.0	6.0	8.38	139.0
7H	14	1455	53.0–62.5	9.5	9.95	105.0
8X	14	1610	62.5–72.0	9.5	9.87	104.0
9X	14	1645	72.0–81.9	9.9	9.81	99.1
10X	14	1720	81.9–91.5	9.6	9.60	100.0
11X	14	1755	91.5–101.2	9.7	9.84	101.0
12X	14	1830	101.2–110.8	9.6	9.84	102.0
13X	14	1900	110.8–120.5	9.7	9.89	102.0
14X	14	1925	120.5–130.1	9.6	9.89	103.0
15X	14	1955	130.1–139.7	9.6	9.71	101.0
16X	14	2030	139.7–149.4	9.7	9.88	102.0
17X	14	2100	149.4–159.0	9.6	10.23	106.5
18X	14	2130	159.0–168.7	9.7	9.89	102.0
19X	14	2200	168.7–178.3	9.6	9.67	101.0
20X	14	2230	178.3–188.0	9.7	9.81	101.0
21X	14	2300	188.0–197.6	9.6	9.83	102.0
22X	14	2325	197.6–207.2	9.6	9.84	102.0
23X	14	2350	207.5–216.8	9.3	9.92	106.0
24X	15	0015	216.8–226.5	9.7	9.58	98.7
25X	15	0045	226.5–236.0	9.5	8.96	94.3
26X	15	0115	236.0–245.7	9.7	9.46	97.5
27X	15	0215	245.7–255.3	9.6	7.38	76.9
28X	15	0300	255.3–265.1	9.8	9.87	101.0
29X	15	0330	265.1–274.8	9.7	9.81	101.0
30X	15	0400	274.8–284.6	9.8	9.27	94.6
31X	15	0435	284.6–294.4	9.8	7.71	78.7
32X	15	0520	294.4–304.2	9.8	8.94	91.2
33X	15	0600	304.2–314.0	9.8	8.01	81.7
34X	15	0630	314.0–323.8	9.8	9.78	99.8
35X	15	0700	323.8–333.2	9.4	8.54	90.8
36X	15	0745	333.2–342.5	9.3	7.74	83.2
37X	15	0815	342.5–352.2	9.7	9.56	98.5
38X	15	0850	352.2–361.8	9.6	8.35	87.0
39X	15	0925	361.8–371.5	9.7	7.80	80.4
40X	15	1020	371.5–381.1	9.6	9.52	99.1
41X	15	1125	381.1–390.8	9.7	4.01	41.3
42X	15	1220	390.8–400.3	9.5	2.12	22.3
43X	15	1320	400.3–409.8	9.5	0.20	2.1
44X	15	1410	409.8–419.3	9.5	0.37	3.9
45X	15	1500	419.3–428.8	9.5	6.13	64.5
46X	15	1555	428.8–438.6	9.8	8.59	87.6
47X	15	1635	438.6–448.2	9.6	8.89	92.6
48X	15	1740	448.2–457.9	9.7	9.73	100.0
49X	15	1830	457.9–467.5	9.6	7.00	72.9
50X	15	1930	467.5–477.2	9.7	9.33	96.2
51X	15	2100	477.2–486.8	9.6	7.96	82.9
52X	15	2145	486.8–496.5	9.7	9.19	94.7
53X	15	2300	496.5–506.2	9.7	9.77	101.0
54X	15	2330	506.2–515.8	9.6	9.88	103.0
55X	16	0015	515.8–525.3	9.5	9.64	101.0
56X	16	0100	525.3–534.8	9.5	9.86	104.0
57X	16	0145	534.8–544.5	9.7	9.30	95.9
58X	16	0230	544.5–554.2	9.7	6.60	68.0
59X	16	0415	554.2–563.8	9.6	1.28	13.3
60X	16	0515	563.8–565.5	1.7	1.43	84.1
61X	16	0615	565.5–567.5	2.0	0.42	21.0
62X	16	0745	567.5–573.5	6.0	1.00	16.6
63X	16	0850	573.5–583.2	9.7	0.28	2.9
64X	16	0100	583.2–586.3	3.1	0.87	28.0
65X	16	1125	586.3–592.8	6.5	1.13	17.4
66X	16	1230	592.8–594.4	1.6	1.45	90.6
67X	16	1430	594.4–598.9	4.5	0.49	10.9
68X	16	1600	598.9–602.4	3.5	0.25	7.1
Coring totals				602.1	511.69	85.0

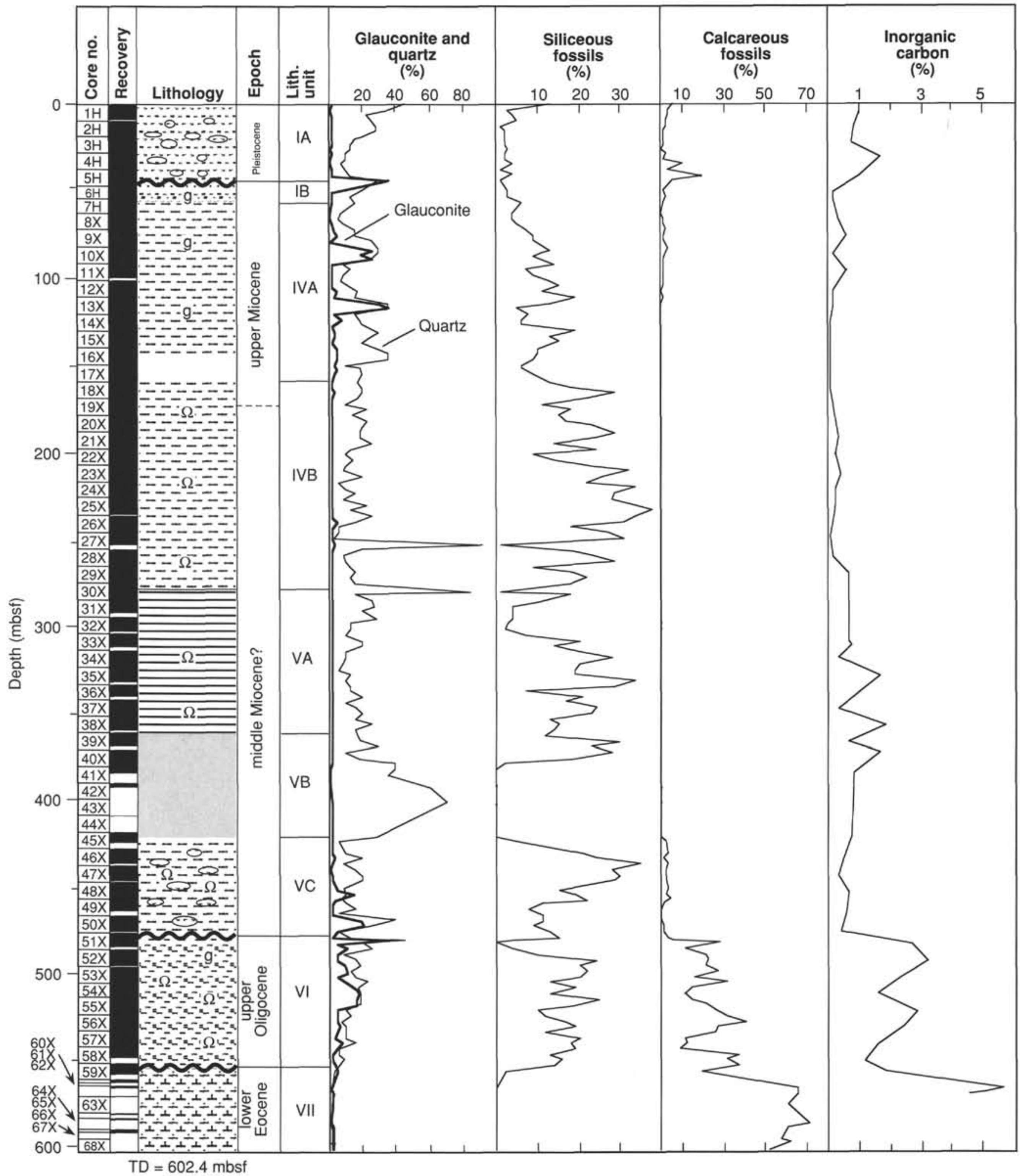

Figure 3. Generalized summary lithologic column for Hole 906A, showing glauconite and quartz, siliceous and calcareous fossil content (determined from smear slides), and inorganic carbon.

conite sand at the base, occurs above the boundary, and homogeneous gray clay occurs below (55.4 mbsf; Section 150-906A-7H-2, 90 cm).

Considering Unit I as a whole, smear slides show that sand content is negligible, except locally in Subunit IB where 65% was recorded. As silt-sized particles, quartz and feldspar are fairly abundant at the top of Subunit IA (~45%), but they decline steadily in abundance toward the base (~10%). Subunit IB shows a slight increase in the abundance of these minerals. The general trends for calcite and dolomite combined are very similar to those of quartz and feldspar, albeit with a range from 0% to 15%. This parallel of carbonate with quartz and feldspar content is also seen in the Pleistocene of all the other slope sites. Siliceous microfossils are common only in the uppermost

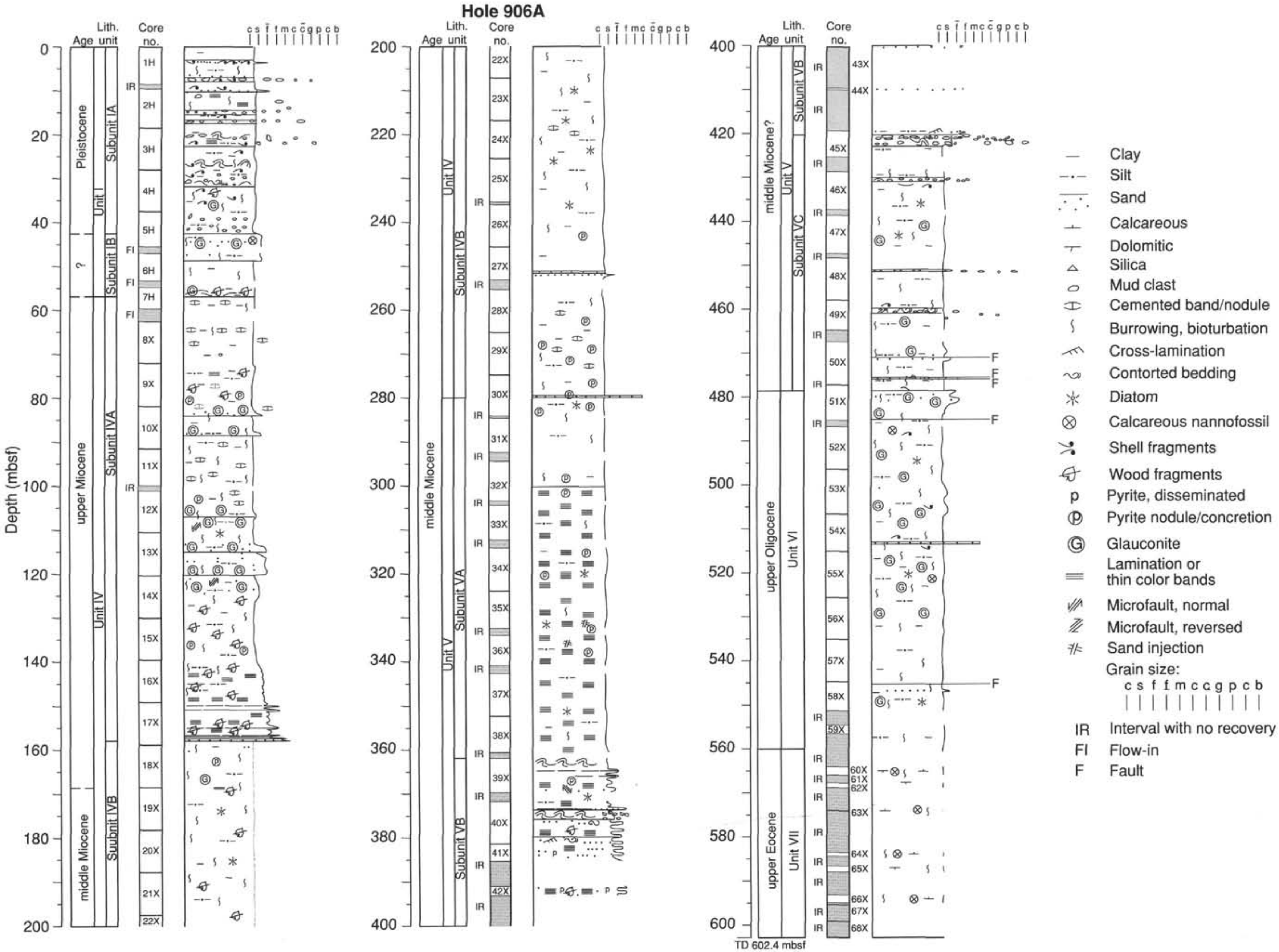

Figure 4. Detailed summary lithologic column, Hole 906A. See also Plate 2 (in back-pocket foldout). TD = total depth.

Table 2. Lithostratigraphy, Site 906.

Unit or subunit	Series	Interval (depth)	Lithology	Process
IA	Pleistocene	0–43.3 mbsf (150-906A-1H through 150-906A-5H-4, 130 cm)	Color-banded silty clay, silty clay with mud clasts, diatomaceous silty clay, rare quartz-rich sand.	Predominantly mass-wasting and hemipelagic deposition; minor gravity-controlled flows.
IB	upper Miocene	43.3–55.4 mbsf (150-906A-5H-4, 130 cm, through -7H-2, 90 cm)	Silty clay with abundant glauconite as burrow fill, glauconite sand and clay with mud clasts.	Predominantly hemipelagic, rare gravity-controlled flows, and mass-wasting.
		Major disconformity		
IVA	upper Miocene	55.4–157.4 mbsf (150-906A-7H-2, 90 cm, through -17X-6, 150 cm)	Homogeneous silty clay with siderite nodules and bands, glauconitic silty clay, sandy clay, and land plant debris.	Predominantly hemipelagic and gravity-controlled flows; alteration of processes.
IVB	upper to middle Miocene	157.4–279.2 mbsf (150-906A-17X-6, 150 cm, through 30X-3, 135 cm)	Glauconitic silty clay with pyrite and siderite nodules.	Predominantly hemipelagic; alteration of sediments by diagenetic processes.
VA	middle? Miocene	279.2–361.8 mbsf (150-906A-30X-3, 135 cm, through -38X-CC, 35 cm)	Laminated and thinly bedded silty clay.	Predominantly hemipelagic; alteration of sediments by diagenetic processes.
VB	middle? Miocene	361.8–421.1 mbsf (150-906A-38X-CC, 35 cm, through -45X-2, 33 cm)	Thinly bedded, fine-grained quartz sand, silty sand, and silt interbedded with silty clay; contorted silty clay.	Predominantly gravity- controlled flows and mass-wasting; minor hemipelagic deposition.
VC	middle? Miocene	421.1–478.2 mbsf (150-906A-45X-2, 33 cm, through 51X-1, 101 cm)	Gray brown silty clay and mud-clast conglomerates.	Predominantly hemipelagic and mass-wasting.
		Major disconformity		
VI	upper Oligocene	478.2–555.3 mbsf (150-906A-51X-1, 101 cm, through -59X-CC, 40 cm)	Dark gray green silty claystones with abundant glauconite and calcareous microfossils.	Hemipelagic to pelagic and gravity-controlled flows.
		Major disconformity		
VII	upper Eocene	563.8–602.4 mbsf (150-906A-60X-1, 0 cm, through -68X-CC)	Clayey, nannofossil chalk.	Predominantly pelagic.

smear-slide sample at Hole 906A. Calcareous nannofossils are generally very scarce, but a significant increase to ~20% is apparent at around the boundary between Subunits IA and IB.

Unit IV

Interval: Sections 150-906A-7H-2, 90 cm, to -30X-3, 135 cm
Depth: 55.4–279.2 mbsf
Age: upper to middle Miocene

Subunit IVA

Interval: Sections 150-906A-7H-2, 90 cm, to -17X-6, 150 cm
Depth: 55.4–157.4 mbsf

Subunit IVB

Interval: Sections 150-906A-17X-6, 150 cm, to -30X-3, 135 cm
Depth: 157.4–279.2 mbsf

Unit IV at Site 906 consists of similar lithofacies to those observed in the upper Miocene strata at Sites 902 and 903 (Fig. 4). The dominant lithologies of this unit at all three sites are greenish gray silty clays with common siderite nodules and bands, glauconitic silts and silty clays, and brown gray silty clays. A consistent characteristic of Unit IV is the occurrence of gravity-flow deposits, rich in terrigenous material, approximately in the middle and near or at the base of the unit. However, the relative thickness of these lithofacies, and the spatial relationship of the silty clays with the gravity-flow deposits, varies significantly between sites.

At Site 906, Unit IV can be divided into two subunits. Subunit IVA (55.4 to 157.4 mbsf; Sections 150-906A-7H-2, 90 cm, to -17X-6, 150 cm) consists of greenish gray silty clay with common buff-colored sideritic nodules and bands, glauconitic silty clay and sandy clay and a basal interval with abundant quartz sand and comminuted plant material. Subunit IVB (157.4–279.2 mbsf; Sections 150-906A-17X-6, 150 cm, to -30X-3, 135 cm) is predominantly slightly glauconitic, brown gray silty clay with common pyrite and siderite nodules near the base.

The glauconitic silty clay and sandy clay of Subunit IVA occur interbedded with greenish gray silty clay, and in a thick interval in the lower half of the subunit. The interbedded intervals typically are 2 to 3 m thick, with sharp, heavily burrowed bases. Two beds of glauconitic sandy clay between 82 and 88 mbsf (Core 150-906A-10X), with very distinctive burrowed bases, are very similar to intervals observed at Site 903 (579.0–582.8 mbsf; Core 150-903A-64X), Site 902 (257.7–262.4 mbsf; Core 150-902D-30X) and, possibly, at Site 904 (133.6–137.8 mbsf; Core 150-904A-15H). Between 104.9 and 142.7 mbsf (Sections 150-906A-12X-3, 70 cm, to -16X-2, 150 cm), Subunit IVA is predominantly a dark gray to dark olive gray, glauconitic silty clay and sandy clay. This interval is largely homogeneous to heavily bioturbated, with *Chondrites* the dominant burrow. Comminuted woody plant material is common below 125 mbsf.

An interval of thinly laminated, gray brown micaceous clayey silt and silty fine sand with very abundant woody plant material comprises the basal portion of Subunit IVA and is 14.7 m thick. Individual laminae are typically 1–5 mm thick, ungraded, possibly locally cross-laminated, and rarely disturbed by burrowing. Thin beds of fine quartz sand become thicker and more common downsection. The very abundant plant material typically occurs as small (<2 mm) black flakes, concentrated in 1–3 mm laminae (Fig. 5). Larger woody fragments occur in the fine quartz sand beds. The base of this interval, which defines the base of Subunit IVA (Section 150-906A-17X-6, 150 cm), is sharp and burrowed, with silty sand piped down 10 cm below the contact.

Uniform, slightly glauconitic, brown gray silty clay comprises Subunit IVB. Bioturbation is ubiquitous throughout the subunit with fine to medium quartz sand commonly filling burrows. *Chondrites* is the dominant burrow. The silty clays are slightly micaceous and comminuted plant material is common. Minor glauconite is disseminated throughout, with abundances typically less than 2% (according to smear-slide data). Pyrite and siderite nodules are rare between 157.4

and 260.8 mbsf; they are abundant below 260.8 mbsf where the pyrite nodules are commonly rimmed by siderite. Zoned marcasite nodules occur just above the base of Unit IV (Section 150-906A-30X-3, 69 cm).

A siderite- and calcite-cemented bed occurs between 250.7 and 251.7 mbsf (Interval 150-906A-27X-4, 50–150 cm). This is underlain by a thin, fine quartz sand. Geophysical logs (see "Downhole Logging" section, this chapter) suggest the existence of a second, similarly cemented bed around 254 mbsf, where there was no core recovery.

Two thin sand beds occur near, and at, the base of Subunit IVA (252.4 and 279.0 mbsf, respectively). Both beds are poorly consolidated and were poorly recovered. The upper bed is 7 cm thick, consists primarily of fine to medium quartz sand, and has gradational boundaries. The lower bed, which marks the base of Unit IV, consists of medium quartz sand, is in part pyrite-cemented, and has a sharp base.

Smear-slide analyses of Unit IV as a whole show that quartz and feldspar combined vary between 5% and 30%, with the greatest abundance in the lower part of Subunit IVA. Glauconite content is variable in the upper subunit, ranging from 0% to 35%; the lower subunit contains 2% or less throughout. Woody plant material is an important component in the smear slides from Unit IV and is generally >2% throughout, reaching a maximum of 15% a few meters above the boundary of Subunits IVA and IVB, at around 138 mbsf. Diatom content shows a steady increase from near zero at the top to more than 30% near the base of the unit. Calcareous nannofossils are almost entirely absent.

Unit V

Interval: Sections 150-906A-30X-3, 135 cm, to -51X-1, 101 cm
Depth: 279.2–478.2 mbsf
Age: middle? Miocene

Subunit VA

Interval: Sections 150-906A-30X-3, 135 cm, to -38X-CC, 35 cm
Depth: 279.2-361.8 mbsf

Subunit VB

Interval: Sections 150-906A-38X-CC, 35 cm, to -45X-2, 33 cm
Depth: 361.8-421.1 mbsf

Subunit VC

Interval: Sections 150-906A-45X-2, 33 cm to -51X-1, 101 cm
Depth: 421.1-478.2 mbsf

A package of heterolithic sediment, 200 m thick, comprises the fill of a submarine valley cut into middle to lower Miocene strata (Fig. 4). Both the fill of the valley, and the bulk of the sediment into which it is cut, belong to Unit V as recognized at Sites 902 to 904. The valley also cuts into the top of Unit VI (see "Seismic Stratigraphy" section, this chapter).

Unit V at Site 906 can be divided into three distinct subunits (Fig. 4). Subunit VA (279.2–361.8 mbsf; Sections 150-906A-30X-3, 135 cm to -38X-CC, 35 cm) is predominantly a laminated and thinly bedded, light to dark brown silty clay; Subunit VB (361.8–421.1 mbsf; Sections 150-906A-38X-CC, 35 cm to -45X-2, 33 cm) is composed of light gray, thinly bedded, fine quartz sand; Subunit VC (421.1–478.2 mbsf; Sections 150-906A-45X-2, 33 cm to -5X-1, 101 cm) comprises mainly gray brown silty clay interspersed with mud-clast conglomerates.

The uppermost 22 m of sediment in Subunit VA are similar to the lowermost sediments of Unit IV and comprise slightly bioturbated, green-gray to dark green-gray silty clay. Lamination and very thin beds characterize the light and dark gray-brown silty clays from 300.8 mbsf downward (150-906A-33X to -38X; Fig. 6). The lighter laminae and thin beds appear to be less silty. In addition to the compositional variation shown on the millimeter- to centimeter-scale, the laminae

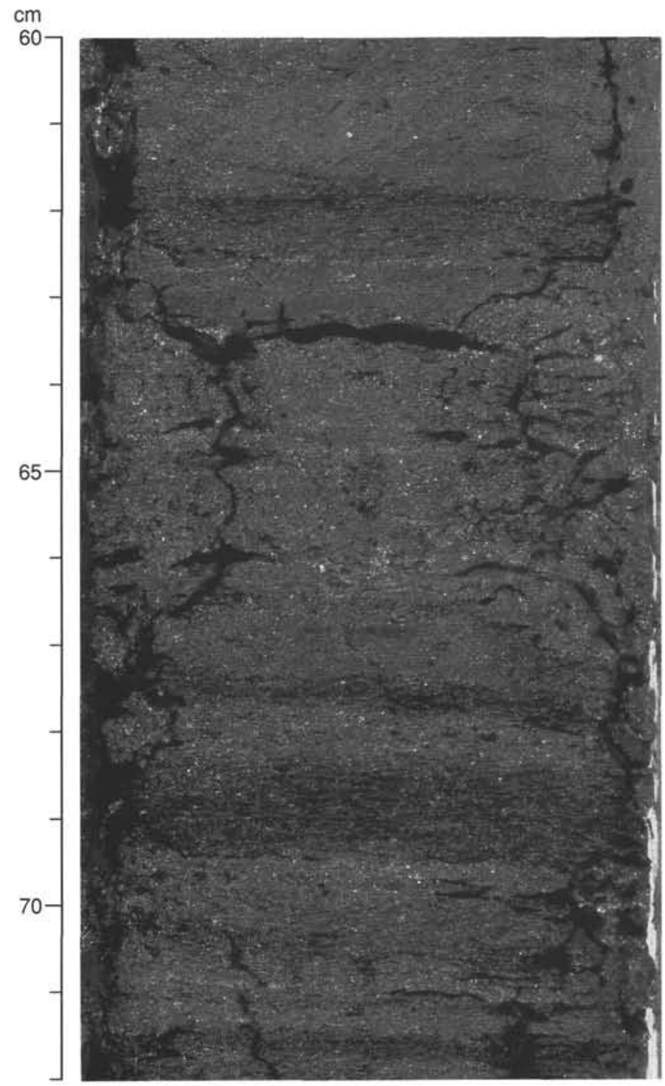

Figure 5. Silty clay and fine sand with very abundant woody fragments defining crude laminae near the base of Subunit IVA (Interval 150-906A-17X-5, 60–72 cm; 155.0–155.1 mbsf).

and thin beds are alternately more and less distinctly developed in beds 0.1 to 0.5 m thick. Burrows are very rare. Unexpectedly, total organic-carbon (TOC) values (see "Organic Geochemistry" section, this chapter) are significantly *lower* than is typical for the Miocene silty clays at other localities, although they are still high (1.1%–1.8%) relative to average marine sediments.

Clastic dikes occur at two levels: 329.1 and 336.2 mbsf. The upper dike is at an angle of ~45°, is 2 cm wide, and contains fine quartz sand cemented with pyrite. It also contains mud clasts, <0.5 cm across, that abut against the upper wall (Fig. 7). The lower dike was less completely recovered. The upper wall, which was the only one retrieved, dips at ~45°. Below it is a medium to coarse quartz sand, cemented with sparry dolomite and containing abundant pyrite framboids. Microfaults through the silty clay just above the margin have a normal offset of a few millimeters. In thin section, the upper wall of the dike is seen to be unfaulted. The silty clay above and below the dike is completely replaced by ankerite and calcite.

Smear slides show that woody organic material is common (~10%) at the top of the subunit, declining in abundance downsection. In contrast, diatoms are rare in the upper 25 m, reaching a peak of ~35% in the middle of the subunit and declining slightly below this level.

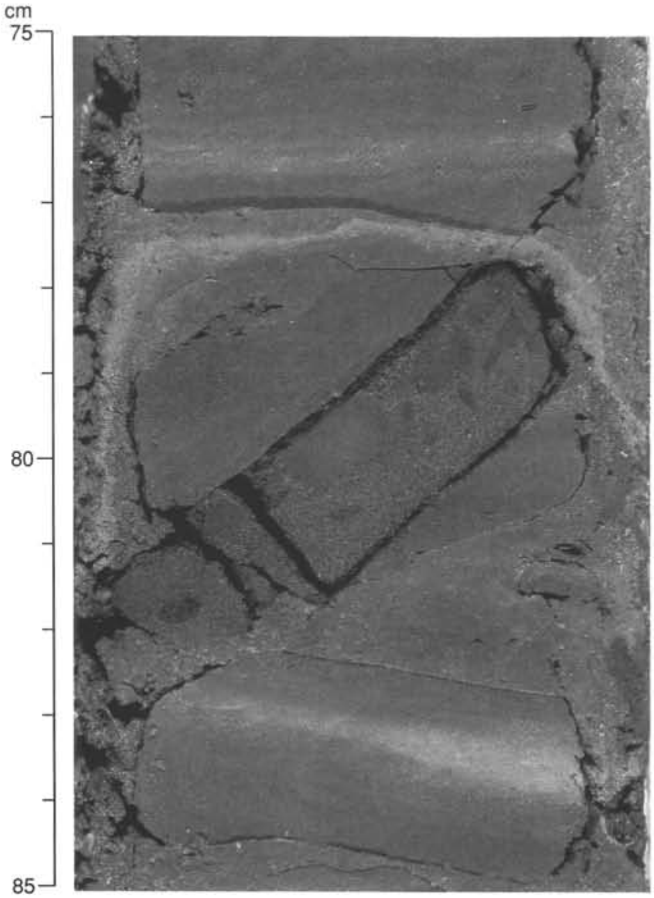

Figure 6. Clastic dike cross-cutting laminae and thin beds of laminated and thinly bedded silty clay in Subunit VA (Interval 150-906A-35X-4, 75–85 cm; 329.1–329.2 mbsf). The host rock is typical of this subunit and comprises alternating, light brown, sideritic layers and dark brown, calcitic layers. The dike contains fine quartz sand and mud clasts, the latter concentrated against the upper wall. The dike is cemented with pyrite.

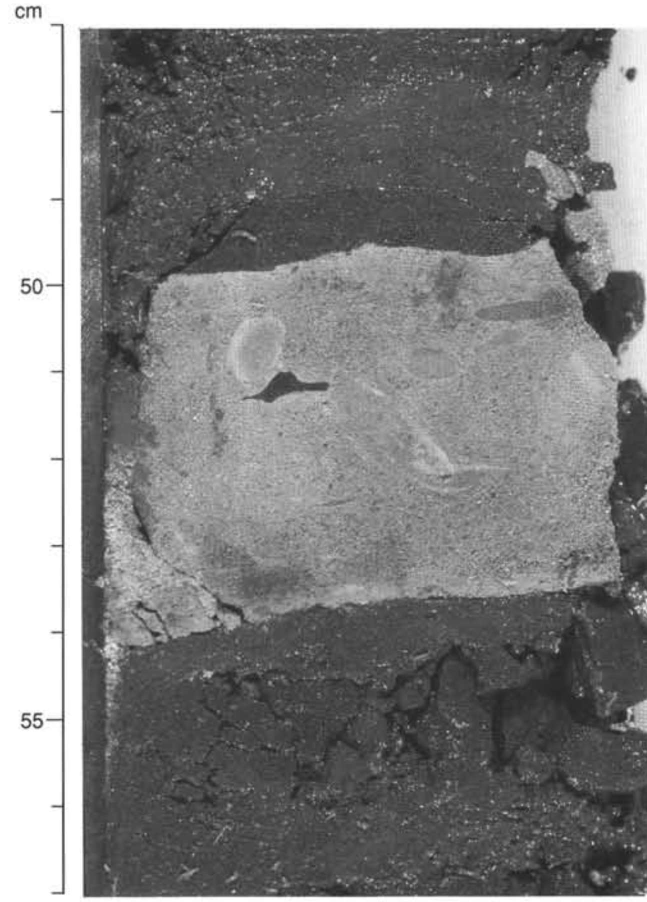

Figure 7. Possible clastic sill, intruded into silty claystones of Unit VI (Interval 150-906A-54X-5, 47–57 cm; 512.7–512.8 mbsf). Note the sharp upper and lower contacts. The matrix of the dike is a mixture of fine-grained calcite and siderite. Matrix-supported grains include quartz, glauconite, mica, and woody debris, which all occur in high concentrations.

Pyrite occurs commonly throughout the subunit as irregular to spherical nodules as large as 2 cm in diameter. In the uppermost few meters, composite nodules contain both marcasite and, in lesser quantities, pyrite.

Subunit VB is characterized by an abundance of fine quartz sand and contorted silty clay and sand. In the upper part, beds of gray silt, sandy silt, and fine sand (1–10 cm thick) occur interlayered within the laminated light and dark brown silty clay facies typical of the overlying subunit. These gray silt and sand beds commonly have sharp lower contacts and more diffuse upper contacts and were probably deposited from turbidity currents in an otherwise hemipelagic regime. The thicknesses and frequency of the silt and fine sand beds increases progressively downsection.

Slump folding is common and affects alike the brown silty clay and the gray silt and sand. Clasts of both these lithologies also occur in the slumped intervals (e.g., 373.8–375.8 mbsf). Micaceous fine-grained quartz sand, containing woody plant fragments, predominates from about 381 mbsf downward; however, poor core recovery over this interval precludes detailed description. Bioturbation in the subunit is generally slight with only rare *Planolites* observed. Diagenetic phases include pyrite, in millimeter-scale nodules and thin layers throughout, and carbonate, as a patchy cement in the sand beds.

Subunit VC is mainly a silty clay with interspersed beds of mud-clast conglomerate. The dark green-gray to brown-gray, silty clay that makes up the bulk of the subunit are homogeneous or slightly to moderately bioturbated. Glauconite abundance is variable, from 0% to 20% according to smear-slide observations; overall, however, its abundance increases downward. Diatoms are abundant at the top of the subunit (~35%) and decrease in abundance downsection. Calcareous nannofossils occur sparsely in the top of Subunit VC.

The mud-clast conglomerates are probably debris-flow deposits. The thickest conglomerate bed, about 2.5 m, occurs at the top of the subunit. It contains brown-gray to buff mud clasts that range in size from <1 cm to 30 cm. This bed is clast-supported at the top and matrix-supported at the base, where isoclinal folding was also observed. The thinner mud-clast conglomerates present lower in the subunit are also matrix-supported and commonly associated with folding and soft-sediment microfaulting (e.g., 459.9–461.9 mbsf). Possible macrofaults occur close to the base of the unit at 471.0, 475.2, and 475.8 mbsf.

At the base of Unit V is a slump bed, about 10 cm thick, that sits with a sharp contact on the underlying, well-indurated glauconitic sandstone at the top of Unit VI (Fig. 8). This is inferred to be the base of the canyon, because below this horizon the succession is similar to that seen at Sites 902 and 903.

Unit VI

Interval: Sections 150-906A-51X-1, 101 cm, to -59X-CC, 40 cm
Depth: 478.2–555.3 mbsf
Age: upper Oligocene

Dark gray-green and brown silty claystone and clayey siltstone with abundant glauconite and calcareous fossils is the predominant lithology in this unit (Fig. 4). Heavily bioturbated glauconitic sand occurs in the uppermost 3 m. Below this level, glauconite remains an important constituent, particularly between 500 and 520 mbsf (>15% according to smear-slide observations). Calcareous nannofossils range from 10% to 40% and show a slight downward increase. Trace fossils are commonly well preserved and include *Chondrites, Planolites, ?Teichichnus, ?Thalassinoides,* and *Zoophycos.* The calcareous fossils include thin-shelled bivalves, foraminifers, and the calcareous sponge *Sagarites* (*vel Makiyama*).

A possible clastic sill occurs between 512.70 and 512.74 mbsf (Interval 150-906A-54X-5, 50–54 cm; Fig. 7). This is a pale gray- to buff-colored bed composed predominantly of microcrystalline calcite and siderite. The carbonate matrix supports a variety of grain types, including abundant fine quartz sand and less abundant glauconite, mica, and woody flakes. Thin-section observations show the platy grains to be perpendicular to the margins in the middle of the bed, and parallel to the margins toward the edges. Both contacts are very sharply defined. These relationships are compatible with an intrusive origin, and the lithology is similar to that of a clastic dike observed in Unit V of Hole 903D.

Macrofaults occur at two levels within the unit: from 484.8 to 485.1 mbsf and from 544.5 to 545.3 mbsf. In the upper interval, two parallel faults occur that dip ~45° and have slickensides on the slip planes indicative of normal displacement. In the lower interval, relationships are less clear because of a combination of structural and drilling disturbance. Between 27 and ~50 cm in Section 150-906A-58X-1, brown-gray silty claystone appears to dip ~45°, based on the orientation of compacted *Planolites* burrows. Below this level, between 70 and 80 cm in the same section, a fracture dipping ~60° juxtaposes 12 cm of glauconitic silty sandstone above, against silty claystone below. A clean, fine, quartz sand occurs as the matrix to drilling breccia lower in the same core (Interval 150-906A-58X-3, 0–20 cm); beds of clean quartz sand have not been recorded in Unit VI at Sites 902 through 904. Taking all the evidence together, there appears to have been significant structural dislocation at around 545 mbsf in the upper part of Core 150-906A-58X.

The basal contact with Unit VII was not recovered at Hole 906A.

Unit VII

Interval: Core 150-906A-60X to Section 150-906A-68X-CC
Depth: 563.8–602.4 mbsf
Age: upper Eocene

Unit VII consists of clayey nannofossil chalk (Fig. 4). Recovery of this unit was poor, and much of the core was badly disturbed by the drilling. The chalk is moderately to heavily bioturbated and light gray to light greenish gray in color. Burrows include *Chondrites, Planolites,* and *Zoophycos* and are commonly filled with dark gray clay.

Smear-slide observations show the chalks to consist mainly of nannofossils (~50%) with minor foraminifers (1%–5%), and the remainder is primarily clay (Fig. 3). Glauconite and opaque minerals are minor components (1%–2%). Opal-CT is most likely present in Unit VII of Site 906, but X-ray diffraction analyses, which may have detected it here, were not performed.

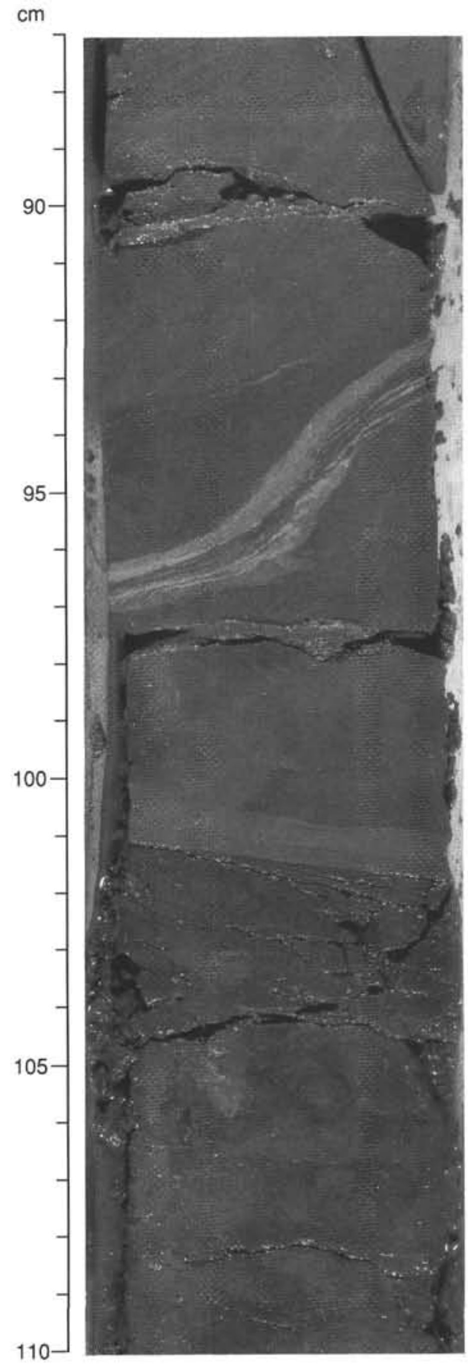

Figure 8. Inferred floor of the valley cut into lower Miocene strata, coinciding with the junction of Unit V with Unit VI (Interval 150-906A-51X-1, 87–110 cm; 478.1–478.3 mbsf). The contact is at 101 cm and is sharply defined. Above the boundary is a slump-folded silty claystone; below the boundary is a fine glauconitic sandstone.

BIOSTRATIGRAPHY

Introduction

Site 906 is located in approximately 913 m water depth and was drilled as a single hole site. The 602.4 m of sediment cored yielded remarkably good recovery except toward the bottom of the hole. Fossil recovery is spotty, and large intervals are barren of calcareous microfossils. However, there are abundant siliceous microfossils, and, it was possible to develop an adequate biostratigraphy (Fig. 9). The section comprises four unconformable units: upper Pleistocene, middle to upper Miocene, upper Oligocene, and upper Eocene.

The upper and middle Pleistocene (calcareous nannofossil Zones NN21 and NN20) extend to a level between Samples 150-906A-5H-4, 106 cm, and -5H-5, 45 cm (43.06 and 43.95 mbsf). The nannofossils indicate that the record extends back beyond the lowest occurrence of *Emiliania huxleyi* (i.e., beyond 0.275 Ma), but is younger than *P. lacunosa* (<474 ka).

A major unconformity separates the upper Pleistocene from the Miocene below. Sample 150-906A-5H-5, 45 cm (43.95 mbsf) immediately below the unconformity, yields calcareous nannofossil assem-

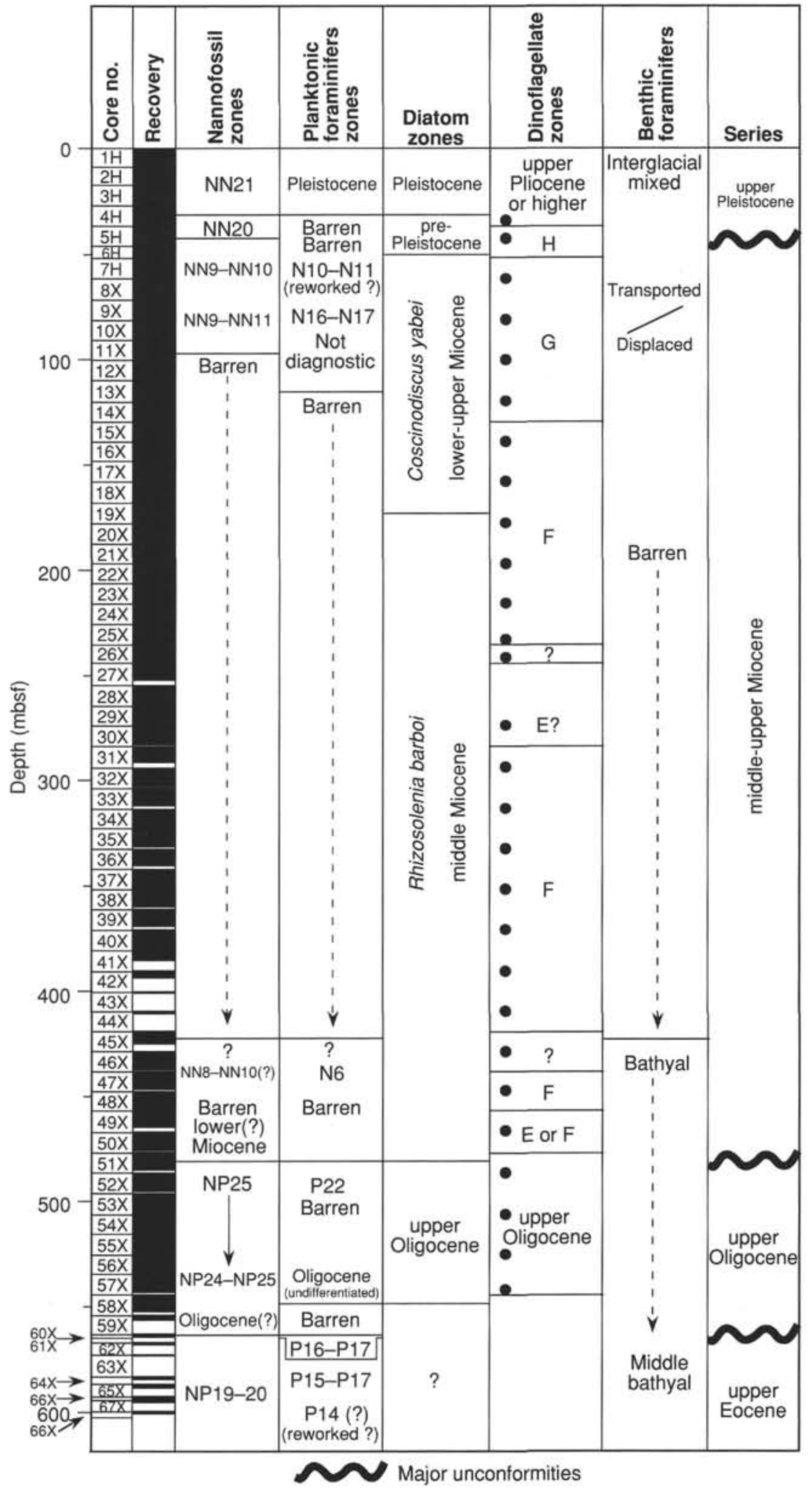

Figure 9. Summary of biostratigraphic results from Hole 906A for calcareous nannofossils, planktonic and benthic foraminifers, diatoms, and dinoflagellates.

blages suggestive of a lower upper Miocene Zone NN10 (or NN11). Long-ranging calcareous nannofossil species occur down to Sample 150-906A-10X-CC (91.5 mbsf), whereas planktonic foraminifers occur sporadically down to Sample 150-906A-12X-CC (111.04 mbsf). The lowest calcareous microfossils occur in Core 150-906A-13X-1, 20 cm (111 mbsf; see "Lithostratigraphy" section, this chapter) in the upper Miocene as determined by diatom and dinocyst stratigraphy. Below, abundant siderite crystals, often clearly showing the shapes of the nannofossils that were replaced to form the siderite.

The interval from Cores 150-906A-12X through -44X (111.04–410.17 mbsf) yields no calcareous microfossils but abundant siliceous microfossils. The diatoms indicate that this section is an upper Miocene (to Sample 150-906A-18X-CC; 168.98 mbsf) and middle Miocene (to Sample 150-906A-50X-CC; 476.83 mbsf). However, dinoflagellate cyst stratigraphy on spot samples suggests that the upper middle Miocene occurs above Core 150-906A-15X-CC (139.80 mbsf).

The base of the middle to upper Miocene unit is marked by a significant unconformity, probably within Core 150-906A-51X (477.2–485.16 mbsf). The core catcher of that core contains Oligocene microfossils.

The Oligocene extends from Samples 150-906A-51X-CC through -58X-CC (485.16–551.10 mbsf). The top of the interval is assigned to planktonic foraminifer Zone P22 and calcareous nannofossil Zone NP25. Much of the remainder of the Oligocene section is barren of planktonic foraminifera except for Sample 150-906A-57X-CC (544.10 mbsf), which yields an undifferentiated Oligocene foraminifer assemblage. Upper Oligocene Zone NP25 extends down at least to Section 150-906A-55X-CC (525.44 mbsf) (and possibly Zone NP24 based on less certain assemblages from Cores 150-906A-56X, -57X, and -58X [535.16–551.10 mbsf]). The lower part of this Oligocene interval is barren of planktonic foraminifers and diatoms but contains sparse nannofossils.

The lowermost unit is entirely upper Eocene. Nannofossils indicate Zone NP19–20 and upper Zone NP19 for Cores 150-906A-59X, -60X, and -61X (555.48–565.92 mbsf). The interval from there through Core 150-906A-68X (568.50–599.15 mbsf) lies in the lower part of Zone NP19–20. Planktonic foraminifers indicate Zone P16–P17 near the top of the Eocene interval and Zone P15–P17 in Core 150-906A-67X (594.89 mbsf).

The benthic foraminifers from the Pleistocene interval suggest predominance of interglacial indicators, with a mixture of indigenous and transported species. Transported species dominate in the uppermost part of the Miocene interval. The middle part of the interval is barren. Predominantly in situ bathyal assemblages were recovered from the lowermost part of the Miocene interval (middle Miocene) and from the upper Oligocene, whereas the upper Eocene yields middle bathyal assemblages.

The biostratigraphic subdivision of Hole 906A is given in Table 3.

Table 3. Biostratigraphic zonations and datum levels, Site 906.

Zone (base unless specified) and/or datum level	Code	Sample number	Depth (mbsf)
NN21	Cn	150-906A-2H-CC	19.40
NN20	Cn	150-906A-4H-CC	37.87
LO *P. doliolus*	Dm	150-906A-4H-CC	
LO *G. truncatulinoides*	Pf	150-906A-4H-CC	
NN10 or NN11	Cn	150-906A-5H-CC	47.47
Dinocyst Zone H	Df	150-906A-5H-CC	
HO *T. grunowii*	Dm	150-906A-7X-CC	
N16–N17	Pf	150-906A-8X-CC	72.37
Dinocyst Zone G	Df	150-906A-13X-CC	120.69
HO *D. punctata hustedtii*	Dm	150-906A-18X-CC	168.89
NN8 to NN10	Cn	150-906A-45X-CC to 150-906A-47X-CC	425.43 to 447.49
Dinocyst Zone F	Df	150-906A-47X-CC	
N6	Pf	150-906A-47X-CC	
Dinocyst Zone E or F	Df	150-906A-49X-CC	464.90
P22	Pf	150-906A-51X-CC	485.16
upper Oligocene*	Df	150-906A-57X-CC*	544.10
NP19 or NP20	Cn	150-906A-61X-CC	
P16–P17	Pf	150-906A-60X-CC to 150-906A-62X-CC	565.92 to 568.50
NP19	Cn	150-906A-62X-CC to 150-906A-68X-CC	568.50 to 599.15
P15–P17	Pf	150-906A-67X-CC	594.89
P14	Pf	150-906A-68X-CC	599.15

Note: An asterisk (*) means that the datum level was not reached and is below the lowest sample. Dm = diatoms, Cn = calcareous nannofossils, Df = dinocysts, and Pf = planktonic foraminifers. LO = lowest occurence, HO = highest occurrence.

Planktonic Foraminifers

Pleistocene sediments in Hole 906A extend downward from Sample 150-906A-1H-CC at a depth of 9.5 mbsf to at least Sample 150-906A-4H-CC at 37.9 mbsf. Based on the presence of *Globorotalia truncatulinoides,* which first appeared just before the Olduvai Subchron at 1.9 Ma (BKV85), Sample 150-906A-4H-CC is the stratigraphically lowest Pleistocene recovered in Hole 906A. Numerically dominant species are *Neogloboquadrina pachyderma, Globigerina bulloides,* and *Globorotalia inflata.* They occur in approximately equal relative abundances in all samples analyzed, which, combined with the persistence of warm-water indicators such as *Globigerinoides ruber,* implies interglacial conditions. *Globigerinoides ruber,* usually rare when present, is common in Sample 150-906A-4H-CC, indicating a full interglacial interval. Samples 150-906A-5H-CC and -6H-CC at 47.5 and 55.4 mbsf, respectively, are barren of planktonic foraminifers.

An assemblage of stained and abraded specimens of middle Miocene age occurs in Sample 150-906A-7H-CC at 63.0 mbsf. Based on the co-occurrence of *Globorotalia acrostoma* with a last appearance datum (LAD) near the top of Zone N11 (Kennett and Srinivasan, 1983) and *Globorotalia praemenardii* which ranges in Zones N10 to N12 (Kennett and Srinivasan, 1983; Bolli and Saunders, 1985), the fauna indicates the N10–N11 zonal interval. Long-ranging species in the sample support this interpretation. It is possible, however, that these specimens were reworked and subsequently redeposited in younger sediments. Sample 150-906A-8X-CC at 72.4 mbsf contains a sparse fauna that is not age diagnostic, but Sample 150-906A-9X-CC at 81.8 mbsf yielded a mixed assemblage containing both upper and middle Miocene indicators. Collectively, the well-preserved specimens are assignable to upper Miocene Zones N16-N17, whereas the forms suggesting middle Miocene Zones N10-N11 are abraded, stained, and often encrusted with secondary mineral growth. Hence, the latter asssemblage is interpreted to be reworked, as is the fauna encountered in the overlying Sample 150-906A-7H-CC. The N16 to mid-N17 zonal assignment is based on the co-occurrence of *Globorotalia jaunai* with a first appearance datum (FAD) at the base of Zone N16 (Kennett and Srinivasan, 1983; Bolli and Saunders, 1985), *Globorotalia paralenguaensis* with an LAD in mid-N17 (Kennett and Srinivasan, 1983), and *Globorotalia acostaensis* with an FAD in Chron C5n at 10.2 Ma (BKV85).

Samples 150-906A-10X-CC through -13X-CC (91.5–120.3 mbsf) contain sparse faunas that are non-age diagnostic. Samples 150-906A-14X-CC through -44X-CC (130.4 to 410.2 mbsf) are barren of planktonic foraminifers.

The association of *Globorotalia acrostoma, Globorotalia siakensis,* and *Neogloboquadrina continuosa* in Sample 150-906A-45X-CC (425.4 mbsf) indicates upper lower to lower middle Miocene. Sample 150-906A-47X-CC at 447.5 mbsf contains a more diverse fauna that can be constrained to Zone N6. In addition to the species noted in Sample 150-906A-45X-CC, the co-occurrence of *Globigerinoides altiaperturus* with a FAD at the top of Chron C6A at 20.9 Ma (BKV85) and a LAD in upper Zone N6 (Bolli and Saunders, 1985) and *Globorotalia praescitula* with a FAD in Chron C5D at 17.7 Ma (BKV85) serves as the basis for this zonal assignment.

Samples 150-906A-48X-CC at 457.9 mbsf through -50X-CC at 476.8 mbsf contain no planktonic foraminifers. However, an assemblage in Sample 150-906A-51X-CC at 485.2 mbsf is assignable to upper Oligocene Zone P22. In addition to longer ranging species such as *Globigerina ciperoensis angustiumbilicata* and *Catapsydrax* spp., the co-occurrence of *Globorotalia siakensis* with a FAD at the base of Zone P22 (Kennett and Srinivasan, 1983) and *Subbotina tripartita* with a LAD in mid-Zone P22 (Bolli and Saunders, 1985) supports the zonal assignment.

With the exception of Sample 150-906A-57X-CC at 544.1 mbsf, the interval from Samples 150-906A-53X-CC (506.3 mbsf) through -59X-CC (555.5 mbsf) is barren of planktonic foraminifers.

Age-diagnostic assemblages indicating the upper Eocene (Zones P16-P17) are encountered in Samples 150-906A-60X-CC through -62X-CC (565.2 to 568.5 mbsf). Species supporting the mid-Zone P16 to P17 zonal assignment include *Globorotalia cerroazulensis cunialensis, G. cerroazulensis cerroazulensis,* and *G. cerroazulensis pomeroli* (all with LADs in Chron C13 at 36.6 Ma; BKF85); and

Globorotalia postcretacea (with a FAD in the middle of Zone P16; Toumarkine and Luterbacher, 1985). According to the latter authors, *Globorotalia cerroazulensis cunialensis* also first occurs in the middle of Zone P16. Other species that first occur in the upper middle to lower upper Eocene include *Globorotalia increbescens, Globigerina ampliapertura, G. officinalis,* and *G. corpulenta.*

The underlying stratigraphic section down to Sample 150-906A-67X-CC (594.9 mbsf) contains faunas that constrain its age to the late Eocene zonal interval P15–P17. A more precise zonal assignment is not possible based on the species present.

The basal sample in Hole 906A (150-906A-68X-CC at 599.2 mbsf) contains appreciable numbers of well-preserved specimens belonging to taxa that last occur at the top of Zone P14 (Toumarkine and Luterbacher, 1985). These taxa include *Truncorotaloides rohri* and *Acarinina spinuloinflata,* both with LADs in Chron C17 at 40.6 Ma (BKF85), and *Globigerinatheka subconglobata* with a LAD at the top of Zone P14 (Toumarkine and Luterbacher, 1985). Associated with these taxa are *Globorotalia cerroazulensis, G. cerroazulensis pomeroli,* and species of *Globigerina,* all of which support the P14 zonal assignment although they also range upward through the remainder of the Eocene. It is possible that the older elements of this assemblage are reworked, but their abundance and excellent preservation suggest minimal exposure to abrasion and chemical alteration.

Benthic Foraminifers

One sample (Sample 150-906A-4H-CC) was analyzed in the thin Pleistocene section (Sections 150-906A-1H-CC to -4H-CC). It yields an interglacial assemblage with both transported and in situ taxa. The high-diversity assemblage contains both shallow-water fauna (e.g., *Elphidium* spp., *Cassidulina* spp., *Rosalina* spp., *Fursenkoina* spp., and *Bulimina marginata*) and deeper water fauna (*B. marginata/aculeata, B. aculeata, Cibicides* sp., *Cibicidoides pachyderma, Planulina* sp., *Melonis barleeanum, Nonionellina* spp., and *Pullenia bulloides*). The percentage of *Elphidium* spp. is very low, implying they were deposited in situ (Streeter and Lavery, 1982) rather than transported from the shelf during a glacial period (see "Biostratigraphy" section, Site 902 chapter, this volume). At the other sites, the interglacial interval is characterized by the presence of deeper water transported and in situ fauna. The presence of rare interglacial planktonic foraminifers, *Globorotalia truncatulinoides* and *G. menardii,* and the high relative percentages of deeper water taxa suggest deposition during an interglacial interval; however, a significant percentage of the transported shelf fauna suggests transport during a glacial stage. It is not possible to determine whether the glacial material, the interglacial assemblage, or both are transported.

Uvigerina juncea dominates the benthic foraminifer assemblages examined from Miocene Samples 150-906A-7H-CC (62.95 mbsf) through -11X-CC (101.34 mbsf), indicating probable downslope transport. Other taxa found in these samples include *Globobulimina* sp., *Globocassidulina subglobosa, Fissurina* spp., *Lenticulina* spp., *Martinotiella* sp., *Melonis barleeanum, Nonionellina* spp., and *Stilostomella* spp. Sample 150-906A-7H-CC also contains *Chilostomella* sp., *Elphidium* spp., and *Nonionellina pizzarensis,* indicating a possible transported shelf fauna. Rare *Martinotiella* sp. were found in Samples 150-906A-14X-CC (130.39 mbsf), -18X-CC (168.89 mbsf), and -20X-CC (188.11 mbsf). Other core-catcher samples were barren down through Section 150-906A-44X-CC (410.17 mbsf).

Below the barren interval, many core-catcher samples contained benthic foraminifers. However, Samples 150-906A-48X-CC (457.93 mbsf), -49X-CC (464.90 mbsf), -50X-CC (476.83 mbsf), -53X-CC (506.27 mbsf), -55X-CC (525.44 mbsf), and -59X-CC (555.48 mbsf) were barren. The Miocene and Oligocene section from Samples 150-906A-45X-CC (425.43 mbsf) through -57X-CC (544.10 mbsf) contain bathyal benthic foraminifer assemblages, including *Bolivina* spp., *Bulimina alazanensis, Cibicidoides pachyderma, Dentalina* spp., *Eggerella* spp., *Globocassidulina subglobosa, Marginulina* spp., *Martinotiella* sp., *Melonis barleeanum, Nonionellina* sp., *Planulina* spp., polymorphinids, *Pullenia bulloides, Pullenia quinqueloba, Sphaeroidina bulloides, Stilostomella* spp., and *Uvigerina hispida.* Sample 150-906A-45X-CC (425.43 mbsf) contains well-preserved *Cibicidoides crebbsi,* which may indicate an upper bathyal paleodepth (200-600 m) (van Morkhoven et al., 1986); however, there are abundant *Buliminella elongata* in this sample, possibly indicating downslope transport. *Osangularia* spp. occurs in and below Sample 150-906A-51X-CC (485.16 mbsf). Sample 150-906A-53X-CC (506.27 mbsf) contains *Laticarinina pauperata.* Samples 150-906A-53X-CC and -57X-CC (544.10 mbsf) contain *Melonis pompilioides.*

The Eocene section from Cores 150-906A-60X-CC (565.23 mbsf) through -68X-CC (599.15 mbsf) contains abundant, well-preserved benthic foraminifers. The fauna includes *Bulimina* spp., *Cibicidoides* spp., and agglutinants and is more diverse and abundant than in the overlying Miocene section. Taxa identified in the Eocene section include *Bulimina alazanensis, Bulimina macilenta, Cibicidoides bradyi, Cibicidoides* spp., *Dentalina* spp., *Dorothia* sp., *Eggerella* sp., *Gyroidinoides* spp., *Karreriella* spp., *Lenticulina* spp., miliolids, *Nonion* sp., *Osangularia* spp., *Plectofrondicularia* spp., polymorphinids, *Pullenia bulloides, Pullenia quinqueloba, Sigmoilopsis schlumbergeri, Spiroplectammina spectabilis, Spiroplectammina* spp., *Spirosigmoilinella tenuis, Stilostomella* spp., *Tritaxia* spp., *Uvigerina havanensis,* and *Vulvulina mexicana.* Several species typically found in bathyal Eocene sediments occur in and below Sample 150-906A-64X-CC (584.07 mbsf). These are *Anomalinoides semicribratus, Cibicidoides eocaenus, Cibicidoides micrus, Cibicidoides subspiratus,* and *Planulina costata. Uvigerina havanensis* was found in most Eocene samples, indicating middle bathyal assemblages (600-1000 m) (van Morkhoven et al., 1986).

Calcareous Nannofossils

Nannofossil recovery is uneven and not always adequate for age determination. The interval between sections 150-906A-1H-CC to -5H-4, 106 cm (0 to 43.06 mbsf) is Pleistocene. The interval from 0 to 19.4 mbsf yielded *Emiliania huxleyi* and is assigned to upper Pleistocene nannofossil Zone NN21; the interval from 19.40 to 43.06 mbsf belongs to Zone NN20. The age of Samples 150-906A-5H-CC to -11X-CC (47.47–101.34 mbsf) is less certain. Sample 150-906A-5H-5, 45 cm (43.95 mbsf), yielded an assemblage which includes *Discoaster neohamatus, D.* cf. *bollii,* and *D.* cf. *quinqueramus.* These species are incompatible and suggest a possible mixture of Miocene assemblages from nannofossil Zones NN11 and NN10 (possibly also NN9; SG). Sample 150-906A-5H-CC (47.47 mbsf) yielded *Discoaster bollii, Reticulofenestra pseudoumbilicus,* and *Coccolithus pelagicus,* which suggest assignment to nannofossil Zone NN9 or NN10. The interval between Sample 150-906A-5H-CC to 11X-CC (47.47 to 101.34 mbsf), yielded only long-ranging taxa. From Samples 150-906A-11X-CC to -44X-CC (101.34–410.17 mbsf) no coccoliths were recovered. Carbonate in the form of siderite is abundant, and occasionally a coccolith or a discoaster shape, made of siderite crystals, can be discerned. No species identification was possible.

Samples 150-906A-45X-CC through -47X-CC (425.43-447.49 mbsf) yielded rare but diverse nannofossils, including *Reticulofenestra pseudoumbilicus, Calcidiscus macintyrei, Helicosphaera carteri, Discoaster challengeri,* cf. *Discoaster bollii, Coccolithus miopelagicus, Calcidiscus leptoporus, Sphenolithus neoabies,* and *Pontosphaera multipora,* but not *Cyclicargolithus floridanus.* This suggests a middle to early late Miocene age. Sample 150-906A-49X-CC (464.90 mbsf) is barren, whereas Sample 150-906A-50X-CC (476.83 mbsf) yielded an equivocal assemblage, including *Reticulofenestra pseudoumbilicus, Coccolithus pelagicus, Coccolithus miopelagicus, Helicosphaera carteri, Discoaster sanmiguelensis,* and cf. *Cyclicargolithus floridanus,* which suggests lower middle Miocene (possibly Zone NN6; MPA).

Between Sample 150-906A-51X-CC and -58X-CC (485.16–551.10 mbsf), the sediments recovered are assigned to the upper Oligocene, although the assemblages are not entirely representative and may be residual, possibly with reworked older taxa. Very rare *Sphenolithus ciperoensis* occur in Sample 150-906A-51X-CC (485.16 mbsf), and none are present in Sample 150-906A-52X-CC (495.99 mbsf); they are present again, however, in Samples 150-906A-53X-CC (506.27 mbsf) and -55X-CC (525.44 mbsf). This indicates the upper Oligocene Zone NP25 (MPA). *Chiasmolithus altus* also occurs as a very rare element in Sample 150-906A-51X-CC (485.16 mbsf); questionable specimens occur in Sample 150-906A-52X-CC (495.99 mbsf); the species is present consistently from Samples 150-906A-54X-CC (516.08 mbsf) through -58X-CC (551.10 mbsf). The compilation of Perch-Nielsen (1985) indicates that the interval with *Chiasmolithus altus* should be assigned to Oligocene Zone NP24 (SG). Sample 150-906A-59X-CC (555.48 mbsf) yielded only the long-lived *Cyclicargolithus floridanus*.

Between Samples 150-906A-60X-CC to -68X-CC (565.23–599.15 mbsf), upper Eocene sediments which yield abundant and diverse nannofossil assemblages were recovered. In Samples 150-906A-60X-CC and -61X-CC (565.23–565.92 mbsf), *Isthmolithus recurvus, Chiasmolithus oamaruensis, Discoaster saipanensis,* and *Discoaster barbadiensis* occur without *Cribrocentrum reticulatum.* This indicates the upper part of Zone NP19 or Zone NP20 (see fig. 58 of Perch-Nielsen, in Bolli and Saunders, 1985 [SG]). *Cribrocentrum reticulatum* occurs below Sample 150-906A-62X-CC together with *Isthmolithum recurvus.* This indicates the lower part of nannofossil Zone NP19.

The tektite layer recognized at Sites 903 and 904 in the lower part of this interval was not recognized at Site 906. Very probably, it was not reached. Alternatively, because of poor conditions it was not recovered (SG).

Diatoms

Diatom concentrations ranged from rare to abundant; they were entirely absent from Eocene sediments and were sporadic in occurrence throughout the Pleistocene.

Samples 150-906A-1H-CC to -4H-CC (0–37.5 mbsf) belong to the *Pseudoeunotia doliolus* Zone. In lower latitude sediments, the nominate taxon first appears near the Pliocene/Pleistocene boundary (Burckle, 1972); its occurrence, therefore, indicates a Pleistocene age for this interval. Associated species found in this zone include *Actinocyclus senarius, Azpeitia crenulata, Coscinodiscus curvatulus, C. marginatus, Cyclotella stylorum, Nitzschia marina, Rhizosolenia calcar avis, Roperia tesselata, Thalassionema nitzschioides, Thalassiosira lineata,* and *T. oestrupii.* Several specimens of the fresh-water diatom, *Melosira italica,* were also observed. Samples 150-906A-5H-CC and -6H-CC (47–53 mbsf) have few diatoms; although several genera were identifiable, the only species observed was *Thalassionema nitzschioides.* It is suggested, however, that these samples are pre-Pleistocene in age; the degree of preservation and the overall aspect of the assemblage, even though impoverished, are not those of Pleistocene assemblages.

Samples 150-906A-7H-CC to -18X-CC (62.5–168.7 mbsf) belong to the lower upper Miocene *Coscinodiscus yabei* Zone. As noted previously, the top of this zone is defined by the last occurrence of the nominate taxon and the base by the last occurrence of *Denticulopsis punctata* var. *hustedtii.* However, as Baldauf (1984) pointed out, *C. yabei* does not occur consistently throughout the zone; the top of the zone, therefore, is characterized by the last occurrence of *Thalassiosira grunowii* which has essentially the same range as the nominate taxon. Other species found in this zone include *Actinocyclus ingens, A. senarius, A. tenellus, Coscinodiscus endoi, C. temperi, Denticulopsis hustedtii, Rhizosolenia barboi, R. miocenica* and *Stephanogonia actinoptychus. Delphineis novaecaesaraea* also occurs consistently in this zone. As noted in the previous discussions, this species is used by Andrews (1988) to subdivide Miocene sediments along the coastal plain of the U.S. Further, in other sites we have found this species in lower upper Miocene sediment. The presence of *D. hustedtii* also suggests lower upper Miocene; Burckle et al. (1982) found that this species last occurs in Chron 10 (= C4Ar). Although *D. hustedtii* is diachronous between the equatorial and North Pacific (its last occurrence in the North Pacific is younger), this does not seem to be the case in the North Atlantic. Baldauf (1984), for example, also noted the last occurrence for this species in lower upper Miocene sediments from sites occupied well to the north of Site 906.

Samples 150-906A-19H-CC to -50X-CC (178.3–477.2 mbsf) belong to the *Rhizosolenia barboi* Zone. As noted for previous sites, the age span for this zone and the overlying *C. yabei* Zone may differ from that of Baldauf (1984), who identified an intervening interval, the *Denticulopsis praedimorpha* Zone, at sites located further north. However, we failed to find this zone during Leg 150. Originally, we suggested that this may be due to a hiatus; we are increasingly of the opinion, however, that markers used to identify this zone never penetrated this far south and that no hiatus is indicated. We identified the base of the *C. yabei* Zone, as did Baldauf (1984), on the highest occurrence of *Denticulopsis punctata* var. *hustedtii.* Baldauf (1984) also used the highest occurrence of this variety to identify the middle/upper Miocene boundary. Other species present in the *D. praedimorpha* Zone include *Actinocyclus ellipticus, A. ingens, Actinoptychus senarius, Delphineis novaecaesaraea, Coscinodiscus endoi, C. temperei, C. tuberculatus, Craspedodiscus coscinodiscus, Cymatosira immunis, Denticulopsis hustedtii, D. hyalina, D. nicobarica, Paralia sulcata, P. sulcata* var. *coronata, Rhizosolenia miocenica, Rossia paleacea, Stephanopyxis grunowii* and *Thalassiosira grunowii.*

The *R. barboi* Zone is unusually thick in Hole 906A and may be correlative in part with the *R. barboi* and *Denticulopsis nicobarica* Zones of Baldauf (1984). We did not recognize the latter zone in sediments from Hole 906A; zonal markers, particularly *D. nicobarica,* were rare in Hole 906A and there is no floral justification for identifying this zone. The reader should be aware, therefore, that the *R. barboi* Zone at this site may not be stratigraphically-equivalent with the *R. barboi* Zone of Baldauf (1984) and, indeed, may also include his *D. nicobarica* Zone. A significant hiatus is recognized between Samples 150-906A-50X-CC and -51X-CC (477.2 and 486.8 mbsf), with part of the lower middle Miocene and all of the lower Miocene missing. This is well documented by the absence of *Delphineis penelliptica* which, at other sites, ranges from the lower Miocene to the lower middle Miocene and *Coscinodiscus lewisianus* which also ranges from the lower Miocene to the lower middle Miocene. Oligocene and Oligocene-early Miocene species occur in Sample 150-906A-51X-CC (486.8 mbsf). Samples 150-906A-51X-CC to -57X-CC (486.8–544.5 mbsf) contain such species as *Bogorovia veniamini, Cavitas jouseana, Coscinodiscus rhombicus, Melosira architecturalis, Pseudopyxilla rossica, Rocella gelida, R. vigilans, Stephanogonia grunowii* and *S. grossecellulata.* No zonal designations are given but the assemblage characterizes the upper Oligocene. Samples 150-906A-58X-CC to -68X-CC (544.2–602.4 mbsf) are essentially barren of diatoms. A few fragments are present in some samples, but their state of preservation defies identification to species or even generic levels.

Dinoflagellate Cysts

A total of 28 samples from Hole 906A were analyzed for dinocysts, comprising essentially every second core catcher from Samples 150-906A-4H-CC to -57X-CC (37.87–544.10 mbsf) (Fig. 9 and Table 4). Almost all samples yielded common to abundant dinocyst assemblages that are moderately to poorly preserved. In several samples, taphonomic bias resulting from differential biodegradation of peridinioid taxa is evident. Nevertheless, an unambiguous biostratigraphy based on the dinocyst assemblages has been achieved for the interval studied (Fig. 9 and Table 3).

Sample 150-906A-4H-CC (37.87 mbsf) is the only sample examined from the silty clays of lithologic Subunit IA (see "Lithostratigraphy" section, this chapter). The organic residue > 25 µm is a mixture

Table 4. Dinocyst data, Site 906.

Core, section	Depth (mbsf)	Zone
150-906A-		
4H-CC	37.87	upper Pliocene or higher
5H-CC	47.47	H
7H-CC	62.95	G
9X-CC	81.81	G
11X-CC	101.34	G
13X-CC	120.69	G
15X-CC	139.81	F
17X-CC	159.63	F
19X-CC	178.37	F
21X-CC	197.83	F
23X-CC	217.12	F
25X-CC	235.46	F
26X-CC	245.46	?
29X-CC	274.91	E?
31X-CC	292.31	F
33X-CC	312.21	F
35X-CC	332.34	F
37X-CC	352.06	F
39X-CC	369.60	F
41X-CC	385.11	F
43X-CC	400.50	F
45X-CC	425.43	?
47X-CC	447.49	F
49X-CC	464.90	E or F
51X-CC	485.16	upper Oligocene
53X-CC	506.27	upper Oligocene
55X-CC	525.44	upper Oligocene
57X-CC	544.10	upper Oligocene

of roughly even amounts of marine amorphous and terrestrial structured kerogen, plus common pine (*Pinus*) and spruce (*Picea*) pollen. Subordinate amounts of dinocysts are well preserved and moderately diverse. The presence of *Bitectatodinium tepikiense* indicates that this level is not older than upper Pliocene. However, the absence of other common late Pliocene species, in particular *Habibacysta tectata,* suggests that the sample is Pleistocene (see "Biostratigraphy" section, "Site 905" chapter, this volume). The rest of the assemblage is composed primarily of species of *Spiniferites* spp., *Operculodinium centrocarpum* s.l., and various protoperidinioid and probable protoperidinioid taxa including *Quadrina*? *condita.* The warm-water-mass indicators *Tectatodinium pellitum* and *Tuberculodinium vancampoae* are present in low numbers. The cold-water-mass indicator *Spiniferites elongatus* is more common. This apparent mixing of cool and warm water assemblages occurs in the Pleistocene sections at other sites (see "Biostratigraphy" sections in Chapters 6, 7, and 8, this volume). Quantitative study of these trends, integrated with detailed site to site correlations, will provide important insights on the water-mass provenance and climatic events during the Pleistocene.

Sample 150-906A-5H-CC (47.47 mbsf) is from the top of lithologic Subunit IB at 43.30 mbsf. The upper part of this subunit is a greenish gray clay and sand with common glauconite (see "Lithostratigraphy" section, this chapter). The presence of *Hystrichosphaeropsis obscura* and *Barssidinium evangelineae* indicate that this sample belongs to middle upper Miocene dinocyst Zone H. This result supports the placement of the unconformable Pleistocene/upper Miocene contact between lithologic Subunits IA and IB. The assemblage in this sample is moderately preserved and is anomalously dominated by dinocysts at the expense of less resistant nonreproductive tissues. Non-opaque HF insoluble minerals are common. All of this suggests transport, sorting, and biodegradation of the assemblage. Reworked specimens of Oligocene *Chiropteridium* sp. occur in trace amounts. Rare specimens of *Palaeocystodinium golzowense* may be reworked from upslope. Alternatively, this species may range into the lower part of Zone H. The same situation was observed at adjacent Site 902 (see "Biostratigraphy" section, "Site 902" chapter, this volume). Other biostratigraphically important species that are present in Sample 150-906A-5H-CC are *Labyrinthodinium truncatum, Filisphaera filifera, Achomosphaera andalousiensis* s.s., and *Batiacasphaera sphaerica* s.s. Another feature of the assemblage is the diversity of peridinioid cyst types, including some rare and other undescribed taxa. The most common species in the assemblage, however, is an unidentified thick-walled, spherical, algal cyst with a slightly helicoidal, equatorial dehiscence. This species is also dominant in basal Zone H assemblages at Site 903 (see "Biostratigraphy" section, "Site 903" chapter, this volume).

The next sample analyzed (Sample 150-906A-7H-CC; 62.95 mbsf) occurs within lithologic Subunit IVA, just below the base of lithologic Subunit IB at 55.40 mbsf. A clear unconformity and a change in lithology and color are associated with the contact between these two clay-rich subunits (see "Lithostratigraphy" section, this chapter). The organic residue in Sample 150-906A-7H-CC is co-dominated by terrestrial plant tissue (cuticle and woody tissue) and by reproductive palynomorphs (pollen, spores, dinocysts, and other algal cysts). Based on the presence of *Sumatradinium soucouyantiae* and *S. druggii,* and the absence of *Cannosphaeropsis* sp. cf. *C. utinensis,* this level belongs to dinocyst Zone G. *Barssidinium evangelineae* is not present, which suggests that the H/G zonal boundary may be coincident with the lithologic Subunit IB/IVA contact. However, the spacing of the samples analyzed to date is too coarse to assert this (Fig. 9). Dinocyst Zone G extends down to Sample 150-906A-13X-CC at 120.69 mbsf and has been additionally documented in Samples 150-906A-9X-CC and -11X-CC (81.81 and 101.34 mbsf). In these three samples, the organic residue is dominated by marine amorphous pelloidal kerogen but is characterized by diverse and well-preserved dinocyst assemblages including several undescribed protoperidinioid species. In this and other respects they are compositionally similar to the assemblages that occur in Zone G at nearby Site 902 (see "Biostratigraphy" section, "Site 902" chapter, this volume).

Lower upper Miocene Sample 150-906A-13X-CC (120.69 mbsf) is from a glauconitic sandy silt about 4.5 m above the top of a distinctive dark gray glauconitic silty clay characterized by common macroscopic organic matter at 125.00 mbsf (Section 150-906A-14X-3, 150 cm). This latter facies extends down to the base of lithologic Subunit IVA at 157.40 mbsf (Section 150-906A-17X-6, 150 cm; see "Lithostratigraphy" section, this chapter). Sample 150-906A-15X-CC (139.81 mbsf) falls within this woody interval and belongs to the upper middle Miocene dinocyst Zone F. This is the level of the highest recorded occurrence of *C.* sp. cf. *C. utinensis* at Site 906. The organic residue in this sample is dominated by terrestrial structured kerogen, although dinocysts are common, and in this respect differs markedly from the overlying Zone G kerogens. This suggests that the Zone G/Zone F boundary may occur at 125 mbsf. Further sampling will be required to confirm this. The dominance of terrestrial structured macerals over all other types in the >25-μm organic fraction is a consistent feature of the residues from Zone F samples.

The total range of *C.* sp. cf. *C. utinensis* defines the extent of Zone F. The lowest recorded occurrence of this species in Hole 906A is in Sample 150-906A-47X-CC (447.49 mbsf; Fig. 9). The duration of Biochron F is estimated to be about 2.5 m.y. (from 10.5 Ma to 13 Ma; L. de Verteuil and G. Norris, unpubl. data, 1993). An average sedimentation rate of 12 cm/k.y. can, therefore, be inferred for the roughly 300 m-thick Zone F at Site 906.

Dinocyst assemblages within Zone F at Site 906 vary somewhat in composition but are nevertheless characteristic of other Zone F assemblages which occur in the Baltimore Canyon Trough. Common gonyaulacoid taxa in this zone include *Operculodinium centrocarpum* s.s., *Cordosphaeridium minimum* s.l., *Hystrichosphaeropsis obscura, Habibacysta tectata, Reticulatosphaera actinocoronata, Cannosphaeropsis* sp. cf. *C. utinensis, Batiacasphaera sphaerica, Nematosphaeropsis lemniscata,* and *Dapsilidinium pseudocolligerum.* The peridinioid component of assemblages is generally quite diverse and usually contains several well known and as yet undescribed species of *Lejeunecysta* complex, *Trinovantedinium, Brigantedinium* types (round browns), *Sumatradinium,* and *Algidasphaeridium* types.

Of the 17 samples examined within the interval belonging to Zone F, 13 contain the zonal species *C.* sp. cf. *C. utinensis.* Sample 150-

906A-26X-CC (245.46 mbsf) developed a precipitate during processing that obscured the organic residue; no floral list was generated from this sample. Sample 150-906A-29X-CC (274.91 mbsf) yielded a well-preserved dinocyst assemblage and associated palynofacies. However, *C.* sp. cf. *C. utinensis* is not present among over 30 other taxa recorded during a careful examination of the residue. The dinocyst assemblage indicates dinocyst Zones E, F, or G. The assemblage in this sample appears anomalous with regard to the Zone F assemblages which occur above and below. Sample 150-906A-45X-CC (425.43 mbsf) contains very little organic matter that is >25 µm, but it does contain a residue of nonsilicate HF insoluble nonopaque mineral grains between 25 and 150 µm that dominate the residue. This sample is essentially barren with respect to dinoflagellates. Samples 150-906A-47X-CC and -49X-CC (425.43 and 464.90 mbsf) also contain a high concentration of HF insoluble nonopaque mineral grains in the >25-µm fraction. The structured kerogen is also darker and more biodegraded than in overlying Zone F. All three samples are from lithologic Subunit VC, which comprises silt, clay, and fine sand conglomeratic gravity deposits interbedded with hemipelagic silty clay (see "Lithostratigraphy" section, this chapter). Sample 150-906A-47X-CC (425.43 mbsf) contains a typical middle Miocene dinocyst assemblage, including the Zone F marker *C.* sp. cf. *C. utinensis.* However, Sample 150-906A-49X-CC (464.90 mbsf) contains only a poorly preserved, low-diversity dinocyst assemblage that cannot be constrained better than to Zones E, F, or G. Thus, this level may be as old as middle middle Miocene, although it is more likely slightly younger and in Zone F.

Lithologic Subunit VC unconformably overlies upper Oligocene lithologic Unit VI at 478.20 mbsf (Section 150-906A-51X-1, 102 cm; see "Lithostratigraphy" section, this chapter). Sample 150-906A-51X-CC (485.16 mbsf) is uppermost Oligocene, based on the presence of *Distatodinium biffii* and the absence of *Thalassiphora*? *pansa.* The highest known occurrence of *D. biffii* is within the uppermost part of calcareous nannofossil Zone NP25 (Brinkhuis et al., 1992). However, calcareous nannofossil data from Hole 903C suggest that this species may range as high as Zone NN2 (see "Biostratigraphy" section, "Site 903" chapter, this volume). The further common occurrence of *Chiropteridium galea* places this level within dinocyst Zone Pre-A. Other biostratigraphically important taxa in Sample 150-906A-51X-CC are *Riculacysta perforata, Systematophora ancyrea-placacantha* complex, *Apteodinium spiridoides, Membranophoridium aspinatum,* and *Distatodinium paradoxum. R. perforata,* in particular, has only been recorded from the upper Oligocene. The preservation of the assemblage in general is moderate to poor, but the absence of *Homotryblium* spp. and *Deflandrea phosphoritica* is notable and surprising.

The next two samples analyzed (Samples 150-906A-53X-CC and -55X-CC; 506.27 and 525.44 mbsf, respectively) contain *T.*? *pansa* and therefore are older than dinocyst Zone Pre-A. According to Stover (1977), *T.*? *pansa* has its highest occurrence near the middle of the upper Oligocene planktonic foraminifer *Globigerina ciperoensis* Zone. The assemblages that they contain are otherwise similar to those in Sample 150-906A-51X-CC, but in addition they contain *Distatodinium ellipticum, Caligodinium amiculum, Hystrichokolpoma truncata, H. cinctum, Cordosphaeridium cantharellum, Cerebrocysta mediterranea,* and *Deflandrea phosphoritica.*

Sample 150-906A-57X-CC (544.10 mbsf) was the lowest sample analyzed for dinocysts. The assemblage contains many taxa found in the overlying upper Oligocene samples. These include *D. phosphoritica, H. truncata, C. cantharellum, D. pseudocolligerum, C. mediterranea, M. aspinatum,* and *D. paradoxum.* However, *D. biffii* and *T.*? *pansa* are conspicuously absent from the assemblage. This, together with the absence of common lower Oligocene markers such as the *Areosphaeridium arcuatum* complex, suggest that this level is lowermost upper Oligocene. The most common species in Sample 150-906A-57X-CC, however, is an undescribed species of *Systematophora* that differs from the *S. ancyrea-placacantha* complex in having distally branched processes and well-developed, recurved, denticulate, distal bifurcations. Head and Norris (1989) illustrated a possibly synonymous specimen, as *Surculosphaeridium*? sp. A, from the lower upper Oligocene (calcareous nannofossil Zone NP24) of ODP Hole 647A in the Labrador Sea.

PALEOMAGNETISM

Similar to our experience at other Leg 150 sites, magnetostratigraphic analysis of sediments recovered at Site 906 is hindered by weak magnetization. Where recovery permitted, we measured and demagnetized whole sections of split core from Hole 906A (total depth = 602.4 mbsf) and, to augment the pass-through data, discrete samples were taken from the upper 100 m for more thorough demagnetization.

Magnetization intensities are relatively strong in the dark gray clays at upper levels in the core (0–107 mbsf), but they diminish downhole as the sediments gradually trend toward green clayey silts and silty clays (generally 0.1 mA/m or less). A zone of very strong magnetization is present, however, between about 282 and 465 mbsf, where intensities can reach 100 mA/m. The sediments in this zone are green; in addition, between 300 and 390 mbsf, centimeter-scale yellow bands that possibly contain siderite occur (see "Lithostratigraphy" section, this chapter). As in nearly all sediments recovered on Leg 150, magnetic susceptibility variations in Hole 906A, including those within the banded "siderite zone," tend to follow variations seen in magnetization intensity (Fig. 10).

Following the removal at 15 mT of a drilling-induced overprint, demagnetized remanence yields a fairly uniform zone of normal polarity in the upper 47.5 m of Hole 906A (Fig. 10); this is confirmed by analysis of discrete samples. Between 47.5 and 86.0 mbsf, magnetization are somewhat scattered but consistently negative in inclination (Fig. 10). Demagnetized remanence becomes very shallow below 86 mbsf; and, unfortunately, below about 107 mbsf, magnetization intensities drop to below practical cutoff limits.

Unlike most other Leg 150 sites, the shipboard biostratigraphy at Site 906 does not provide very many clear biozones needed to establish a working framework for magnetostratigraphy in an environment of discontinuous sedimentation. However, the upper 43.06 m are slumped Pleistocene clayey silts, and below 43.95 mbsf diagnostic nannofossils indicate a late Miocene age (i.e., late Miocene; see "Biostratigraphy" section, this chapter). Therefore, a disconformity may be present near 43.5 mbsf, separating an incomplete record of the Brunhes Chron (Chron C1n) from late Miocene magnetic fields below (Fig. 10). The presence of Zones N16–N17 between roughly 72 and 82 mbsf suggests that the normal polarity zone from 37.5 to 47.5 mbsf and the reversed interval between 47.5 and 86.0 mbsf are post-Chron C5n (BKV85; Table 5).

Weak magnetization intensities in the lower 500 m of Hole 906A frustrate our attempts at a magnetostratigraphic zonation. However, over the interval 282–465 mbsf, several subintervals of strong magnetization occur (including the banded "siderite" zone), in which polarity interpretation is feasible (Fig. 10). A relatively long reversed polarity zone takes place between 282 and 383 mbsf, an interval of no recovery from 394–400 mbsf, followed by a thin normal polarity zone to 396 mbsf. Below a zone of strong, but very scattered magnetization, a normal polarity zone occurs between 437 and 457 mbsf, followed by a thin reversed zone to 465 mbsf (Fig. 10). At this stage of the study, we urge caution when interpreting the magnetization in the sediments within and surrounding the banded "siderite" zone. Zoned authigenic pyrite nodules occur at various stratigraphic levels between 270 and 390 mbsf (see "Lithostratigraphy" section, this chapter), and the role of diagenesis on the genesis of the very strong, perhaps secondary, magnetization in these sediments is unknown. Nonetheless, we can attempt a working correlation to the geomagnetic polarity time scale. The only shipboard biostratigraphic age information directly available for the interval from 290 to 420 mbsf is middle Miocene *R. barboi* Zone (approximately 11 Ma) (see "Biostratigraphy" section, this chapter). However, between about 420 and

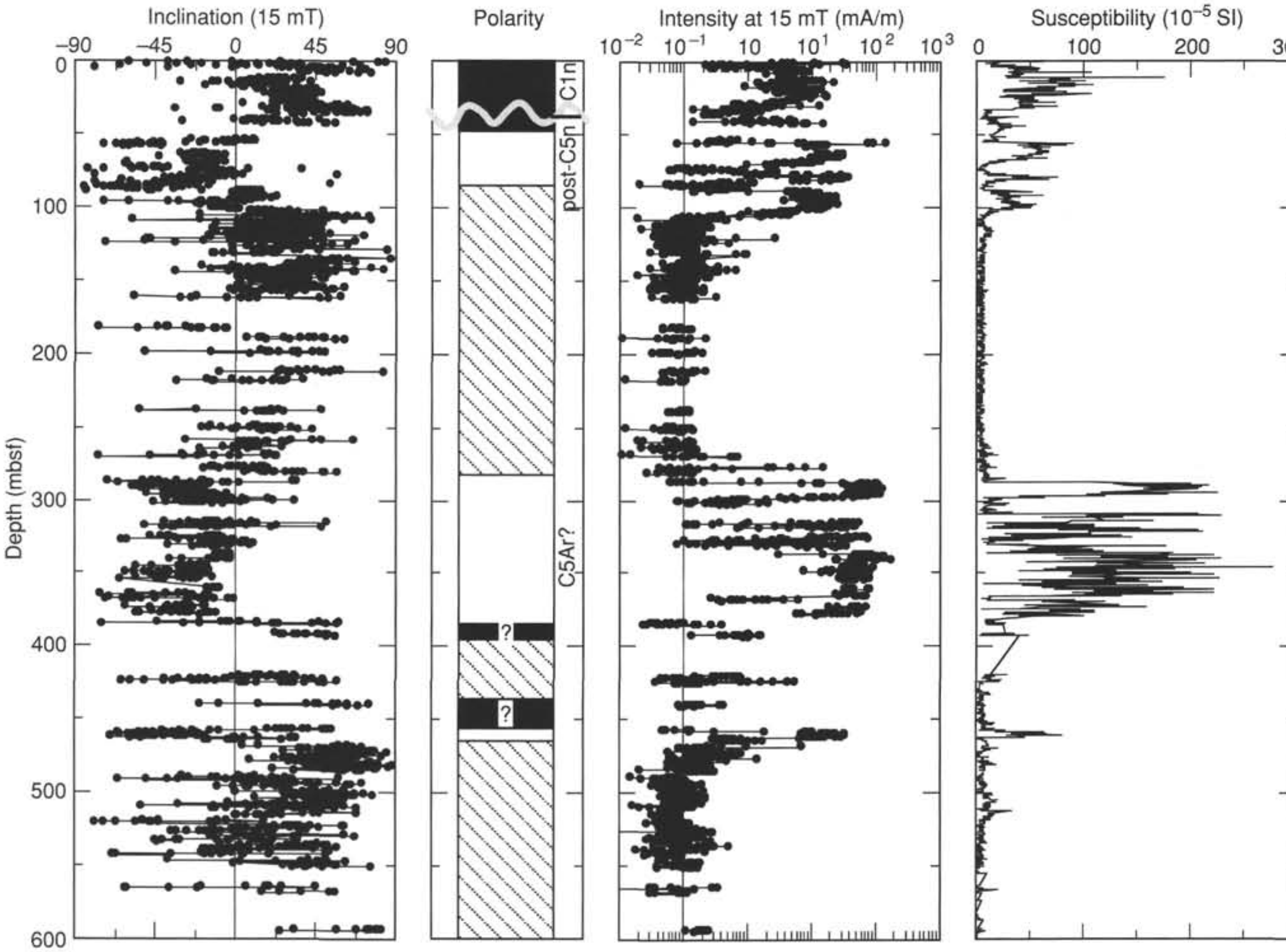

Figure 10. Inclination, magnetic polarity zones, magnetization intensity, and volume susceptibility of pass-through measurements for the interval from 0 to 600 mbsf in Hole 906A. Intensity cut-off value is 0.1 mA/m for pass-through measurements. In the polarity column, black = normal polarity, white = reversed polarity, and cross-hatch = uninterpretable.

Table 5. Reversal boundary depths, Hole 906A.

Depth (mbsf)	Polarity	Interpreted polarity zone
0.0–43.06	N	C1n
43.06–47.5	N	(post-C5n)
47.5–86.0	R	(post-C5n)
86.0–282.0	?	No zonation
282.0–383.0	R	C5Ar?
383.0–396.0	N?	No zonation
396.0–437.0	?	No zonation
437.0–457.0	N?	No zonation
457.0–465.0	R	No zonation
465.0–602.4	?	No zonation

Note: N = normal, R = reversed, and ? = uncertain.

475 mbsf where, unfortunately, magnetizations are very weak, diagnostic nannofossils are present that suggest a correlation to Zones NN5–NN7. Thus, the relatively long reversed interval from 282 to 383 mbsf could correlate to Chron C5Ar of the middle middle Miocene (Fig. 10).

The correlations presented in this summary are judged tentative pending more precise biozonations and shore-based paleomagnetic and rock magnetic analyses of the various sediments recovered at Site 906.

SEDIMENTATION RATES

A 602.4-m-thick Pleistocene to upper Eocene section was penetrated at Site 906. It comprises a 43-m-thick Pleistocene succession of silty clays, fine sands, and mass-flow deposits (see lithologic Unit IA; "Lithostratigraphy" section, this chapter) younger than 0.474 m.y. These unconformably rest on redeposited lower upper Miocene glauconitic sands and hemipelagic silty clays of Subunit IB ("Lithostratigraphy" section, this chapter). The thickness of the upper Miocene is uncertain. The highest occurrence of *D. punctata* var. *hustedtii* at 168.89 mbsf (see Fig. 11) can be used to approximate the top of the middle Miocene, although at Hole 902C and 903C this taxon last occurs within the upper middle Miocene. Much of the remaining Miocene section below this highest occurrence (169–485.16 mbsf) is barren of calcareous plankton; this section belongs to the *R. barboi* diatom Zone. Calcareous microfossils indicate that a ~66-m section of upper Oligocene glauconitic silty clay overlies an upper Eocene nannofossil clayey chalk (lithologic Units VI and VII, respectively; see "Lithostratigraphy" section, this chapter).

The Pleistocene section is thin (43 m) and younger than the *Pseudoemiliania lacunosa* LAD (<474 ka). No attempt was made to correlate this section to the SPECMAP scale on the ship because of time constraints.

The upper Miocene section at Site 906 comprises Zones NN9–NN10 and N16–N17 and thus is lower upper Miocene (8.2–10.4 Ma). This indicates that the reversed polarity zone noted at 47.5–86.0 mbsf

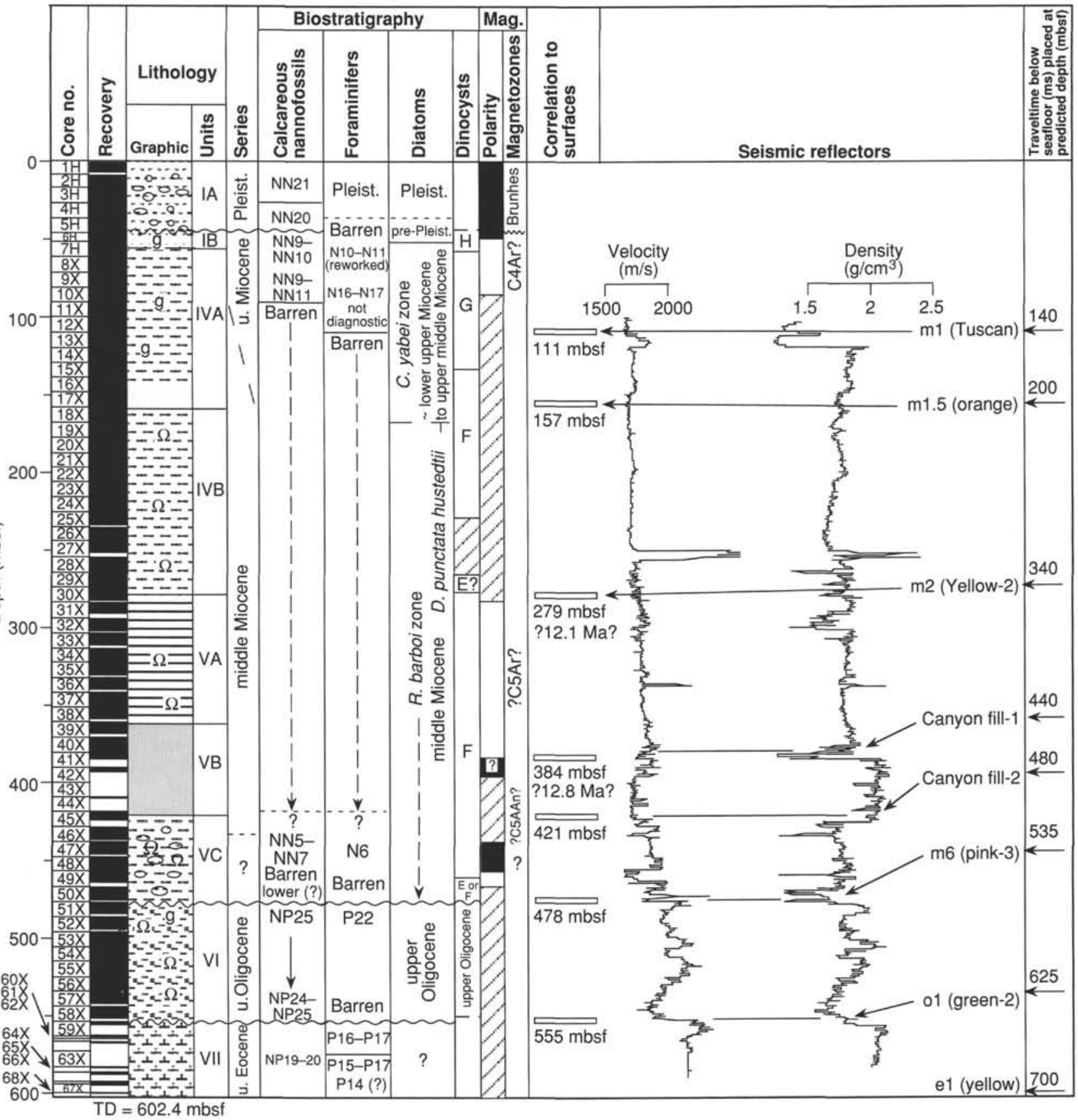

Figure 11. Seismic-core correlations for Hole 906A showing lithology, series, biostratigraphic zones, magnetozones, velocity and density log data, and seismic reflectors discussed in the text.

(see "Paleomagnetism" section, this chapter) may correlate with part of Chron C4Ar (~8.7–8.9 Ma). The boundary between the upper and middle Miocene is not recognizable using biostratigraphic criteria. No estimate of sedimentation rate for the upper Miocene at Site 906 is possible.

Stratigraphic interpretation of the middle Miocene section recovered at Hole 906A is the least constrained of any of the slope sites because of a thick interval (~90–420 mbsf) barren of calcareous microfossils. Biostratigraphic control for this interval is provided by diatoms (*R. barboi* Zone) and dinoflagellate cysts (Zones G, F, and E).

Stratigraphic uncertainties exist in the correlation of the *R. barboi* Zone. The top of this zone is defined by the highest occurrence of *D. punctata* var. *hustedtii*. In the equatorial Pacific, *D. punctata* var. *hustedtii* last appeared in late middle Miocene Chron 10 (= C5r), with an age of ~11 ± 0.5 Ma (Burckle et al., 1982). At Hole 902C, this taxon disappears above reflector m2 (Yellow-2) in a reversed polarity zone that could correlate with either Chron C5r or C5Ar (within the lower half of dinoflagellate Zone F). At Sites 903 and 905, the highest occurrence of this taxon is in the upper middle Miocene. This problem is complicated further by evidence from Hole 904A in which the highest occurrence of *D. punctata* var. *hustedtii* is well above the section assigned to upper Miocene Zones N16–N17, although this discrepancy may be the result of reworking. Despite uncertainties in its exact age, it is clear that the youngest occurrence of *D. punctata* var. *hustedtii* was in late middle Miocene Chron C5r (= Chron 10 as noted by Burckle et al., 1982).

All of the canyon fill at Hole 906A is assigned to the *R. barboi* Zone (older than 11 ± 0.5 Ma, as outlined above) and to dinoflagellate cyst Zones F and E. At Site 903, the base of the *R. barboi* Zone correlates with the mid-part of Zone NN5 (~15 Ma). Assuming that the diatom-nannofossil correlation made at Site 903 is applicable at Site 906 it is possible that the thick reversed magnetozone noted between 282 and 383 mbsf could correlate to Chron C5Ar (12.1–12.8 Ma; see Fig. 11). This yields very high sedimentation rates for this section (minimum rate of 14 cm/k.y. uncorrected for compaction). A similar value (12 cm/k.y.) is estimated using dinoflagellate stratigraphy (see "Biostratigraphy" section, this chapter). Reflector m2 (Yellow-2) lies at the top of the fill. It its age is 12.4 Ma, as estimated at Site 903, then the sedimentation rates were even higher (>25 cm/k.y.). Seismic stratigraphic relations indicate that reflector m3 (Blue) is cut by the canyon, thus dating the erosion as younger than ~13.5 (see "Seismic Stratigraphy" section, this volume). Thus, it appears that the entire cutting and filling of the canyon occurred between ~13.5 and 12.4 Ma.

Lithologic Subunit VC (421.1–478.2 mbsf) is a mud-clast conglomerate found at the base of the canyon fill. This unit contains both lower Miocene (Zone N6) and middle Miocene fossils (*R. barboi* Zone, undifferentiated Zone NN6–NN7). We assume that the older ages reflect the reworking of older sediment as clasts, and that the canyon fill is middle middle Miocene and younger (*R. barboi* Zone and Dinocyst Zone F; <~15 Ma). No estimates of sedimentation rate for the lower part of the canyon fill are possible.

The Oligocene section is assigned to Zones NP25 and P22 (upper part). The upper Eocene section is assigned to Zones NP19–20 and P15–P17. No estimates of the late Oligocene and late Eocene sedimentation rates are possible.

ORGANIC GEOCHEMISTRY

Shipboard organic geochemical studies of sediments from Hole 906A included volatile hydrocarbon and nonhydrocarbon gases, Rock-Eval, and elemental analysis. The instrumentation, operating conditions, and procedures are summarized in Chapter 3 (this volume).

Volatile Gases from Sediments

Gases released from the sediments at Site 906 were continuously measured as part of the shipboard safety and pollution monitoring program. Samples for headspace gases were taken as soon as the core arrived on the deck (Table 6 and Fig. 12). The composition of headspace gas at Hole 906A is predominantly methane, accompanied by minor amounts of ethane and traces of propane toward the bottom of the hole. The headspace gas is considered to be of biogenic, rather than thermogenic, origin. Headspace methane concentrations are highly variable and range from 586 to 83,019 ppm. The highest values occurred in two discrete zones. The upper zone between 32.5 and 317.0 mbsf is directly below the zone of sulfate reduction, and has C_1/C_2 ratios in excess of 1000, indicating its biogenic origin. In general, microorganisms are not thought to generate vast quantities of gas by degradation of organic matter in situ; consequently, this gas observed at Site 906 was not considered to be a hazard to the ship or the surrounding environment. A gas-lean interval occurs in lithologic Subunits VA–VC (328.3–433.3 mbsf) in unusual, thinly interbedded sediments composed of light brown sideritic clays and dark brown silty clays (see "Lithostratigraphy" section, this chapter). This interval is also characterized by lower TOC contents (Fig. 13). The paucity of organic matter is the most likely explanation for the depressed gas concentrations. A deeper gas-enriched zone lies between 443.1 and 663.8 mbsf within lithologic Subunit VC and Unit VI. Within this interval, ethane accompanies methane in concentrations that generally increase with depth (from 1 ppm at 420.8 mbsf to a maximum of 432 ppm at 555.1 mbsf). Propane occurs occasionally (in concentrations as much as 5 ppm). C_1/C_2 values drop dramatically across the Miocene/Oligocene unconformity (478.2 mbsf) and remain below 500 down to 539.3 mbsf. However, TOC values within the same interval are some of the highest in the section, and in the deeper Eocene sediments, C_1/C_2 values rise. The irregularity of the C_1/C_2 ratio with depth, coupled with the high organic-carbon content, suggests that bacterial degradation of organic material is the source of the gas in the Oligocene sediments of this site.

Seventeen vacutainer samples were obtained from expansion voids that formed in sediment within the core liners between 133.2 and 535.6 mbsf (Table 7). Vacutainer hydrocarbon-gas concentrations are consistently higher than those from samples obtained from the same sediments by the headspace method (see also Behrmann, Lewis, Musgrave, et al., 1992). Vacutainer samples contain particularly high concentrations of methane because of methane's greater lability (in comparison to high-molecular-weight volatiles), which permits rapid evolution as pressure decreases as the core is raised to the sea surface. At Hole 906A, vacutainer-sample methane concentrations range from 0 to 802,203 ppm (80.2 vol%). This maximum value is 164 times the headspace value obtained from the same core; thus, caution should be exercised when evaluating hydrocarbon-gas data for safety and pollution-monitoring purposes. Vacutainer measurements were obtained from expansion voids that formed in irregular cores between 239.5 and 451.3 mbsf; however, hydrocarbon gases were absent and only CO_2, N_2, and O_2 were detected. The data from this interval may be an artifact of vacutainer leakage. Concentrations of CO_2 in Cores 150-906A-26X and -30X are well above those found in the atmosphere.

Elemental Analysis

Sixty samples were freeze dried and analyzed for total carbon, nitrogen, and sulfur at Site 906 by elemental analysis. Total inorganic carbon was measured by carbon dioxide coulometry, and the difference between total carbon and inorganic carbon provided the total organic-carbon (TOC) content of the sediments (Table 8).

Carbonate carbon was translated to $CaCO_3$ (wt%) for comparison with previous sites. Diagenetic siderite and dolomite appear to be important components in Miocene sediments at Site 906 (see "Lithostratigraphy" section, this chapter) and, according to smear-slide analysis, biogenic carbonate only exerts control on the carbonate profile in Oligocene and Eocene sediments (Fig. 14). Total inorganic carbon as $CaCO_3$ varies from 0.2 to 47.5 wt% in the sediments at Hole 906A. In lithologic Subunit IA, carbonate ranges from 6.4 to 14.0 wt%, and is considered to be of detrital origin, possibly associated with the mass-transport deposits that make up the Pleistocene section. In contrast to the carbonate in the Pleistocene at Site 905, the coulometric carbonate in Pleistocene sediments deeper than 23.0 mbsf at this site appears to correlate with biogenic carbonate observed in smear slides. Values fall in Subunits IB through IVB to less than 5% $CaCO_3$ wt%. This carbonate depletion probably results from the dissolution of calcareous microfossils by low pH interstitial waters. Apart from coccoliths preserved as ghost structures in siderite, the sediments within this interval were barren of calcareous fauna (see "Biostratigraphy" section, this chapter). The slight upturn in the carbonate profile to a value of 5.8 wt% (0.7 wt% TIC) at 298.2 mbsf may result from the occurrence of abundant diagenetic siderite and carbonate nodules at the base of this unit (see "Lithostratigraphy" section, this chapter). The sediments of Subunits VA and VB (279.2–420.0 mbsf) consist of laminated and thinly bedded silty clays, which contain siderite (see "Lithostratigraphy" section, this chapter). The carbonate values of these units average 7.4 wt%; however, $CaCO_3$ values fluctuate from 2.7 to 15.5 wt% in the interval from 317.7 to 383.3 mbsf. The heterogeneity may be caused by the variation in siderite content in association with the laminae that characterize this zone.

The top of the Oligocene at 481.0 mbsf is marked by an increase in carbonate values from 3.7 to 22.9 wt%. This increase probably reflects the increased abundance of calcareous microfossils in the Oligocene strata. $CaCO_3$ continues to increase downward to a maximum of 47.5 wt% in the Eocene clayey chalks (from 564.3 to 602.4 mbsf) (Fig. 14).

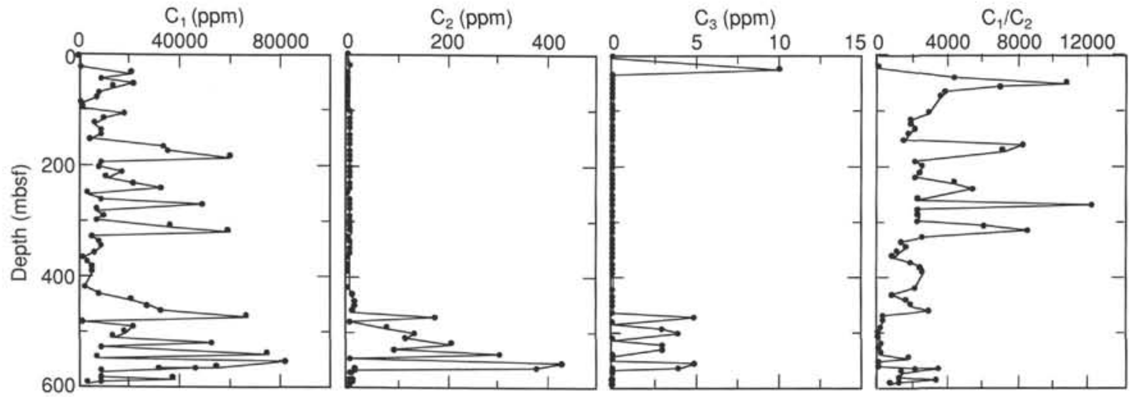

Figure 12. Headspace volatile hydrocarbon composition and C_1/C_2 ratios vs. depth for sediment samples from Hole 906A.

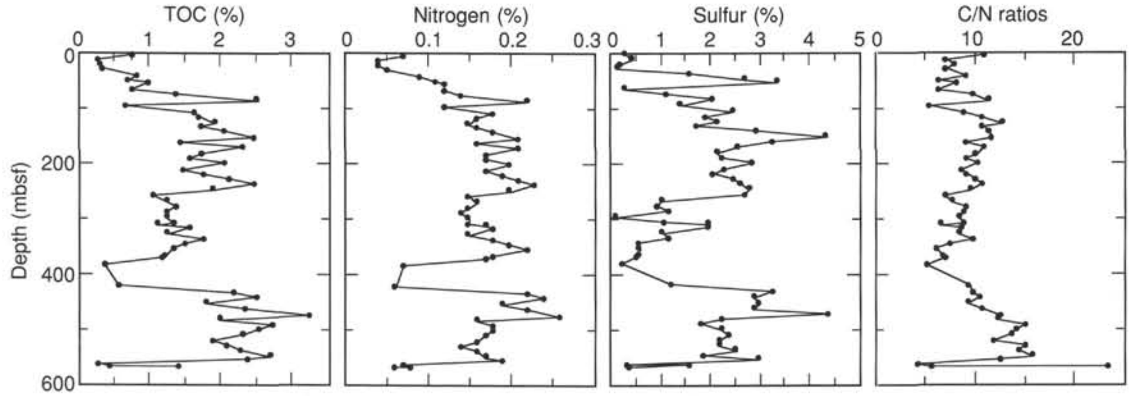

Figure 13. Total organic carbon (TOC), nitrogen, sulfur, and organic C/N atomic ratios vs. depth for sediment samples from Hole 906A.

Total organic-carbon (TOC) values at Hole 906A ranged from 0.29 wt% in Pleistocene sediments to 3.27 wt% in the Oligocene (Fig. 13). The low values recorded in the Pleistocene may be a function of rapid sedimentation rates, which have a clastic dilution effect on organic-matter content. Alternatively, a highly oxygenated sedimentary environment (as a result of dynamic sedimentation processes) and heavily oxidized, redeposited terrestrial and marine organic matter may produce organically lean sediments. Organic-carbon contents in the upper Miocene (50.7–238.1 mbsf) average 1.7 wt%; a deeper zone within Subunit IVA and Unit V between 248.1 and 371.7 mbsf exhibits slightly lower values (average = 1.4 wt%). This lower interval consists of the laminated sediment interval described earlier. It is surprising to see depressed TOC contents in the presence of such thinly bedded, burrow-free silty clays, because this type of sediment is generally characteristic of low-oxygen conditions (see "Lithostratigraphy" section, this chapter). The severe decline in the TOC profile and the sparsity of data between 372.0 and 432.5 mbsf are caused by an unconsolidated sandy interval where recovery was poor. Sands permit a higher diffusion of oxygen between grains than finer grained sediments because of poorer grain packing; thus, the sand's ability to isolate organic matter from oxidation processes is greatly reduced. Core 150-906A-17X (149.4-159.0 mbsf) was observed to contain vast quantities of woody material in the sandy debris. Pieces of this carbonaceous material are up to 1 cm^3 in size and appear to be coated with iron oxide. Despite this large volume of terrigenous material, the TOC values of these sediments are lower than those found in more pelagic facies in the Oligocene (average 2.4 wt%). Such high TOC contents in hemipelagic and pelagic facies are considered to result from a high-productivity water column that exerted high oxygen demands on bottom waters, which, in turn, increased organic-matter preservation potential in surface sediments.

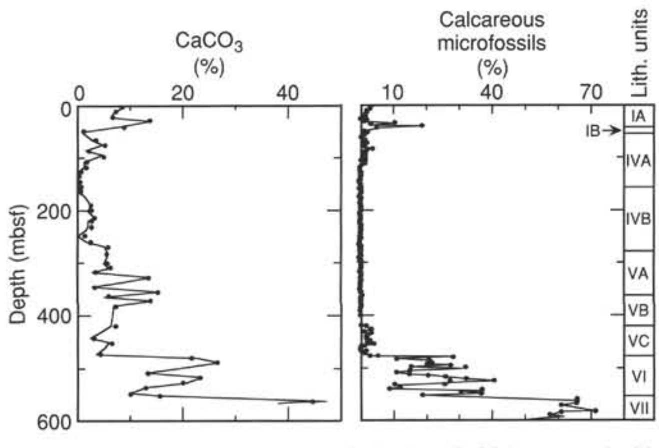

Figure 14. Carbonate concentration (calculated as $CaCO_3$) compared with calcareous nannofossil data (estimated in smear slides) vs. depth for sediment samples from Hole 906A.

Total nitrogen values of sediments vary between 0.04 and 0.26 wt% (Fig. 13), and, as at the other sites, nitrogen parallels the TOC profile with depth. Sulfur ranges from 0.21 and 3.26 wt% down the entire profile and covaries with TOC and total nitrogen, with the exception of a zone between 248.1 and 308.3 mbsf in which content drops from 2.8 down to 0.12 wt%.

Table 6. Headspace gas composition from sediments at Site 906.

Core, section, interval (cm)	Depth (mbsf)	C_1 (ppm)	C_2 (ppm)	C_3 (ppm)	C_1/C_2
150-906A-					
1H-2, 0–5	1.5	37	0	0	
3H-4, 0–5	23.0	534	5	10	107
4H-4, 0–5	32.53	20710	0	0	
5H-4, 0–5	42.0	8854	2	0	4430
6H-4, 0–5	51.5	21740	2	0	10900
7H-4, 0–5	57.5	14008	2	0	7000
8X-4, 0–5	67.0	7978	2	0	3990
9X-4, 0–5	76.5	7372	2	0	3690
10X-4, 0–5	86.4	586	0	0	
11X-4, 0–5	96.0	1254	0	0	
12X-4, 0–5	105.6	18005	6	0	3000
13X-4, 0–5	115.3	10075	5	0	2020
14X-4, 0–5	125.0	6008	3	0	2000
15X-4, 0–5	134.6	8899	4	0	2220
16X-4, 0–5	144.2	9053	5	0	1810
17X-4, 0–5	152.9	4902	3	0	1630
18X-4, 0–5	163.5	33549	4	0	8390
19X-4, 0–5	173.2	36104	5	0	7220
20X-4, 0–5	182.8	60167	6	0	10000
21X-4, 0–5	192.5	9207	4	0	2300
22X-4, 0–5	202.1	7896	3	0	2630
23X-4, 0–5	211.7	17059	7	0	2440
24X-4, 0–5	221.3	11221	5	0	2240
25X-4, 0–5	231.0	22166	5	0	4430
26X-4, 0–5	240.5	32674	6	0	5450
27X-4, 0–5	250.2	3190	0	0	
28X-4, 0–5	259.8	9486	4	0	2370
29X-4, 0–5	269.6	49329	4	0	12300
30X-4, 0–5	279.3	6988	3	0	2330
31X-4, 0–5	289.1	9735	4	0	2430
32X-4, 0–5	298.9	6996	3	0	2330
33X-4, 0–5	308.7	37083	6	0	6180
34X-3, 0–5	317.0	60093	7	0	8580
35X-4, 0–5	328.3	5376	2	0	2690
36X-4, 0–5	337.7	8454	6	0	1410
37X-4, 0–5	347.0	8719	5	0	1740
38X-4, 0–5	356.7	6227	5	0	1250
39X-3, 0–5	364.8	1944	2	0	972
40X-4, 0–5	376.0	3865	2	0	1930
41X-2, 0–5	382.6	5066	2	0	2530
42X-2, 0–5	392.3	5325	2	0	2660
45X-2, 0–5	420.8	2227	1	0	2230
46X-4, 0–5	433.3	8311	9	0	923
47X-4, 0–5	443.1	21256	12	0	1770
48X-4, 0–5	452.7	27672	14	0	1980
49X-4, 0–5	462.4	33051	11	0	3000
50X-4, 0–5	472.0	67292	175	5	385
51X-4, 0–5	481.7	1792	5	0	358
52X-4, 0–5	491.3	21649	78	3	278
53X-4, 0–5	501.0	18660	133	4	140
54X-4, 0–5	510.7	13989	117	0	120
55X-4, 0–5	520.3	53494	209	3	256
56X-4, 0–5	529.8	8940	91	3	98
57X-4, 0–5	539.3	75480	307	0	246
58X-3, 0–5	547.5	7349	4	0	1840
59X-CC, 0–5	555.1	83019	432	5	192
60X-1, 0–5	563.8	54725	379	4	144
61X-CC, 0–5	565.5	32075	14	0	2290
62X-1, 0–5	567.5	46718	13	0	3590
63X-CC, 0–5	573.5	9041	6	0	1510
64X-CC, 0–5	583.6	9191	7	0	1310
65X-1, 0–5	586.3	37756	11	0	3430
66X-1, 0–5	592.8	9365	7	0	1338
67X-CC, 0–5	594.4	3190	4	0	798

Characterization of Organic Matter

Organic matter was characterized solely by organic C/N ratios (Fig. 13). Unfortunately, the Rock-Eval malfunctioned during sample analysis at Site 906, and the data obtained from some samples were considered to be unreliable. The organic C/N ratios corroborate the interpretation of the TOC profile, which indicates that marine-derived organic matter controls the TOC content at this site. In the Pleistocene, C/N-ratio values are typically <10 and indicate the predominant contribution of planktonic organisms and bacteria. Values in the upper Miocene are somewhat higher (6 to 13) and indicate a mixture of marine organisms and higher plants. Such low ratios are surprising because terrigenous material is volumetrically abundant within these sediments. Organic C/N ratios show a general decline with depth from a ratio of 12 to 5 in the interval from 153.6 and 383.2 mbsf. This indicates a transition from organic matter of mixed terrestrial and marine components to organic matter composed solely of marine-derived components. This decline also seems to correspond with a decline in TOC and may be caused, at least in part, by inorganic nitrogen held in ammonium associated with clays interfering with the ratio (Müller, 1977). The decline in the organic C/N ratio is unusual and contrary to what is commonly recorded in deep-sea sediments (i.e. organic C/N ratios normally increase with depth because of the preferential loss of more labile compounds during the diagenesis of organic matter.

Table 7. Vacutainer gas composition from sediments at Site 906.

Core, section, interval (cm)	Depth (mbsf)	O_2	N_2	CO_2	C_1	C_2	C_3	C_1/C_2
150-906A-								
15X-3, 11–12	133.2	828	10308	24680	477761	302	0	1582
16X-4, 25–26	144.5	93	1309	43517	604897	360	0	1680
17X-4, 5–6	152.9	567	4876	75265	802203	508	0	1579
18X-1, 10–11	159.1	387	1592	74540	763165	477	0	1600
19X-1, 10–11	168.8	73356	253413	3069	4896	0	0	
20X-2, 60–62	180.4	48668	179038	1173	290	0	0	
21X-6, 0–5	195.5	5119	29123	56080	700769	488	0	1436
22X-5, 10–11	203.7	25773	98909	15112	144323	139	0	1038
23X-2, 15–16	208.9	7	104	85	587	0	0	
26X-3, 50–51	239.5	403	2173	326619	0	0	0	
30X-5, 100–101	281.8	36841	138209	365032	0	0	0	
39X-4, 5–6	366.4	27839	101879	1029	0	0	0	
48X-3, 10–11	451.3	10829	46203	779	0	0	0	
55X-4, 86–87	521.2	713	8319	58513	720171	1071	17	672
55X-5, 60–61	522.4	6	91	199	1813	0	0	
56X-1, 0–2	525.3	6	85	1130	6133	0	0	
57X-1, 80–81	535.6	17249	69596	20584	53870	124	0	434

Note: Volatile gas concentrations given in parts per million (ppm).

INORGANIC GEOCHEMISTRY

The interstitial water trends below the top of the Miocene section at Site 906 are generally similar to those observed at the other slope sites. The Site 906 profiles are different from profiles at the other sites for the section above the top of the Miocene because Site 906 has only 50 m of post-Miocene sediment. For example, the steep chloride gradient occurs below 225 mbsf at Site 903 vs. 30 mbsf at Site 906. Twenty-six interstitial water samples were collected at Site 906 from depths ranging from 1.5 to 539 mbsf. Whole-round core samples were collected from approximately every third core, and half-round samples were collected to provide a sample every 10 m in the uppermost 100 mbsf to better define the pore-water profiles near the sediment/water interface. Analytical results are summarized in Table 9 and Figure 15.

Bacterial degradation of organic matter at this site reduces sulfate from the seawater value of 28 mM to <1 by 32.5 mbsf (Fig. 15). Rapid increases in the byproducts of bacterial sulfate reduction; alkalinity, ammonium, and phosphate occurs down this same interval (Fig. 15). Below 32.5 mbsf, the sulfate concentration remains low and bacterial degradation of organic matter proceeds by methanogenesis. Production of CO_2 causes alkalinity to increase rapidly in the uppermost 100 mbsf to a maximum of 36 mM by 135 mbsf (Fig. 15). Below 136 mbsf, alkalinity decreases gradually to a minimum of 23 mM at 539 mbsf. The alkalinity maximum is associated with an increase in organic-matter content from <0.5 wt% in the uppermost 70 mbsf to values of 1.5–2.5 wt% from 70 to 240 mbsf (see "Organic Geochemistry" section, this chapter). Ammonium shows a local maximum of 5.8 mM at 32.5 mbsf, decreases downward slightly to 5.5 mM, and then increases with depth to an asymptotic value of around 11 to 12 mM (Fig. 15). The maximum phosphate concentration (191 µM) occurs at 23 mbsf (Fig. 15). Phosphate then decreases downward exponentially to trace values at 365 mbsf. The occurrence of the phosphate, alkalinity, and ammonium maxima with increasing sediment depth reflects the preferential metabolism of phosphorus to nitrogen-rich organic matter (Gieskes, 1981).

As observed at the other slope sites, rapid increases in the salinity, chloride, and sodium concentrations occur beneath the top of the Miocene at Site 906. A dramatic drop in pH occurs in this same interval (Fig. 15). The salinity gradient is particularly steep at Site 906 because of the thin (approximately 50 m thick), post-Miocene sedi-

Table 8. Inorganic carbon, organic carbon, and elemental analysis data from sediments at Hole 906A.

Core, section, interval (cm)	Depth (mbsf)	Total carbon (wt%)	Total inorganic carbon (wt%)	Total organic carbon (wt%)	$CaCO_3$ (wt%)	Nitrogen (wt%)	Sulfur (wt%)	C/N	C/S
150-906A-									
1H-4, 77–78	5.27	1.76	0.99	0.77	8.20	0.07	0.31	11	3
2H-3, 77–78	13.27	1.13	0.84	0.29	7.00	0.04	0.45	7	1
3H-3, 78–79	22.28	1.09	0.77	0.32	6.40	0.04	0.21	8	2
4H-2, 67–67	30.17	2.04	1.68	0.36	14.00	0.05	0.13	7	3
5H-3, 60–61	41.10	1.84	1.01	0.83	8.40	0.09	1.59	9	1
6H-3, 69–70	50.69	0.85	0.13	0.72	1.10	0.11	2.71	7	0
7H-1, 72–73	53.72	1.17	0.17	1.00	1.40	0.12	3.35	8	0
8X-3, 70–71	66.20	1.10	0.33	0.77	2.70	0.12	0.28	6	3
9X-3, 77–78	75.77	1.97	0.59	1.38	4.90	0.14	1.13	10	1
10X-3, 77–79	85.67	2.71	0.18	2.53	1.50	0.22	2.08	12	1
11X-3, 78–79	95.28	1.24	0.57	0.67	4.70	0.12	1.43	6	0
12X-5, 75–76	107.89	1.80	0.17	1.63	1.40	0.18	2.47	9	1
13X-5, 67–68	117.47	1.87	0.15	1.72	1.20	0.16	1.92	11	1
14X-5, 42–44	126.92	1.96	0.03	1.93	0.20	0.15	2.17	13	1
15X-3, 82–84	133.92	1.81	0.07	1.74	0.60	0.16	1.72	11	1
16X-3, 45–47	143.15	2.10	0.03	2.07	0.20	0.18	2.93	12	1
17X-4, 78–80	153.63	2.54	0.05	2.49	0.40	0.21	4.36	12	1
18X-3, 77–78	162.77	1.50	0.04	1.46	0.30	0.16	3.25	9	0
19X-3, 83–84	172.53	2.47	0.16	2.31	1.30	0.21	2.59	11	1
20X-3, 78–79	182.08	2.00	0.27	1.73	2.20	0.17	2.16	10	1
21X-3, 60–61	191.60	1.87	0.30	1.57	2.50	0.17	2.23	9	1
22X-3, 44–45	201.04	2.34	0.28	2.06	2.30	0.20	2.87	10	1
23X-4, 59–60	212.29	1.86	0.37	1.49	3.10	0.17	2.30	9	1
24X-3, 78–79	220.58	2.01	0.25	1.76	2.10	0.19	2.08	9	1
25X-3, 79–80	230.29	2.37	0.25	2.12	2.10	0.21	2.48	10	1
26X-2, 62–63	238.12	2.69	0.20	2.49	1.70	0.23	2.60	11	1
27X-2, 90–91	248.10	1.95	0.04	1.91	0.30	0.20	2.80	10	1
28X-3, 87–88	259.17	1.23	0.18	1.05	1.50	0.15	2.72	7	0
29X-3, 76–77	268.86	1.89	0.63	1.26	5.20	0.16	1.04	8	1
30X-3, 75–76	278.55	2.08	0.70	1.38	5.80	0.15	0.94	9	1
31X-3, 83–85	288.43	1.95	0.69	1.26	5.70	0.14	1.18	9	1
32X-3, 80–82	298.20	1.90	0.64	1.26	5.30	0.15	0.12	8	11
33X-3, 105–106	308.25	2.06	0.70	1.36	5.80	0.15	1.09	9	1
33X-5, 58–59	310.78	1.86	0.72	1.14	6.00	0.17	1.98	7	1
34X-3, 73–74	317.73	1.90	0.32	1.58	2.70	0.18	1.98	9	1
35X-3, 72–74	327.52	2.92	1.65	1.27	13.70	0.15	1.05	8	1
36X-3, 86–87	337.06	2.78	1.00	1.78	8.30	0.18	1.18	10	2
37X-3, 84–85	346.34	1.84	0.32	1.52	2.70	0.20	0.55	8	3
38X-3, 76–77	355.96	3.20	1.86	1.34	15.50	0.22	0.59	6	2
39X-3, 74–75	365.54	1.87	0.63	1.24	5.20	0.18	0.55	7	2
40X-1, 17–18	371.67	2.92	1.72	1.20	14.30	0.17	0.50	7	2
41X-2, 72–73	383.32	1.21	0.84	0.37	7.00	0.07	0.25	5	2
45X-1, 72–73	420.02	1.32	0.75	0.57	6.20	0.06	1.22	10	0
46X-3, 79–80	432.59	2.70	0.52	2.18	4.30	0.22	3.26	10	1
47X-3, 82–83	442.42	2.81	0.29	2.52	2.40	0.24	2.89	11	1
48X-3, 68–69	451.88	2.51	0.71	1.80	5.90	0.19	3.01	9	1
49X-4, 76–77	463.16	2.96	0.61	2.35	5.10	0.22	2.88	11	1
50X-5, 76–77	474.26	3.71	0.44	3.27	3.70	0.26	4.40	13	1
51X-3, 83–85	481.03	4.76	2.75	2.01	22.90	0.16	2.26	13	1
52X-3, 73–75	490.53	5.96	3.22	2.74	26.80	0.18	1.82	15	2
53X-3, 72–73	500.22	4.90	2.34	2.56	19.50	0.18	2.23	14	1
54X-3, 80–81	510.00	3.91	1.57	2.34	13.10	0.17	2.37	14	1
55X-3, 78–79	519.58	4.76	2.86	1.90	23.80	0.16	2.21	12	1
56X-3, 74–75	529.04	4.57	2.46	2.11	20.50	0.14	2.19	15	1
57X-3, 74–75	538.54	3.86	1.56	2.30	13.00	0.16	2.54	14	1
58X-3, 56–57	548.06	3.91	1.20	2.71	10.00	0.17	1.89	16	1
59X-1, 39–40	554.59	4.26	1.87	2.39	15.60	0.19	2.97	13	1
60X-1, 48–49	564.28	6.00	5.70	0.30	47.50	0.07	0.33	4	1
61X-CC, 17–18	565.67	5.55	5.09	0.46	42.40	0.08	1.59	6	0
62X-1, 8–9	567.58	6.01	4.60	1.41	38.30	0.06	0.38	24	4

ment cover. The increase in salinity with depth on the slope may be attributable to dissolution of deeply buried salt diapirs (Grow et al., 1988). Salinity initially decreases from 35.5‰ to 34.2‰ by 23 mbsf because of the loss of sulfate, calcium, and magnesium in response to dolomite precipitation in the sulfate-reduction zone (Fig. 10; also see "Inorganic Geochemistry" section in Chapter 8, this volume). Salinity then increases to a maximum of 55.5‰ at 305 mbsf, then decreases to 53.5‰ at 365 mbsf, and then finally increases to 57‰ from 509 to 539 mbsf. The parallel increase in chloride and sodium indicates that the increase in salinity results mainly from diffusion of sodium and chloride ions from below (Fig. 10 in Chapter 8, this volume).

The chloride profile represents the net result of two competing processes: (1) diffusion of Cl ion from a Cl-rich brine below, and (2) the accumulation of sediment above with a Cl concentration of seawater (559 mM). The asymptotic Cl concentration at Site 906 approaches 1000 mM (Fig. 10; also see "Inorganic Geochemistry" section in Chapter 8, this volume) and is somewhat higher than the asymptotic values of around 970 to 990 mM observed at nearby sites. At Site 906, chloride initially increases gradually to 575 mM at 23 mbsf, then increases more rapidly in a series of steplike increases to 788 mM at 106 mbsf (Fig. 10; also see "Inorganic Geochemistry" section in Chapter 8, this volume). Cl increases more gradually to a value of 940 mM at 309 mbsf, then decreases to 929 mM at 422 mbsf, and finally increases gradually to a maximum of 992 mM at 509 mbsf. The steep Cl gradient begins at a depth of 32.5 mbsf within upper Pleistocene lithologic Subunit IA. The inflection in the Cl gradient occurs within a sediment interval that apparently represents the fill of a buried submarine canyon (270–480 mbsf; see "Lithostratigraphy" section, this chapter). The cause of the inverted Cl gradient between 309 and 365 mbsf is uncertain, but similar inversions of the Cl

Table 9. Interstitial water data, Site 906.

Core, section, interval (cm)	Depth (mbsf)	IW (mL)	pH	Alkalinity (mM)	Salinity (‰)	Cl^- (tit) (mM)	Cl^- (chr) (mM)	SO_4^{2-} (mM)	NH_4^+ (mM)	PO_4^{3-} (μM)	SiO_2 (μM)	Sr (μM)	Mn (μM)	Fe (μM)	Na^+ (calc) (mM)	Na^+ (chr) (mM)	K^+ (chr) (mM)	Mg^{2+} (tit) (mM)	Mg^{2+} (chr) (mM)	Ca^{2+} (tit) (mM)	Ca^{2+} (chr) (mM)
150-906A-																					
1H-1, 145–150	1.5	54	7.48	10.909	34.5	563	538	24.01	1.1	72	816	84	3.2	4.4	474	513	12.03	51.94	52.58	9.39	9.27
2H-3, 145–150	14.0	19	7.44	20.313	34.3	573	543	12.18	3.5	116	725	72	1.7	4.3	479	502	12.39	44.72	45.82	5.67	5.61
3H-3, 145–150	23.0	24	7.53	24.055	34.2	575	551	5.60	4.8	191	839	70	1.4	7.9	477	514	12.05	41.63	42.15	4.21	4.13
4H-3, 145–150	32.5	26	7.51	25.367	35.2	606	587	0.61	5.8	164	882	73	2.1	11.0	510	477	12.44	40.42	36.28	3.77	3.41
5H-3, 145–150	42.0	18	7.45	28.178	37.2	629	612	1.23	5.5	67	969	87	3.2	4.8	523	487	11.22	45.62	41.38	4.77	4.38
6H-3, 145–150	51.5	20	7.54	30.920	38.8	663	639	0.82	5.5	84	1003	98	1.4	4.9	558	516	10.71	46.06	40.75	5.77	4.45
7H-3, 145–150	57.5	12	7.40	32.931	39.5	673	661	0.91	6.2	71	980	103	2.8	5.6	563	532	11.36	46.87	41.69	6.83	5.59
8X-3, 145–150	67.0	20	7.56	32.576	40.9	704	699	2.02	6.8	72	930	108	1.9	5.9	575	614	13.66	46.56	48.65	7.35	7.26
9X-3, 145–150	76.5	20	7.37	35.126	43.3	736	727	1.67	7.3	77	1134	122	1.8	8.0	606	643	11.17	48.26	49.43	8.12	7.84
10X-3, 145–150	86.4	14	7.48	33.682	43.8	752	744	1.56	8.1	57	1076	130	2.3	6.8	632	585	11.60	47.55	44.35	8.83	7.68
11X-3, 145–150	96.0	14	7.48	35.126	45.1	780	797	3.71	8.5	45	990	138	2.9	7.9	649	700	11.89	49.60	50.01	9.66	9.29
12X-3, 145–150	105.7	32	7.34	34.948	46.5	788	780	1.19	9.0	45	1177	143	2.7	11.8	653	683	11.76	48.83	49.20	9.41	8.68
15X-3, 145–150	134.6	26	6.73	36.201	49.2	845	849	1.87	9.3	27	1170	172	4.8	13.7	704	722	11.61	49.56	51.70	10.74	10.07
18X-3, 140–150	163.5	37	6.75	35.437	50.9	876	882	1.64	10.6	28	1225	188	3.8	20.7	746	656	13.59	51.34	44.81	11.24	9.41
21X-3, 145–150	192.5	28	6.77	33.068	51.5	899	927	1.19	11.2	9	1172	200	3.8	16.4	756	690	13.91	51.17	48.41	12.23	11.13
24X-3, 145–150	221.3	32	6.75	32.979	52.8	916	919	0.98	11.8	18	1243	219	2.7	19.4	775	691	13.47	51.75	47.07	13.09	11.30
27X-3, 145–150	250.2	17	6.83	31.783	53.5	925	933	1.25	11.7	21	1234	239	2.2	13.7	769	766	12.27	51.54	53.56	14.13	13.97
30X-3, 145–150	279.3	15	6.83	31.535	54.4	940	935	1.25	11.9	13	1188	291	3.0	15.0	787	794	12.41	51.03	50.80	15.88	14.65
33X-3, 140–150	308.7	34	6.73	30.211	55.0	941	949	0.82	11.5	7	1250	327	2.7	36.3	779	776	12.49	49.05	52.06	17.24	17.08
36X-3, 140–150	337.7	32	6.76	29.203	54.2	933	956	1.33	12.1	4	1211	352	2.4	39.9	777	796	12.20	48.78	49.70	15.86	17.05
39X-2, 140–150	364.8	30	6.75	27.623	53.5	929	926	2.20	11.7	0	1177	432	2.6	35.5	772	767	11.95	47.65	49.96	19.27	18.65
45X-2, 140–150	422.3	31	6.62	28.458	55.2	959	988	1.72	11.3	5	1143	501	3.6	83.3	796	809	11.30	47.39	49.48	21.59	21.98
48X-3, 140–150	452.7	22	6.73	26.791	56.0	978	999	1.42	11.1	0	1266	590	3.7	33.0	818	811	11.93	46.33	47.32	23.48	22.06
51X-3, 140–150	481.7	24	6.59	20.541	55.5	976	980	0.99	11.1	11	1287	687	2.5	61.3	814	802	11.41	44.24	46.76	24.12	23.16
54X-2, 140–150	509.2	40	6.57	24.625	57.0	992	963	1.32	11.4	11	1291	769	3.3	148.4	837	729	12.29	45.54	43.07	26.13	22.96
57X-3, 140–150	539.3	44	6.38	23.268	56.7	988	990	1.33	11.0	7	1353	828	3.5	100.5	844	669	12.65	43.60	39.44	22.07	21.09

Note: IW = interstitial water, chr = ion chromatography, and tit = titration.

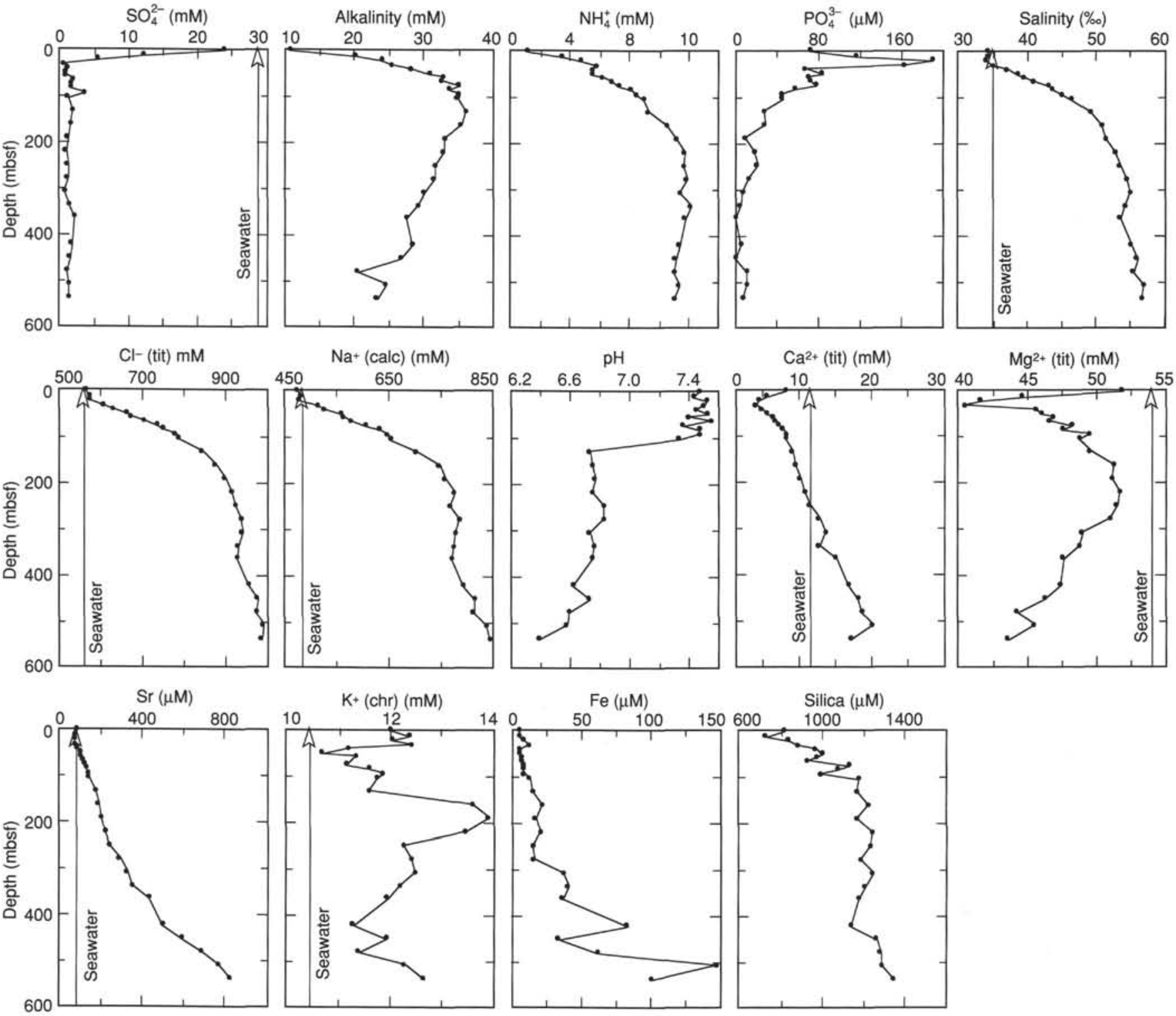

Figure 15. Interstitial-water geochemical data vs. depth, Hole 906A. tit = titration, calc = calculation, chr = chromatography.

gradient were also observed at Sites 902 and 903. The calculated Na profile parallels the Cl trends (Fig. 10; also see "Inorganic Geochemistry" section in Chapter 8, this volume).

A dramatic decrease in pH occurs from 7.48 at 96 mbsf to 6.73 at 135 mbsf (Fig. 10; also see "Inorganic Geochemistry" section in Chapter 8, this volume) and corresponds to an increase in salinity. The top of the sediment in this interval is barren of calcareous fossils (see "Biostratigraphy" section, this chapter). The pH profiles of Site 906 and the other slope sites are generally similar and show a near-surface Pleistocene maximum followed by a gradual decrease to slightly acidic values at depths below the chloride gradient. At Site 906, the pH shows a maximum value of 7.6 at 67 mbsf; pH then decreases to a minimum of 6.4 at 539 mbsf. The relatively high pH values in the uppermost 100 mbsf correspond to low values of Ca, Mg, and Sr, and indicate that carbonate precipitation is occurring at these depths. Dolomite occurs in the uppermost 100 mbsf (see "Lithostratigraphy" section, this chapter).

The increase in alkalinity associated with the degradation of organic matter enhances precipitation of diagenetic carbonates by increasing the degree of supersaturation of the pore waters (Compton, 1988). Precipitation of diagenetic carbonate at depths centered around the base of the sulfate-reduction zone (32.5 mbsf) is indicated by Ca, Sr, and Mg ion minima at 32.5 mbsf (Fig. 15). Ca decreases to 3.8 mM by 32.5 mbsf and then increases rapidly to 9.7 mM at 96 mbsf (Fig. 15). Ca increases more gradually to a maximum of 26.1 mM by 509 mbsf. Sr is similar to Ca, decreasing to a minimum of 70 μM by 23 mbsf, then increasing gradually to 239 μM by 250 mbsf, and then increasing more rapidly to a maximum of 828 μM by 539 mbsf (Fig. 15). The increase in Sr concentrations with depth probably reflects the recrystallization of increasingly abundant biogenic carbonate below 250 mbsf at Site 906 (see "Organic Geochemistry" section, this chapter). Mg decreases to a minimum concentration of 40.4 mM at 32.5 mbsf (Fig. 15). This sharp Mg gradient, combined with the relatively high Mg/Ca ratios, is consistent with dolomite precipitation. Mg increases sporadically to a broad maximum of 51.8 mM centered around 221 mbsf and then decreases to 43.6 mM at 539 mbsf. The sporadic nature of the Mg profile from 58 to 96 mbsf corresponds to the depth interval of steps in the Cl gradient (Fig. 15).

Potassium and iron are important pore-water ions to determine because of the abundance of glauconite (K- and Fe-rich illite), pyrite

(FeS_2), and siderite ($FeCO_3$) in these sediments. Most of the pyrite and siderite is in situ, but the glauconite is probably a mixture of authigenic and reworked shelfal glauconite. In contrast to the other slope sites, the pore-water K minima at Site 906 correspond to sediment intervals of greatest glauconite abundance (see "Lithostratigraphy" section, this chapter). Potassium at Site 906 decreases to 10.7 mM at 52 mbsf, increases to a maximum of 13.9 mM at 193 mbsf, and then decreases to a minimum of 11.3 mM at 422 mbsf (Fig. 15). In contrast to other slope sites, the maximum pore-water K value does not correspond to a glauconite-rich interval. The association of glauconite with lower K concentrations suggests that the glauconite may be a K sink at Site 906. The pore-water K values are higher than the seawater concentration of K and may result from the temperature-of-squeezing effect, an artifact of the sampling procedure that has been observed to cause an increase in K concentration with the higher temperatures attained during squeezing (Waterman, 1973).

The abundant Fe-rich terrigenous material in these sediments provide an ample source of Fe for the formation of diagenetic minerals such as Fe-sulfides, Fe-carbonates, and glauconite. Fe tends to increase with sediment depth (Fig. 15). A minimum Fe concentration of 4 μM occurs at 1.5 mbsf, and Fe remains low (4–11 μM) to 100 mbsf. Fe concentrations increase slightly to a range of 12–21 μM from 106 to 279 mbsf and then increase to a range of 36–40 μM from 309 to 365 mbsf. The highest Fe concentrations occur below 365 mbsf, with values ranging from 33 to 148 μM. These high Fe concentrations are associated with the glauconite interval from 440 to 530 mbsf (see "Lithostratigraphy" section, this chapter). The interval with high pyrite and siderite contents from about 250 to 400 mbsf is associated with decreasing Fe concentrations. Glauconite and pyrite, which occur from 35 to 160 mbsf, are associated with low Fe concentrations. Variations in the Fe concentrations may be related to pyrite, siderite, and glauconite abundance; however, the exact relationship among them is unclear. Dolomite dominates the diagenetic carbonate above 100 mbsf, and siderite tends to dominate below 100 mbsf (see "Lithostratigraphy" section, this chapter). Siderite formation is favored below the sulfate reduction zone because the sulfide sink of Fe is no longer available.

High silica concentrations primarily reflect the abundance of highly soluble opaline (opal-A) silica, which is mostly present as diatoms. Silica increases sporadically from a minimum of 725 μM at 14 mbsf to 1177 μM by 106 mbsf (Fig. 15). Silica concentrations remain fairly constant below 106 mbsf, ranging between 1172 and 1250 μM from 106 to 453 mbsf. Silica then increases to a maximum value of 1353 μM at 539 mbsf.

PHYSICAL PROPERTIES

Sampling Procedures

GRAPE bulk-density and index properties measurements provide the most densely sampled and complete physical properties data set for the definition of units in Site 906 sediments. On average, three to four index properties measurements were made per core, with fewer samples from cores with incomplete recovery.

Compressional-wave velocities were obtained from most Site 906 sediments, except in brittle clays at 30–90 mbsf and from the greater part of a unit rich in unconsolidated sands at 380–420 mbsf. The Digital Sonic Velocimeter (DSV) was used down to Core 150-906A-3H at 28 mbsf. The Hamilton Frame velocimeter was used successfully in sediments from this level to Core 150-906A-11H at 92 mbsf. No compressional-wave velocities were logged on the MST below Core 150-906A-4H at 38 mbsf.

Thermal conductivity was usually measured once every 3 m, except in the uppermost cores that were not thermally equilibrated and in the indurated lowermost cores. Sediments below 545 mbsf became too brittle to insert thermal probes.

The multisensor-track, natural-gamma-ray (MST NGR) emissions were measured every 40 cm on all cores at Site 906. In addition, the emission spectrum of natural gamma rays from whole, sectioned cores was obtained for the first time in ODP/DSDP history on Cores 150-906A-54X through -68X (see Chapter 5, this volume, for details).

GRAPE and Index Properties

Eight major physical properties units distinguished by GRAPE bulk-density and index properties are recognized at Site 906 (Fig. 16). Three of the units are further divided into subunits. Boundaries between adjacent units are placed at the location of the lowermost index properties measurement in the upper unit.

Units I and II

Unit I is characterized by a steep downhole increase in bulk density from 1.52 g/cm^3 near the seafloor to a peak of 1.77 g/cm^3, before declining downhole to 1.61 g/cm^3. This unit is middle Pleistocene to Holocene.

Unit II (10.2–34.8 mbsf; Samples 150-906A-2H-1, 74–76 cm, to -4H-5, 74–76 cm) is also broadly cyclic in nature. It is middle Pleistocene. Bulk density rises abruptly to 1.91 g/cm^3 at the top of Unit II, is variable for much of the unit (ranging from 1.65 to 2.07 g/cm^3, and declines abruptly to 1.62 g/cm^3 at the base.

Unit III

A marked downhole increase in bulk density to 1.96 g/cm^3, with a continued rise to a peak of 2.08 g/cm^3, occurs in the uppermost 10 m of Unit III (34.8–248 mbsf; Samples 150-906A-4H-5, 74–76 cm, to -27X-2, 81–83 cm). Unit III is middle Pleistocene to middle Miocene. Bulk density decreases gently downhole to 1.77 g/cm^3 at the base of Subunit IIIA at 111.5 mbsf (Sample 150-906A-13X-1, 73–75 cm) near the level of reflector m1 (Tuscan; ~106 mbsf; see "Seismic Stratigraphy" section, this chapter). A single peak of 2.4 g/cm^3 occurs at 90.6 mbsf. The top of Subunit IIIB (111.5–155.0 mbsf; Samples 150-906A-13X-1, 73–75 cm, to -17X-5, 63–65 cm) is marked by a sharp rise to a peak of 2.02 g/cm^3. This well-defined peak is about 10 m thick. Bulk density decreases rapidly downhole to 1.83 g/cm^3 beneath the peak and thereafter decreases gradually to around 1.78 g/cm^3 at the base of Subunit IIIB. A thin sand layer, with a bulk-density peak of 2.05 g/cm^3, marks the top of Subunit IIIC (155.0–248.0 mbsf; Samples 150-906A-17X-5, 63–65 cm, to -27X-2, 81–83 cm), probably correlating with reflector m1.5 (orange; see "Seismic Stratigraphy" section, this chapter) and the boundary between lithologic Subunits IVA and IVB (see "Lithostratigraphy" section, this chapter). Bulk density beneath this peak is 1.77 g/cm^3 and rises slightly to 1.8–1.82 g/cm^3 between 190 and 200 mbsf, before falling gradually to 1.63 g/cm^3 at the base of Unit III. The relatively uniform bulk densities in Subunit IIIC may reflect the apparent absence of mass-flow deposits and sand in lithologic Subunit IVB (see "Lithostratigraphy" section, this chapter).

Unit IV

The top of Unit IV (248.0–285.4 mbsf; Samples 150-906A-27X-2, 81–83 cm, to -31X-1, 84–86 cm; middle Miocene) coincides closely with a cemented horizon (bulk density = 2.54 g/cm^3). The unit is middle Miocene. This bed is faintly detected as an unnamed reflector (see "Seismic Stratigraphy" section, this chapter). The remainder of Unit IV is characterized by fairly constant bulk densities between 1.73 and 1.84 g/cm^3. Reflector m2 (Yellow-2) and the base of lithologic Unit IV lie near the base of this unit at 279 mbsf (see "Seismic Stratigraphy" and "Lithostratigraphy" sections, this chapter).

Unit V

Bulk density increases from 1.83 to 1.96 g/cm^3 near the top of Unit V (285.4–378.2 mbsf; Samples 150-906A-31X-1, 84–86 cm, to -40X-

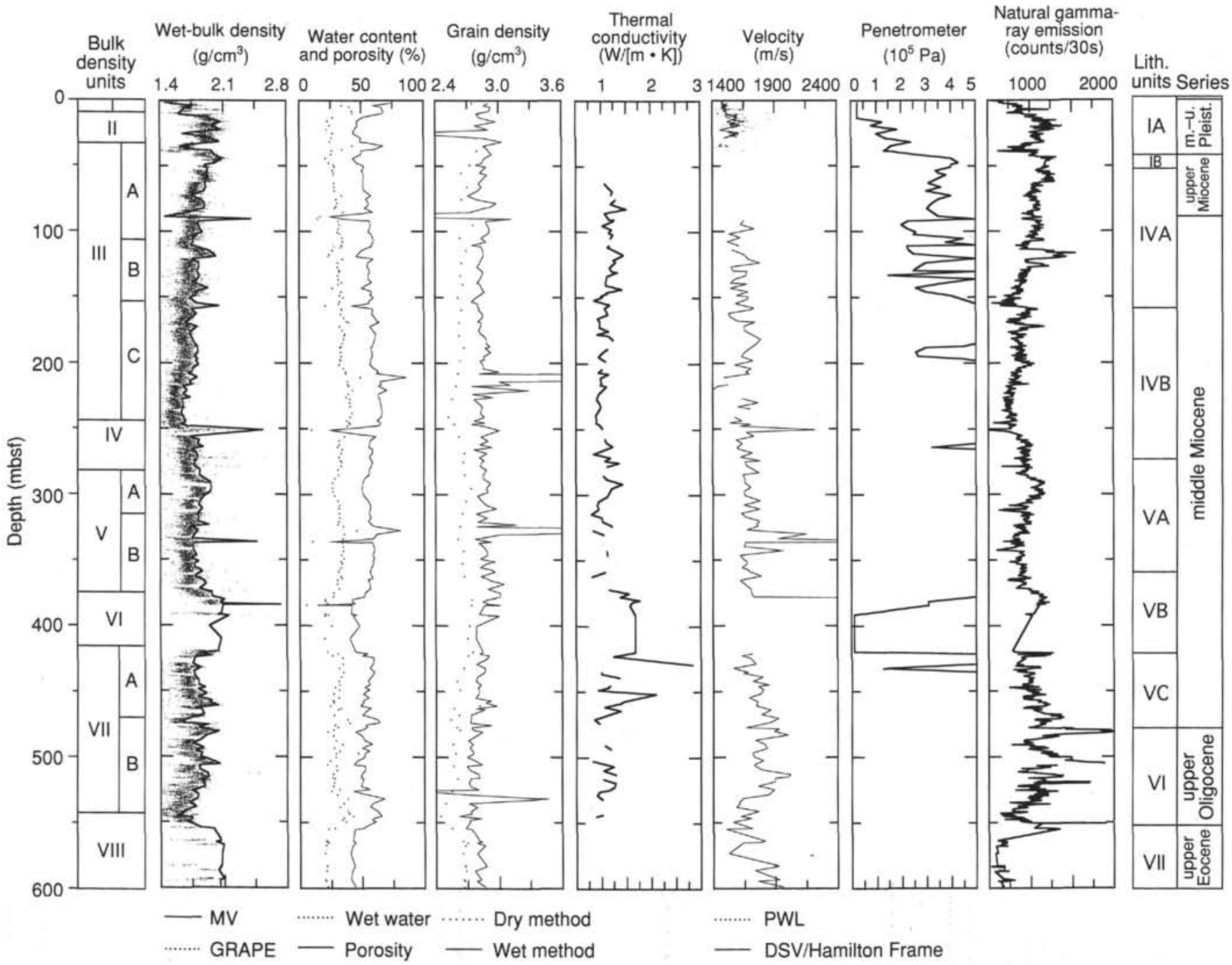

Figure 16. Physical properties results (wet-bulk density, water content and porosity, grain density, thermal conductivity, compressional velocity, penetrometer readings, multisensor-track, and natural-gamma-ray logs), Hole 906A. Compressional-wave measurements above 30 mbsf were made using the digital sound velocimeter (DSV), whereas those below 90 mbsf were made using the Hamilton Frame. MV = mass-volume method. Penetrometer readings exceeding the instrument scale of 4.5×10^5 Pa are plotted at 5×10^5 Pa.

5, 69–71 cm; middle Miocene), then declines gradually to 1.74 g/cm^3 at the base of Subunit VA (285.4–334 mbsf; Samples 150-906A-31X-1, 84–86 cm, to -36X-1, 79–81 cm). This trend reverses in Subunit VB (334–378.2 mbsf; Samples 150-906A-36X-1, 79–81 cm, to -40X-5, 69–71 cm), where density increases gradually from 1.76 to 2.1 g/cm^3 at the base of Unit V. Bulk density increases with depth throughout Subunit VB but more so toward the bottom of the unit. A single peak value of 2.47 g/cm^3 occurs at the boundary between Subunits VA and VB and represents a 50-cm-thick lithified interval in the vicinity of a fault. The top of Unit V corresponds approximately with the top of the fill of the buried canyon drilled at Site 906 (lithologic Unit V; see "Lithostratigraphy" section, this chapter).

Unit VI

Unit VI (378.2–420.0 mbsf; Samples 150-906A-40X-5, 69–71 cm, to -45X-1, 74–76 cm) is characterized by fairly constant, but elevated, bulk densities of 1.94–2.15 g/cm^3. An isolated peak of 2.73 g/cm^3 near the top of the unit is a sample from a cemented sandy layer. Unit VI is a sandy interval (lithologic Subunit VB), particularly in Cores 150-906A-43X and -44X, where recovery was restricted to core catchers that contained uncemented muddy sand. The base of Unit VI corresponds closely with the base of lithologic Subunit VB (see "Lithostratigraphy" section, this chapter). Unit VI is bounded above by seismic reflector canyon-1 and below by seismic reflector canyon-2 (see "Seismic Stratigraphy" section, this chapter).

Unit VII

Bulk density falls abruptly to 1.84 g/cm^3 at the top of Unit VII (420.0–545.3 mbsf; Samples 150-906A-45X-1, 74–76 cm, to -58X-1, 82–84 cm; middle Miocene to upper Oligocene), then rises gently downhole in Subunit VIIA (420.0–474.3 mbsf; Samples 150-906A-45X-1, 74–76 cm, to -50X-5, 78–80 cm) to a peak of 2.03 g/cm^3 at 461.1 mbsf (Sample 150-906A-49X-3, 15–17 cm). Bulk density subsequently decreases rapidly downhole to a low of 1.64 g/cm^3 at the base of Subunit VIIA. A rapid increase to 1.92 g/cm^3 marks the top of Subunit VIIB (474.3–545.3 mbsf; Samples 150-906A-50X-5, 78–80 cm, to -58X-1, 82–84 cm), rising to a peak of 2.04 g/cm^3 just below the top of the subunit. The upper part of Subunit VIIB contains significant fluctuations in bulk density, including a second peak of 2.05 g/cm^3 at 506 mbsf (Sample 150-906A-53X-5, 75–77 cm). Bulk density then declines gently to a low of 1.58 g/cm^3 in a trough at the base of Subunit VIIB. The boundary between Subunits VIIA and VIIB corresponds approximately to the top of lithologic Unit VI and to a major disconformity at the base of the buried canyon (see "Lithostratigraphy" section, this chapter). It also corresponds with seismic reflector m6 (pink-3; see "Seismic Stratigraphy" section, this chapter).

Unit VIII

An abrupt rise in bulk density to 1.98 g/cm^3 occurs just below the top of Unit VIII (545.3 mbsf to total depth; Sample 150-906A-58X-1, 82–84 cm, to Section 150-906A-68X-CC), corresponding approximately with the top of lithologic Unit VII (Eocene chalk). Bulk densities remain fairly constant between 2.0 and 2.1 g/cm^3 throughout the remainder of Unit VIII. The top of this unit coincides approximately with seismic reflector o1 (green-2) (see "Seismic Stratigraphy" section, this chapter).

Porosity and wet water content trends are the inverse of bulk-density trends, suggesting that bulk densities are controlled primarily by porosity (Fig. 16). Average calculated wet water contents are 20%–40%. Porosity values are greater by about 20%–30% and mimic the trend of wet water contents.

Grain densities calculated by the wet volume method (see Chapter 3, this volume; Fig. 16) show an overall tendency to decrease slightly toward the bottom of the hole from an average of 2.9 g/cm^3 to one of 2.8 g/cm^3. Grain densities calculated directly using the dry volume method are generally between 0.1 and 0.2 g/cm^3 less than those calculated using the "wet volume method," the difference being greatest at intermediate depths (150–400 mbsf). Trends in grain density do not appear closely related to those in bulk density. The peak at 210.9 mbsf corresponds to a yellow, probably sideritic, diagenetic layer.

As noted above, many bulk-density unit boundaries correspond approximately to lithostratigraphic units defined at Site 906 (see "Lithostratigraphy" section, this chapter). Lithostratigraphic unit boundaries IA/IB, IVA/IVB, IV/V, VB/VC, V/VI, and VI/VII are at similar depths to bulk-density unit boundaries II/III, IIIB/IIIC, IV/V, VI/VII, VIIA/VIIB, and VII/VIII, respectively.

Compressional-wave Velocity

Velocity values measured using the DSV average 1513 m/s in Unit I (Fig. 16). At the top of Unit II, velocity increases to almost 1600 m/s. Velocities then increase gently to 1800 m/s in Units III through V over the range from 90 to 380 mbsf. A velocity spike of 2200 m/s at 252 mbsf, in a siderite- and calcite-cemented bed, occurs at the top of Unit IV; a double spike reaching 2830 m/s around 335 mbsf corresponds to a strongly cemented zone at the boundary of Subunits VA and VB. The highest velocity recorded in Hole 906A, 4100 m/s, was obtained from a cemented bed in a sand-rich zone near the top of Unit VI, in Core 150-906A-41X at 380 mbsf, approximately correlative with reflector canyon-1 (see "Seismic Stratigraphy" section, this chapter). Velocity values increase from 1650 m/s at 420 mbsf, reach a maximum value of 2000 m/s at about 500 mbsf, and gradually decrease to about 1650 m/s at 530–575 mbsf. This crudely cyclic trend parallels similar patterns in the bulk densities and in the MST NGR emission data in Subunits VIIA, VIIB, and the upper part of Unit VIII. Velocities again increase within Unit VIII (Eocene chalk) to 1950 m/s at 599 mbsf, the deepest measurement made at this site.

Thermal Conductivity

Thermal conductivity decreases slightly downhole from around 1.25 W/(m · K) at 60 mbsf to around 0.4 W/(m · K) at 240 mbsf, and increases again to 1.4 W/(m · K) at 290 mbsf (Fig. 16). High values of 1.75 W/(m · K) characterize a sand-rich interval at 380–420 mbsf. After peaks of 2.4 W/(m · K) at 430 mbsf and of 2.2 W/(m · K) at 450 mbsf, values remain at around 0.6 W/(m · K) until 545 mbsf.

Penetrometer

Three penetrometer readings were made per core. Values increase rapidly downhole through Units I and II and Subunit IIIA (Fig. 16). Beginning in Subunit IIIB and continuing to total depth, cores became too indurated (>4.5×10^5 Pa) for penetrometer evaluation, except in the sandy interval (Unit VI).

Natural-gamma-ray Emissions

Variations in relative MST NGR counts confirm the choice of bulk-density units chosen for Site 906. Large NGR shifts at 38, 115, 154, 250, 285, 370, 478, and 560 mbsf all correspond closely to unit and subunit boundaries defined from bulk-density data (Fig. 16). Additional shifts at 310 and 500 mbsf are not coincident with bulk-density unit boundaries but reflect variations in biogenic, terrigenous, and hemipelagic sediment contributions (see "Lithostratigraphy" section, this chapter).

DOWNHOLE LOGGING

Introduction

Below we describe the acquisition and preliminary interpretations of log data completed at sea. Additional processing and display were conducted onshore by the Borehole Research Group, and the results are presented at the end of this chapter and on the CD-ROM disk in the back pocket of this volume. FMS data are found only on the CD-ROM disk.

Four logging runs were made at Hole 906A using the sonic-induction, porosity, FMS, and geochemical tool strings (see Chapter 3, this volume, for a description of the tools). The hole was drilled to a total depth of 602.4 mbsf, and a wiper trip was made to the bottom of the hole. Experience from previous sites showed that the side-entry sub (SES) greatly increased the probability of acquiring good quality logs, and the SES was therefore used on all runs. Table 10 summarizes the logging tools and logging parameters in Hole 906A.

The drill pipe and the sonic-induction tool string were lowered to a total depth of 582 mbsf. The logging run continued up across mud line, as can be seen on the gamma-ray curve in Figure 17, to correlate log depths with depths recorded during drilling operations.

The second run with the porosity tool string also started from a total depth of 582 mbsf, as no material had accumulated in the bottom of the hole during the first run. Logging continued up to 85 mbsf. A repeat run was performed from 211 mbsf.

The FMS (third logging run) was run from the bottom of the hole to the base of the pipe, even though the readings from the upper part were affected by hole enlargement. Fill had accumulated in the bottom of the hole, so the entire run spanned 577 to 119 mbsf. A second pass with the FMS was planned, but cable damage was sustained when trying to reenter the drill pipe at the end of the first pass. The tool string was brought back to the surface, and the cable repaired before the fourth logging run.

For the fourth and final run, the geochemical tool string was used for the first time on Leg 150. This tool was run with the older logging system (see "Downhole Logging" section, Chapter 3, this volume), and logging speed was much lower than for the other tool strings. The geochemical log was run from 561 up to 144 mbsf, with a repeat run in the upper part.

Log Quality

The logging heave compensator was used during all the runs in Hole 906A. After each run, only a few meters of the borehole were lost because of fill in the bottom of the hole (see Table 10).

Hole conditions were very good, as can be seen on the caliper curve in Figure 17. Use of the SES from the inception of logging contributed to the good hole conditions by enabling the tool string to go to the bottom of the hole directly without flushing and unnecessary movements of the logging string in attempts to pass tight spots. Only one major tight spot was present in Hole 906A, between 460 and 469 mbsf. Because of these good hole conditions, logging data are generally of high quality and are degraded because of hole enlargement in only a few intervals. The response of the geochemical tool string is particularly sensitive to changes in logging speed. As there were essentially no tight spots in Hole 906A, it was possible to keep logging speeds constant and produce good quality geochemical data.

Depth Shifting

The various logs correlate well and several distinct peak values have been used for depth shifting. A gamma-ray log was recorded on every run and was also used for depth shifting. All logs displayed are in adjusted depth (Fig. 17).

Logging Results

Major changes in the character of the log curves have been used to define 4 log units. Within the units, smaller variations occur. Hole deviation increases from less than 1.5° at 119 mbsf to ~9° at 577 mbsf.

Log Unit 1 (base of pipe [100 mbsf] to 384 mbsf)

Log Unit 1 is characterized by a small decrease in gamma radiation with depth. The gamma-ray values in the lower part of the unit vary around 50 API units. Several thin (10–40 m) upward-fining sequences may be indicated by the gamma-ray curve. All other log values in this unit are fairly constant. A minor decrease in resistivity occurs with depth, however, starting from ~1 Ωm just below the drill pipe to 0.7 Ωm at the lowest part of the unit. Velocity varies around 1700 m/s, increasing slightly with depth, and porosity readings fluctuate around 55%.

At 252 and 254 mbsf, two distinct layers produce readings that differ from surrounding values. The layers have much higher density and velocity and lower porosity and are also revealed on the gamma-ray and resistivity logs. Below these layers, velocity increases with depth to around 1800 m/s. Fluctuation in the density log between 260 and 305 mbsf may be caused by hole enlargement, but also may be related to the top of the buried canyon fill (top of lithologic Unit V, 279 mbsf; see "Lithostratigraphy" section, this chapter).

Table 10. Total drilling depth, SES, tool configuration, logging interval, and logging speed at Hole 906A.

Total depth (mbsf)	SES	Tools (string and combination)	Logging interval (mbsf)	Logging speed (m/hr)
585	Yes	Sonic-induction tool string NGT/SDT/MCD/DIT/LDEO temperature	−35 to 585	275
582	Yes	Porosity tool string NGT/CNT/HLDT/LDEO temperature	85 to 582	275
577	Yes	Formation MicroScanner tool string NGT/MEST/LDEO temperature	119 to 577	275
561	Yes	Geochemical tool string NGT/AACT/GST	144 to 561	153

Note: SES = side-entry sub.

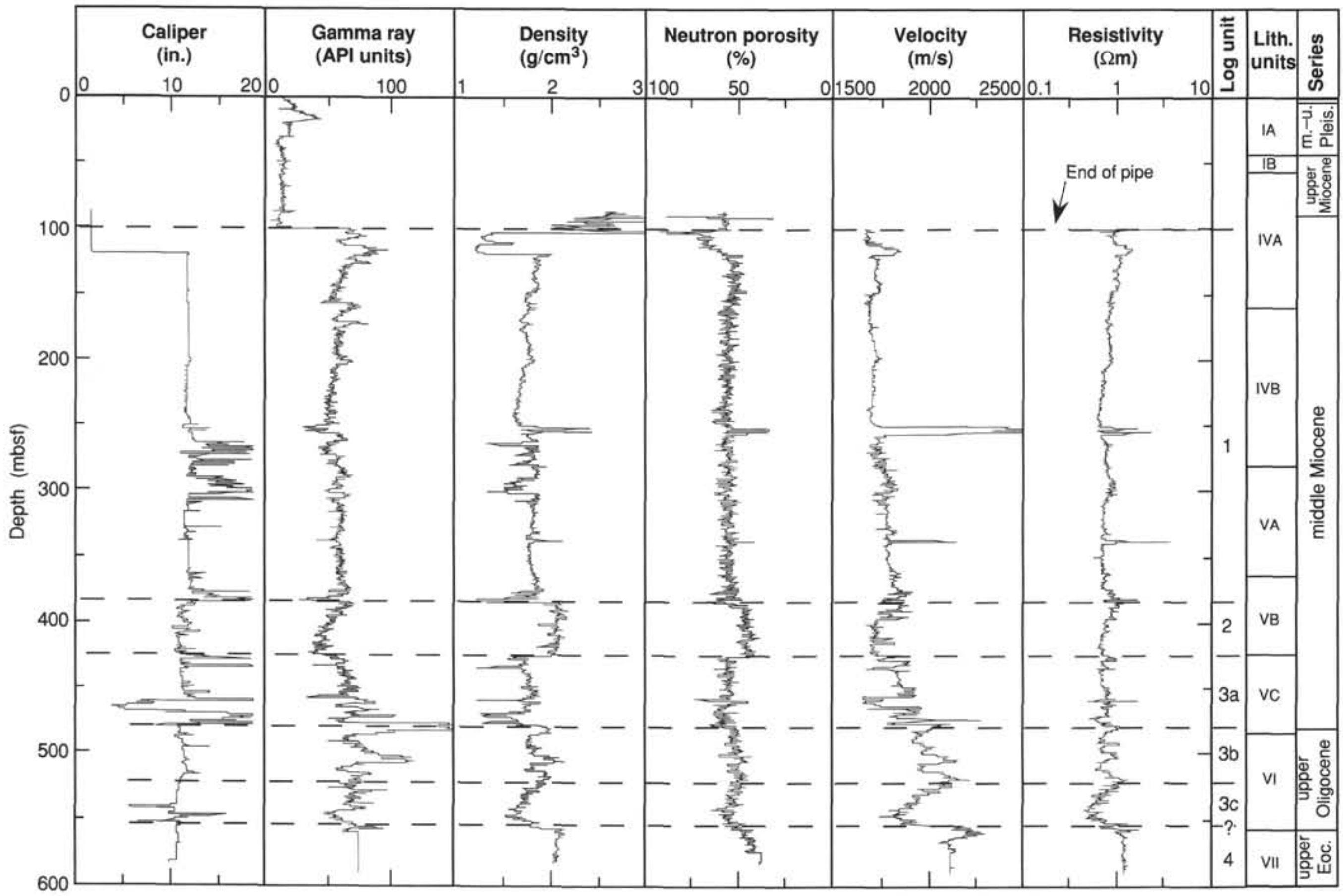

Figure 17. Logging units based on observations of density, caliper, gamma-ray, neutron porosity, sonic velocity, and deep resistivity logs run in Hole 906A.

Log Unit 2 (384–425 mbsf)

Density in log Unit 2 is higher than in log Unit 1, with a mean reading of 2.07 g/cm^3. This unit corresponds to an interval of poor recovery in lithologic Subunit VB. Porosity also decreases to values around 46%. Velocity is almost constant at 1700 m/s, corresponding to the lower part of log Unit 1. The natural-gamma-ray curve shows a decrease with depth. Log Unit 2 corresponds to lithologic Subunit VB and bulk-density Unit VI and represents a sandy interval where recovery was poor. The gamma-ray log suggests that the sediment of log Unit 2 fines upward.

Log Unit 3 (425–561 mbsf [556 mbsf])

It is difficult to define the lower boundary of log Unit 3 exactly because indications differ among the various log curves. The FMS and the natural-gamma-ray curve indicate that the boundary is at 561 mbsf. The resistivity, density, and porosity curves, on the other hand, indicate a change around 556 mbsf. This depth range spans an interval of no core recovery. Siliciclastic sediments of lithologic Unit VI were found above 555 mbsf; carbonates of lithologic Unit VII were found below 564 mbsf.

Log values vary much more in log Unit 3 than in the other log units, and three subunits are recognized.

Log Subunit 3A, between 425 and 478.5 mbsf, is characterized by increasing gamma-ray and velocity values. The respective values at the base of log Subunit 3A are ~75 API and ~2050 m/s. The density, porosity, and resistivity readings are similar to those of log Unit 1 (1.75 g/cm^3, 57%, and 0.7–0.8 Ωm, respectively). The base of log Subunit 3A corresponds with the base of lithologic Unit V and the base of the buried canyon.

Log Subunit 3B, between 478.5 and ~520 mbsf, exhibits velocities of ~2100 m/s. Resistivity and porosity are fairly constant. The upper 5 m of the subunit, between 478.5 and 483 mbsf, contains a peak in the natural-gamma-ray curve caused by high uranium content, as revealed by the geochemical log (see below). The layers with high uranium content can also be seen on the density curve as an increase to 1.99 g/cm^3 above the surrounding values of 1.75 g/cm^3.

In log Subunit 3C, between ~520 and 561 mbsf, velocity, density, and resistivity decrease. In the same interval, a small porosity increase occurs.

Log Unit 4 (561–582 mbsf)

Only the upper part of log Unit 4 (below 561 mbsf) can be seen on all log curves, so it cannot be fully characterized. Abrupt changes in density, neutron porosity, velocity, and resistivity occur at the top of log Unit 4. The unit is recognized by downward decreasing porosity and increasing density. Neutron porosity decreases to a mean value of 43%, whereas the mean density reading is 2.05 g/cm^3. Resistivity remains nearly constant at 1.2 Ωm. Velocities are higher than in log Unit 3 (2100–2300 m/s), but variable. The natural-gamma-ray curve includes only the uppermost few meters of log Unit 4. Log Unit 4 correlates with the Eocene chalk of lithologic Unit VII.

Log-core Correlation

A comparison between laboratory and log measurements of natural-gamma-ray values was also made (Fig. 18; see also Chapter 5, this volume). Laboratory natural-gamma-ray values were measured on cores every 40 cm (see also "Physical Properties" section, this chapter). Correlation between laboratory and log measurements is excellent, even though the units of measurement differ.

Downhole Temperature Measurements

The sonic-induction tool string was run twice, but because of a failure in telemetry, only temperature data were recorded on the first trip. Temperatures were recorded again on the second (successful) run of the sonic-induction tool string. The labels on the temperature profiles in Figure 19 refer to these two runs.

The profiles shown in the figure do not accurately reflect the thermal regime at the site, because they are disturbed by the operations preceding logging and by fluid circulation. Nevertheless, the two curves illustrate a tendency of the borehole to return to thermal equilibrium and to a higher thermal gradient between the two runs, even though the time elapsed between the runs did not exceed a couple of hours.

The different "anomalies" in the profiles are the result of fluid circulation as well as exits/entries of the temperature tool at the bit; thus, they cannot be linked to changes in the properties of the surrounding formation. These data will be processed to obtain more realistic temperature profiles, but the trend of the recorded data provides a minimum estimate of 28°C/km for the thermal gradient.

Synthetic Seismogram

The excellent hole conditions yielded very reliable density and sonic logs, which made it possible to produce a satisfactory synthetic seismogram (Fig. 20).

Reflector m2 (Yellow-2), at 330 ms or 280 mbsf, is the transition between lithologic Units IV and V, whereas m6 (pink-3), at 540 ms or 478 mbsf, corresponds to the boundary between lithologic Units V and VI, and o1 (green-2), at 620 ms or 563 mbsf, correlates with the boundary between lithologic Units VI and VII. Some reflectors also correlate with boundaries between lithologic subunits, e.g., m1.5 (orange), at 190 ms or 160 mbsf, between lithologic Subunits IVA and IVB and the second buried canyon reflector (canyon-2, at 485 ms or 421 mbsf), between lithologic Subunits VB and VC. Note that the traveltime/depth conversions in Figure 20 are slightly different from those presented in the "Seismic Stratigraphy" section, this chapter.

Some other important kicks in acoustic impedance were not labeled as seismic reflectors' and correspond to local features. At ~250 mbsf or 300 ms, a very sharp contrast is produced by two calcite- and siderite-cemented beds (see "Lithostratigraphy" section, this chapter), and at 336 mbsf, or 380 ms, the small kick in acoustic impedance is the signature of a clastic dike (see "Lithostratigraphy" section, this chapter).

Geochemical Tool String

Results of geochemical logging are summarized in Figures 21 and 22. See Chapter 3 (this volume) for a description of the processing of geochemical logging data. A marked increase in uranium content creates a gamma-ray peak at 478 mbsf, just beneath the base of the buried valley at the boundary between log Subunits 3A and 3B (boundary between lithologic Subunit VC and Unit VI). Additional uranium peaks characterize the section below this.

SEISMIC STRATIGRAPHY

Introduction

Numerous buried canyons have been observed in profiles across the New Jersey continental slope (e.g., Poag and Mountain, 1987; Mountain, 1987; Mountain and Miller, 1991). Details concerning how and when they were formed, maintained, and eventually filled have been a matter of speculation due to uncertain ties to the sparsely available wells or outcrop data. One especially broad and deeply incised example, buried several hundred ms beneath the modern Berkeley Canyon, was recognized in seismic data examined before Leg 150. Site 902 was located 3.5 km S of this scar in an "interfluve" region; Site 906 is centered above the axis of this buried feature (Fig. 2), and in conjunction with Site 902 provides an excellent opportunity to examine its evolution.

Cruise Ew9009 Line 1027 crossed but did not provide adequate 3-D control of this buried feature (Fig. 1); hence a third survey was

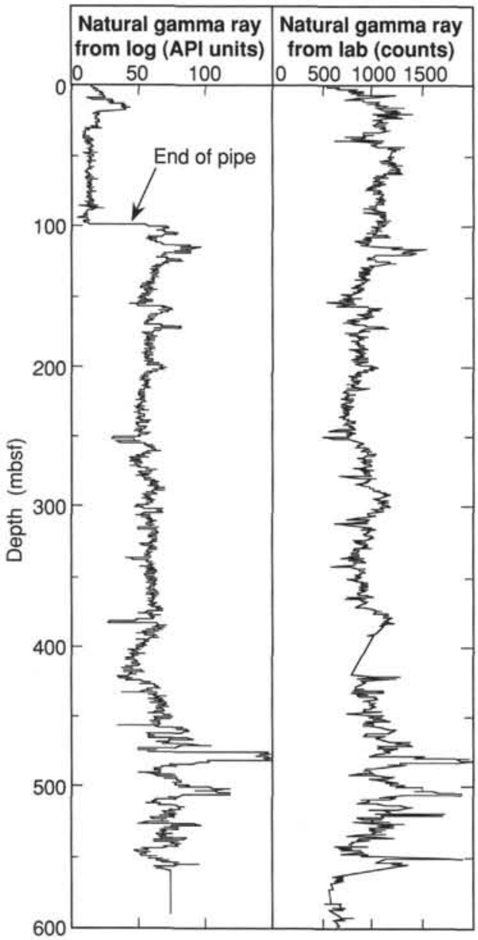

Figure 18. Correlation between gamma-ray values from wireline logs and those from laboratory measurements on cores.

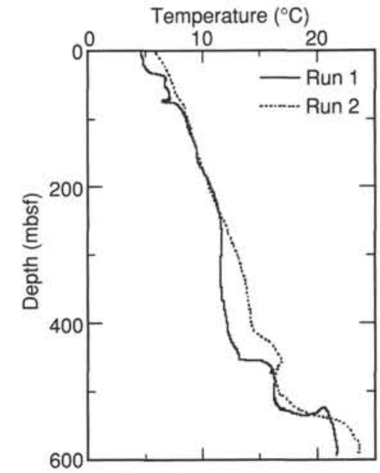

Figure 19. Temperature profiles from Hole 906A based on Lamont-Doherty temperature tool.

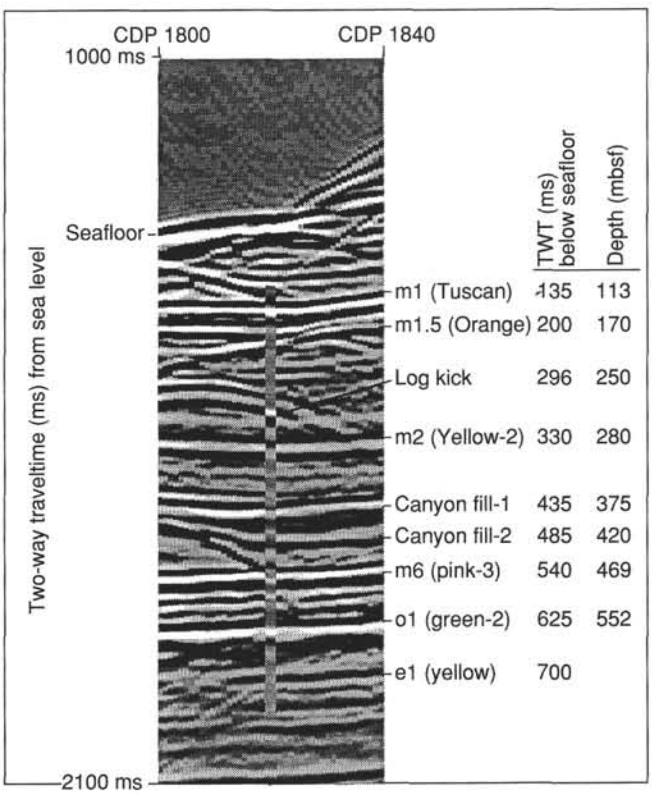

Figure 20. Synthetic seismogram from logging data for Hole 906A inserted between CDP 1800 and 1840 on Ew9009 MCS Line 1027.

conducted by Leg 150 to constrain its boundaries (see Fig. 3 in Chapter 4, this volume). There were two goals to this survey: 1) to locate precisely the thalweg of both the modern Berkeley Canyon and that of the buried target; and 2) to reveal the morphology of this buried feature. Achieving the first goal determined the optimal site location that would minimize post-middle Miocene overburden yet ensure that we would drill into the oldest fill within this buried canyon. Achieving the second goal showed that the buried target was considerably broader and more flat-floored than canyons found on the modern slope, and suggested that this ancient feature had a unique origin and/or that canyon morphology is significantly re-shaped during the in-filling stage.

Reflector Correlations

Several reflectors correlated to Miocene and older strata at Sites 902, 903, and 904 can be traced to Site 906 (Table 11). However, due to erosion by the modern Berkeley Canyon and by the buried Miocene canyon at this site, several reflectors and their corresponding strata documented at the other Leg 150 slope sites are missing. Furthermore, the sediment now filling the buried Miocene canyon at Site 906 is distinct from correlative sediment at the adjacent sites (see "Lithostratigraphy" section, this chapter) and, not surprisingly, has a unique and strictly local seismic character that we describe below.

The floor of the modern Berkeley Canyon at this location on the slope has eroded to roughly the level of reflector m0.7 (blue; Fig. 2), and therefore there is little in situ record of post lower upper Miocene deposition at Site 906. The shallowest reflector crossing the site can be resolved at about 55 to 60 ms sub-bottom, and it dips toward the southwest wall of Berkeley Canyon, reaching a maximum of 100 ms sub-bottom (see Fig. 9 in Chapter 4, this volume). This geometry and the likely correlation to between 40 and 50 mbsf confirms it matches the base of displaced debris flows and slump deposits comprising Pleistocene canyon fill in Cores 150-906-1H to -5H (lithologic Subunit IA; see "Lithostratigraphy", this chapter.) Although logged through the pipe, gamma-ray measurements (Fig. 17) show several peaks in the upper 20 m, corresponding to the matrix-supported debris flows in this upper half of Subunit 1A; gamma-ray values between 20 mbsf and the bottom of the pipe at 100 mbsf remain much more uniform, consistent with the more homogenous character of these sediments.

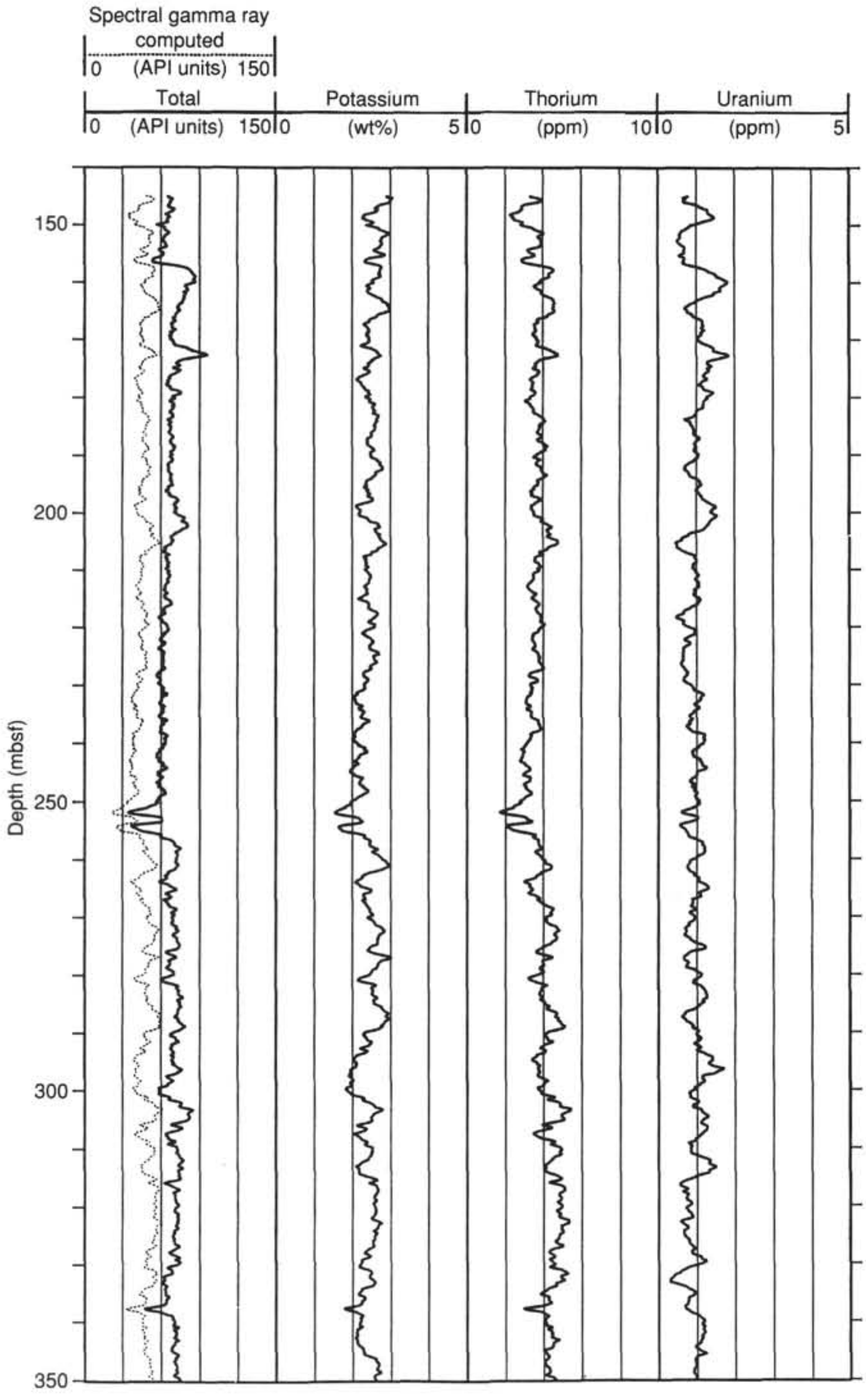

Figure 21. Processed natural-gamma-ray data from Hole 906A.

Reflector m1.5 (orange) lies at 200 ms at Site 906 and approximates the *R. barboi/C. yabei* Zonal boundary. We correlate reflector m1.5 to the laminated quartz sand with plant fragments that comprise the basal 15 m of lithologic Subunit IVA (Fig. 11). This reflector can be traced a few hundred meters south (Fig. 2) to the hyperbolic "bow-tie" artifact at 250 ms, indicating that reflector m1.5 marks the wall of a sharply incised, very narrow canyon. Accordingly, we drilled the edge of this feature at Site 906, as can be seen in numerous crossings of the pre-site Leg 150 SCS survey (see Fig. 9 in Chapter 4, this volume).

The top of another interval of glauconitic sandy silt at Site 906 begins at 111 mbsf (Core 150-906-13X), and is correlated with reflector m1 (Tuscan) at 140 ms. This is expressed in the gamma-ray log as a sharp low as expected in less clay-rich units, and we match the reflector to the base of the coincident velocity increase (Fig. 11).

Laminated quartz sand with plant fragments comprise the basal 15 m of lithologic Subunit IVA, and the IVA/IVB contact at 157 mbsf corresponds to reflector m1.5 (orange; Fig. 11). This surface is at 200 ms at Site 906, and can be traced a few hundred meters south (Fig. 2) to the hyperbolic "bow-tie" artifact at 250 ms, indicating that m1.5 marks the wall of a sharply incised canyon. Site 906, accordingly, drilled the edge of this feature as can be seen in numerous crossings of the pre-site Leg 150 SCS survey (see Fig. 9 in Chapter 4, this volume).

The seismic section is relatively featureless down to the next (unnamed) reflector at 310 ms (250 mbsf using an average velocity

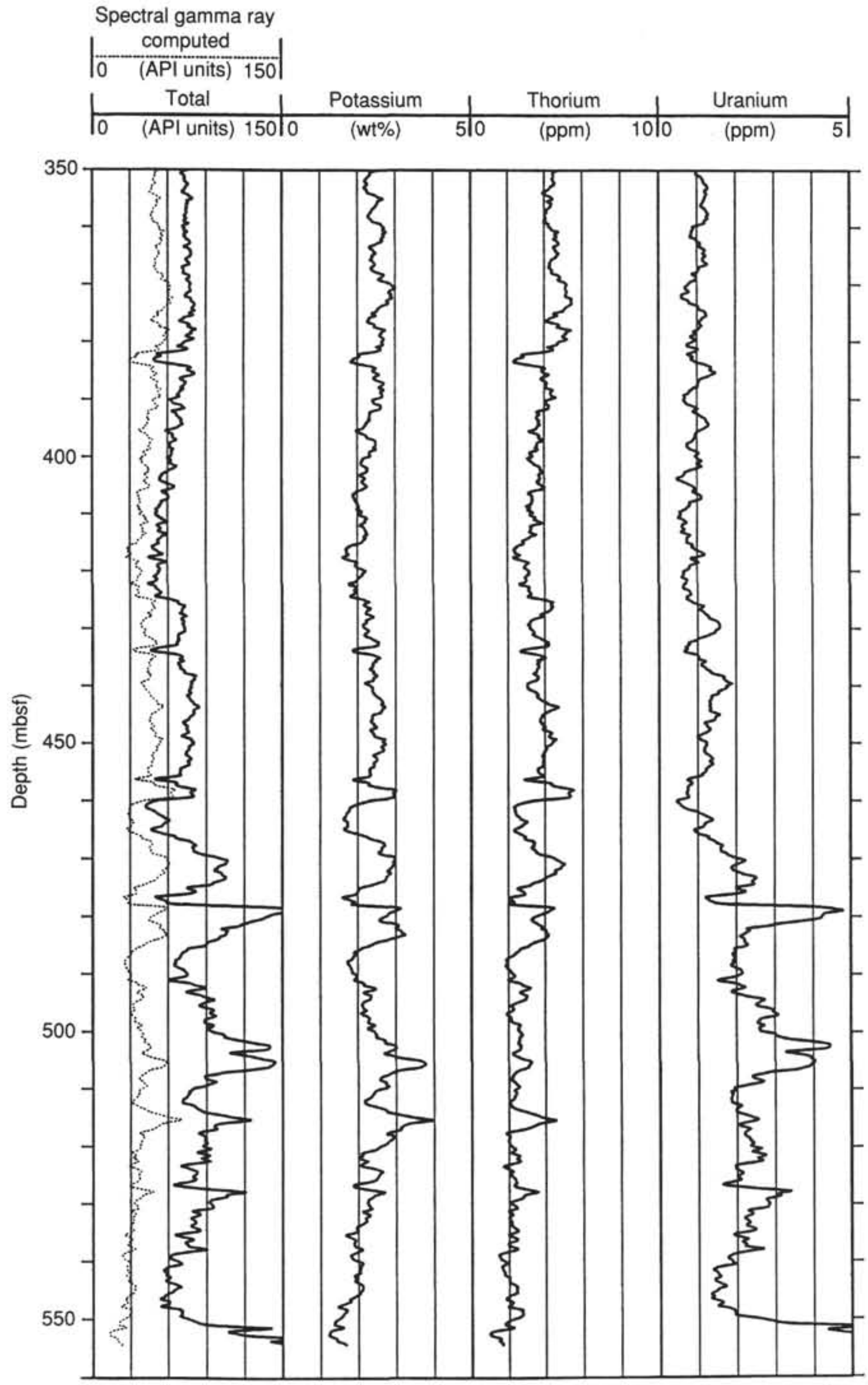

Figure 21 (continued).

of 1613 m/s). The gamma-ray log suggests upward-fining sequences terminate at 120, 157, 175 and 200 mbsf (Fig. 17), although only the second of these (correlating with m1.5 as described) has both seismic and lithologic expression. No other log signatures show dramatic changes throughout this interval (Fig. 11). This uniformity in all but the gamma-ray log agrees with the interpretation that the section immediately beneath m1.5 corresponds to an open slope setting adjacent to, but not within, a formerly active canyon; pre-m1.5 sediments at Site 906 are pelagic and fine-grained deposits that we interpret occasionally spilled out of this adjacent canyon.

The unnamed reflector at 310 ms corresponds with a dramatically sharp and thin increase in log density and velocity caused by a 1-m siderite-calcite bed at 251 mbsf (Fig. 11). This reflector is the youngest surface tracing a remnant of the buried slope canyon that is the primary target of Site 906. It onlaps the wall of this canyon south of the drill site, and outside of this canyon cannot be distinguished seismically from the underlying m2 (Yellow-2) reflector, and no equivalent cemented bed was detected at Site 902.

The high-amplitude reflector m2 (Yellow-2) at 340 ms corresponds with the base of lithologic Subunit IVB at 279 mbsf (Fig. 11). Its log expression is ironically subtle. More impressive are the density and gamma-ray variations in the 20 m above this reflector, corresponding to a significant downhole increase in pyrite and siderite nodules. Perhaps the composite acoustic effect of these nodules cre-

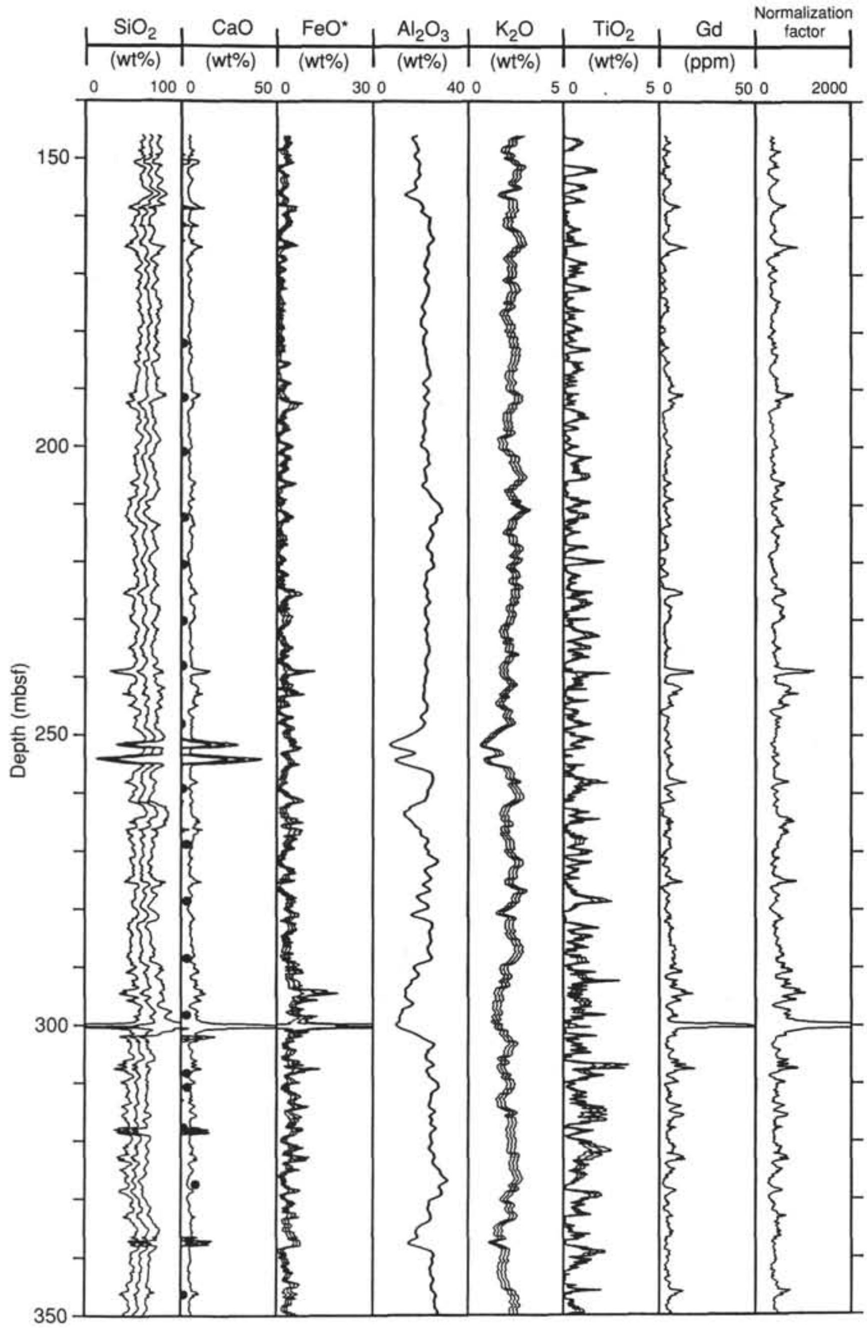

Figure 22. Estimates of major oxide-weight fractions from geochemical logs, Hole 906A. Solid circles represent shipboard carbonate measurements on core material, converted to CaO for comparison to GST-derived CaO. The oxide closure model normalization factor (F) is displayed to the right of the logs. A lower normalization factor represents better counting statistics and therefore higher quality data.

ates the high amplitude of m2 (Yellow-2). This surface traces the target canyon at a time when it had roughly 30 m of topographic relief.

The 100 ms of section (~100 m) beneath m2 (Yellow-2) is seismically nonreflective. It represents late-stage canyon fill composed of thin-bedded silty clays (lithologic Subunit VA). Despite this seismically uniform character, a sharp log density increase is detected at 300 mbsf, corresponding with the top of an especially well-laminated and rarely bioturbated silty clay interval within lithologic Subunit VA. A spike in all log signatures similar to that at 251 mbsf occurs at 337 mbsf and marks another siderite-calcite bed. It lies immediately beneath a fault that cuts across core 906-36X-2. However, its log signature is fairly thin and it has no apparent seismic expression (Figs. 11 and 17).

Two local reflectors (canyon-1 and canyon-2) mark a phase of active canyon cutting and rapid infilling. Lithologic Subunit VB begins at 362 mbsf, and is characterized by sand beds that increase downward in both frequency and thickness. It very likely marks the time of rapid filling of the slope canyon by shallow-water turbidites. The log expression of this change is not apparent until 380 mbsf, however, when a few meters of downward coarsening sands are indicated by the gamma-ray log (Fig. 17). The top of log Unit 2 begins at 384 mbsf with an abrupt change in all log parameters, followed by a clear coarsening downward trend that continues until 421 mbsf. We match the abrupt density increase at 384 mbsf to the locally defined reflector "canyon-1". The equally abrupt density decrease at 421

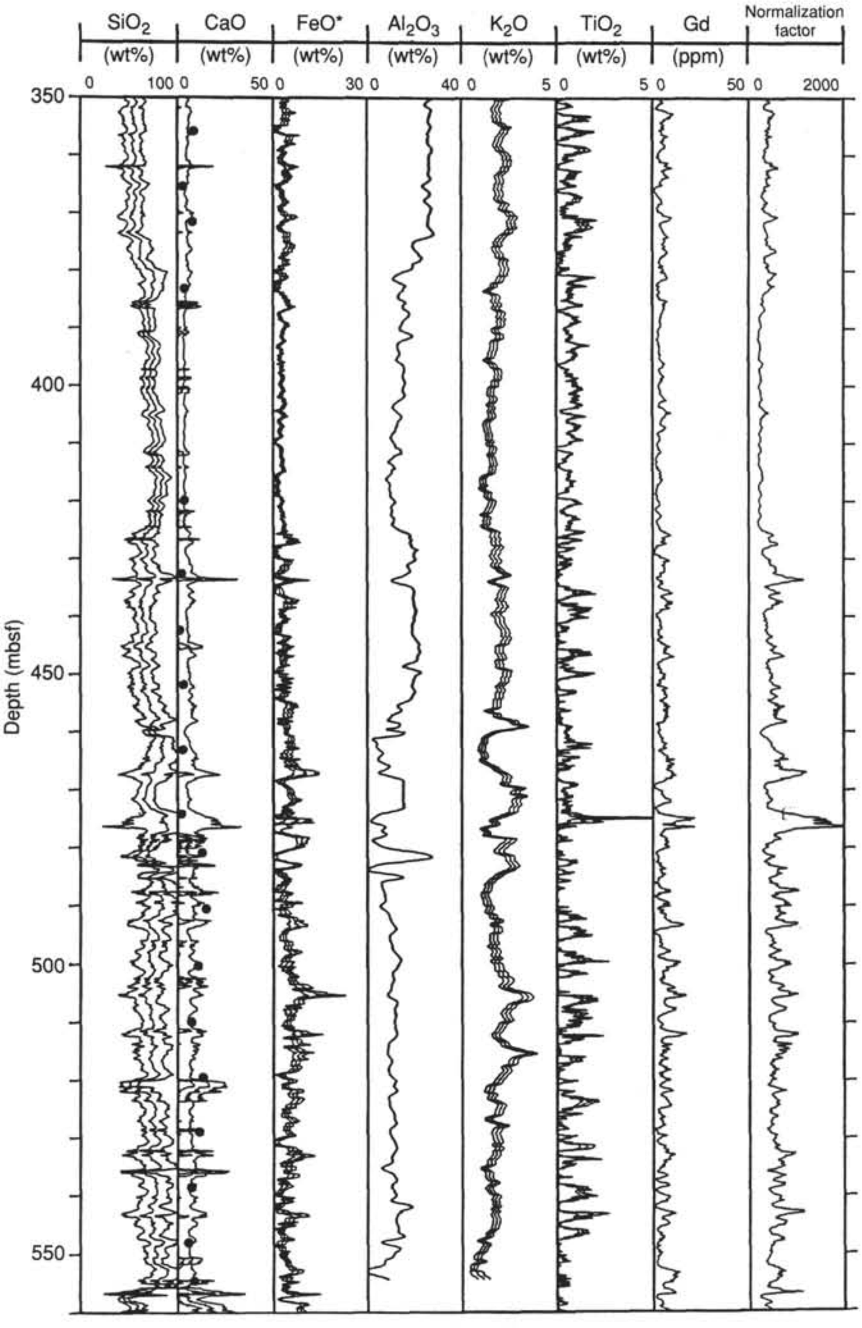

Figure 22 (continued).

mbsf matches the local reflector "canyon-2", and corresponds to the contacts between log Units 2 and 3a and lithologic Subunits VB and VC (Fig. 11). The irregularity of reflector "canyon-1" and the variable thickness between it and "canyon-2" suggest it is an erosional surface. Apparently the late-stage filling processes that followed the time of "canyon-1" removed sediment as well as deposited it.

Irregular, strong reflectors line the floor of the canyon beneath Site 906 between "canyon-2" and m6 (pink-3). We correlate this latter reflector with 478 mbsf, the contact between log Subunits 3a and 3b and lithologic Subunit VC and Unit VI (Fig. 11). This reflector is traced across the slope to other Leg 150 sites, and is the youngest reflector that crosses intact beneath the buried canyon (Fig. 2). Clearly it marks a maximum age for the event that formed the canyon. The contorted, discontinuous nature of reflectors in the "canyon-2" to m6 interval relate to the matrix- and clast-supported debris flows that comprise lithologic Subunit VC. These are the earliest canyon-filling sediments, and in contrast to those in the "canyon-1" to "canyon-2" interval, were derived from the slope, probably the walls of the canyon itself, and were transported only short distances.

The fact that reflector m6 (pink-3) appears to represent a remarkably wide, smooth and nearly level floor of the buried canyon emphasizes the contrast with modern slope canyons. The latter are typically 2 km or less in width, V-shaped or nearly so, with an axial gradient steeper than surrounding stratal surfaces causing the canyon to cut downslope into progressively older sediment. We suggest that the buried Miocene canyon may have originated by one or more bedding plane slides. It is likely that this scar formed over a relatively short period of time. Detailed shore-based work will be conducted to date

Table 11. Seismic reflectors identified at Site 906.

Name	Color	Two-way traveltime (ms)	Depth (mbsf)	Calculated velocities (m/s)		Correlation to borehole
				Interval	Average	
m1	Tuscan*	140	111	1570	1570	
m1.5	orange	200	157.4	1582	1547	Top of sand unit; log velocity increase.
m2	Yellow-2*	340	279.2	1740	1740	Base lithologic Subunit IVB.
canyon-1		440	384	2016	2096	Change in all logs.
canyon-2		480	421.1	2055	1993	Base lithologic Subunit VB; density log kick.
m6	pink-3**	535	478.2	2076	2077	Base lithologic Unit V; density and velocity log kicks.
o1	green-2**	625	555.5	1718	1984	Top lithologic Unit VII; density and velocity log kicks.
e1	yellow	700	620	1720	0	Interval velocities indicate e1 is below total depth (602.4 mbsf).

Note: Single asterisk (*) = possibly equivalent to the shelf reflectors of this color (Greenlee et al., 1992); double asterisk (**) = possibly equivalent to the shelf reflectors of this color (G.S. Mountain, K.G. Miller, and N. Christie Blick, unpubl. data, 1990).

the youngest sediment contained in the basal debris flows between "canyon-2" and m6. This study may reveal that wall collapse and turbidite filling all occurred in the middle Miocene between the time represented by reflectors m3 (blue) and m2 (Yellow-2). With our present age estimates this restricts it to between about 13.5 and 12.4 m.y. (Fig. 11), and it is tempting to equate this slope failure event with the massive debris flows of this same age between 655 and 680 mbsf at Site 905. Furthermore, this narrow window of time between formation and burial would indicate that at one time this slope canyon maintained about 230 m of relief.

The fairly uniform caliper log near bit size shows that hole conditions below 478 mbsf remained very good. The complex log signatures are therefore highly reliable, and are consistent with the depths of several reflectors matched to the profile beneath m6.

Reflector o1 (green-2) is traced to 625 ms beneath Site 906. We match it to 561 mbsf where there is an abrupt velocity and density increase at the top of log Unit 4 (Fig. 11). The exact contact between the silty claystone of lithologic Unit VI and the clayey nanno chalk of Unit VII was not recovered.

It does not seem likely that reflector e1 (yellow) was reached before TD at 602 mbsf. Core recovery was poor in the last 50 meters and no logs provided data below 585 mbsf. No reasonable interval velocity can be invoked to match the observed travel time of 700 ms with anything shallower than 620 mbsf.

SUMMARY AND CONCLUSIONS

We drilled Site 906 in 923 m water depth on the middle continental slope in the thalweg of modern Berkeley Canyon to minimize upper Neogene overburden and to recover the fill of a buried Miocene submarine canyon. Preliminary results confirm that we accomplished our scientific objective which was to determine the sedimentary history of this canyon and compare its sediments with those of the other slope sites drilled on Leg 150. Reflector m3 (Blue) has been sampled at Sites 902, 903, and 904, where its age has been determined to be ~13.5 Ma. This is the youngest surface cut by the buried Miocene canyon at Site 906. Reflector m2 (Yellow-2) is ~12.4 Ma (it has been sampled at Sites 902, 903 and 904 as well) and can be traced across this canyon; at Site 906 there is roughly 200 m of sediment between m2 and the canyon floor. Hence this middle Miocene canyon formed and filled in less than the ~1.1 Ma bracketed by these reflectors. The erosional event may correlate with a glacioeustatic lowering inferred by the middle Miocene $\delta^{18}O$ increase known from previous studies; additional chronostratigraphic analyses are needed to document this relationship rigorously. The oldest sediments within this canyon are debris-flow deposits apparently eroded from the canyon walls and deposited by mass-wasting processes. These are overlain by turbiditic sands deposited while the canyon served as a conduit for turbidity currents flowing downslope. The final unit to fill the canyon was a 100-m-thick interval of laminated mud that marks a period of unusually low bottom-water oxygen that was detected by much thinner laminated intervals at other Leg 150 sites on the slope.

Ms 150IR-110

NOTE: For all sites drilled, core-description forms ("barrel sheets") and core photographs can be found in Section 4, beginning on page 369. Forms containing smear-slide data can be found in Section 5, beginning on page 833. Thin-section data are given in Section 6, beginning on page 875.

SHORE-BASED LOG PROCESSING

Hole 906A

Bottom felt: 924.5 mbrf (used for depth shift to seafloor)
Total penetration: 602.4 mbsf
Total core recovered: 511.69 m (84%)

Logging Runs

Logging string 1: DIT/DSI/NGT
Logging string 2: HLDT/CNT/NGT (upper and lower sections)
Logging string 3: FMS/GPIT/NGT (main and repeat)
Logging string 4: ACT/GST/NGT

Drill Pipe

The following drill-pipe depths are as they appear on the logs after differential depth shift (see **Depth shift** section) and depth shift to the seafloor. As such, there might be a discrepancy with the original depths given by the drillers on board. Possible reasons for depth discrepancies are ship heave and drill-string and/or wireline stretch.

DIT/DSI/NGT: Bottom of drill pipe at ~102.5 mbsf
HLDT/CNT/NGT: Bottom of drill pipe at ~102.5 mbsf (on merged data)
FMS/GPIT/NGT: Bottom of drill pipe at ~102.5 mbsf
ACT/GST/NGT: Bottom of drill pipe at 139 mbsf

Processing

Depth shift: All logs have been interactively depth shifted with reference to NGT from HLDT/CNT/NGT run, and to the seafloor (– 924.5 m).
Gamma-ray processing: NGT data have been processed to correct for borehole size and type of drilling fluid.
Acoustic data processing: DSI (Dipole Sonic Imager) data were reprocessed on the shipboard MAXIS system.
Geochemical processing: (For a detailed explanation of the processing, please refer to the "Explanatory Notes" chapter [this volume] or to the geochem.doc file on the CD-ROM in the back pocket.) The elemental yields recorded by the GST tool represent the relative contributions of only some of the rock-forming elements (iron, calcium, chlorine, silicon, sulfur, hydrogen, gadolinium, and titanium—the last two computed during geochemical processing) to the total spectrum. Because other rock-forming elements are present in the formation (such as aluminum and potassium), caution is recommended in using the yields to infer lithologic changes. Instead, ratios (see acronyms.text on the CD-ROM) are more appropriate to determine changes in the macroscopic properties of the formation. A list of oxide factors used in geochemical processing includes the following:

SiO_2 = 2.139
CaO = 1.399
FeO^* = 1.358
TiO_2 = 1.668
K_2O = 1.205
Al_2O_3 = 1.889

FeO^* = computed using an oxide factor that assumes a 50:50 combination of Fe_2O_3 and FeO factors.
VARCA = variable Ca oxide/carbonate factor used in $CaO/CaCO_3$ calculation.

Quality Control

Hole diameter was recorded by the hydraulic caliper on the HLDT tool (CALI), and by the caliper on the FMS string (C1 and C2).
Invalid gamma-ray data were recorded at 20, 30, 60, and 92 mbsf (DIT/DSI/NGT).
FACT = quality control curve in geochemical processing. The accuracy of the estimates is inversely proportional to the magnitude of the curve.

Hole 906A: Resistivity-Velocity-Natural Gamma Ray Log Summary

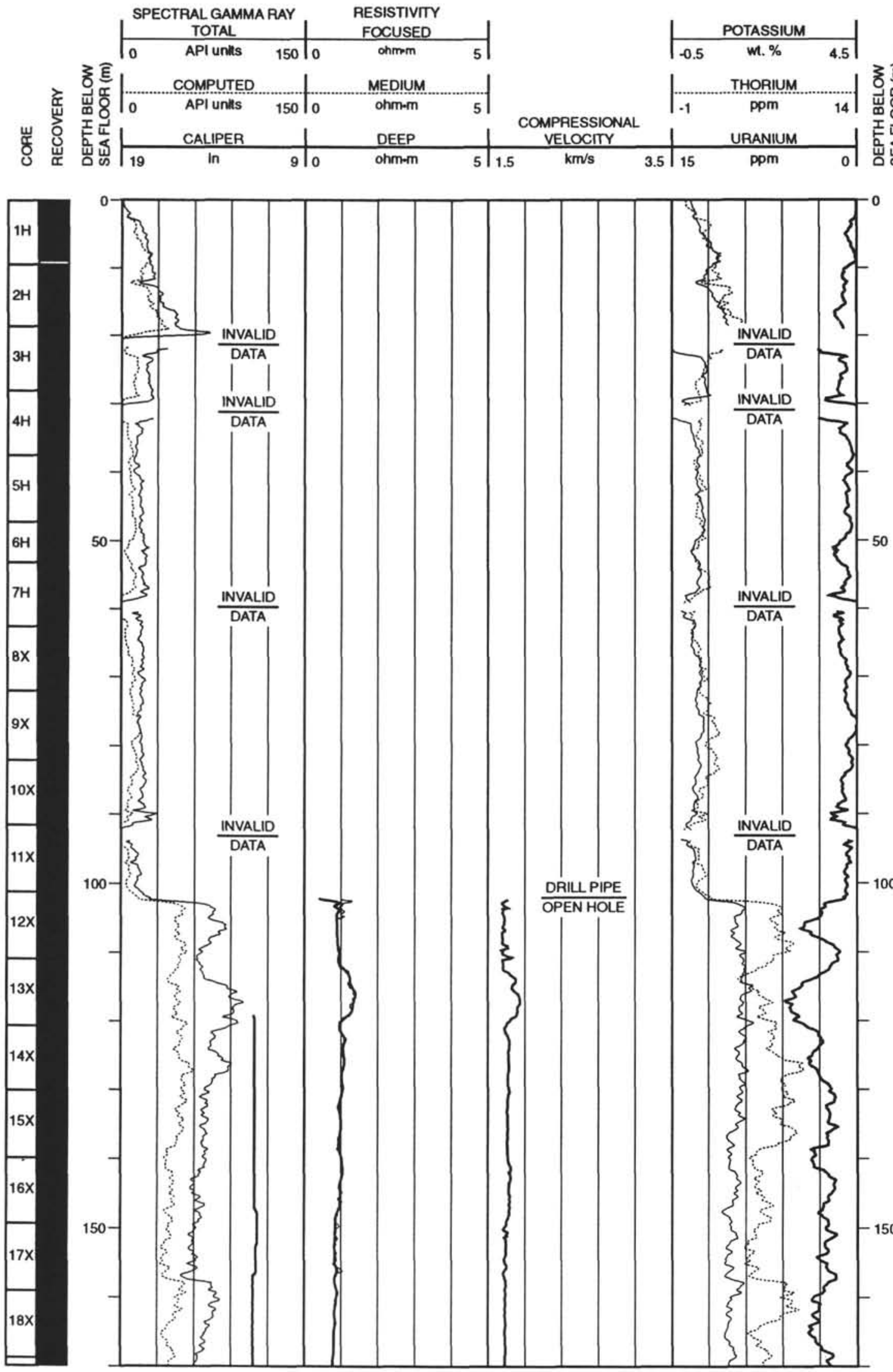

Hole 906A: Resistivity-Velocity-Natural Gamma Ray Log Summary (continued)

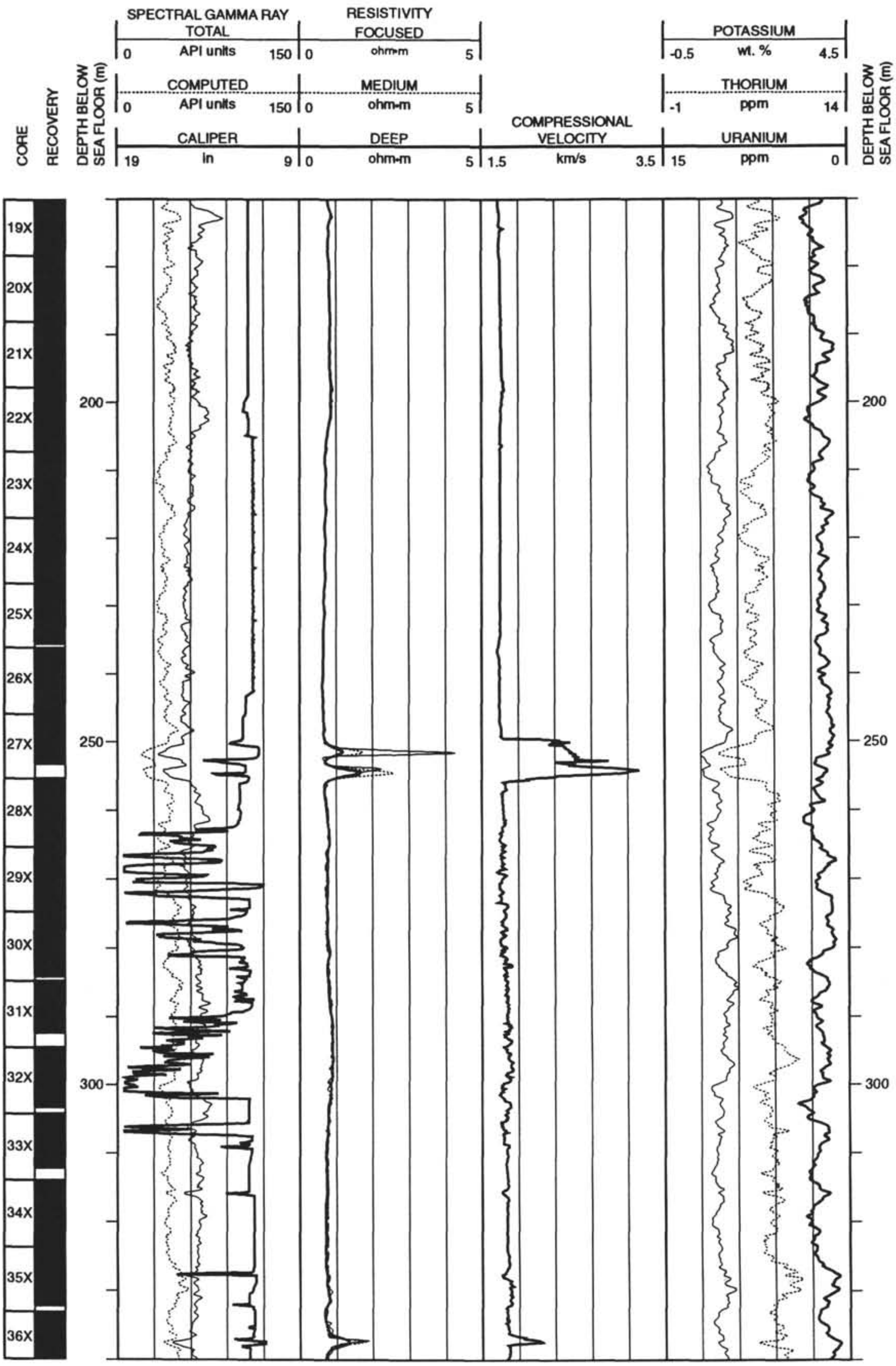

Hole 906A: Resistivity-Velocity-Natural Gamma Ray Log Summary (continued)

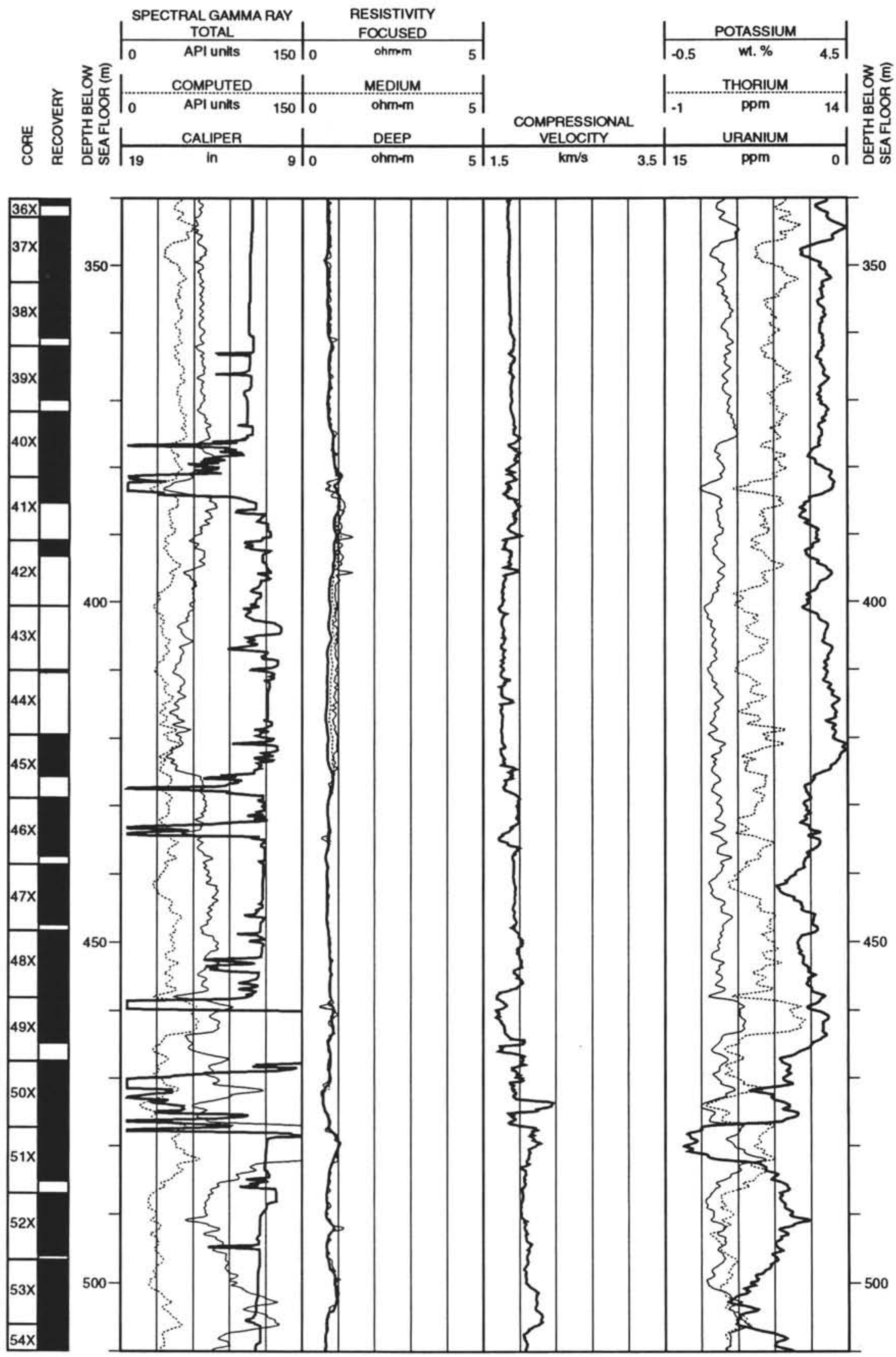

Hole 906A: Resistivity-Velocity-Natural Gamma Ray Log Summary (continued)

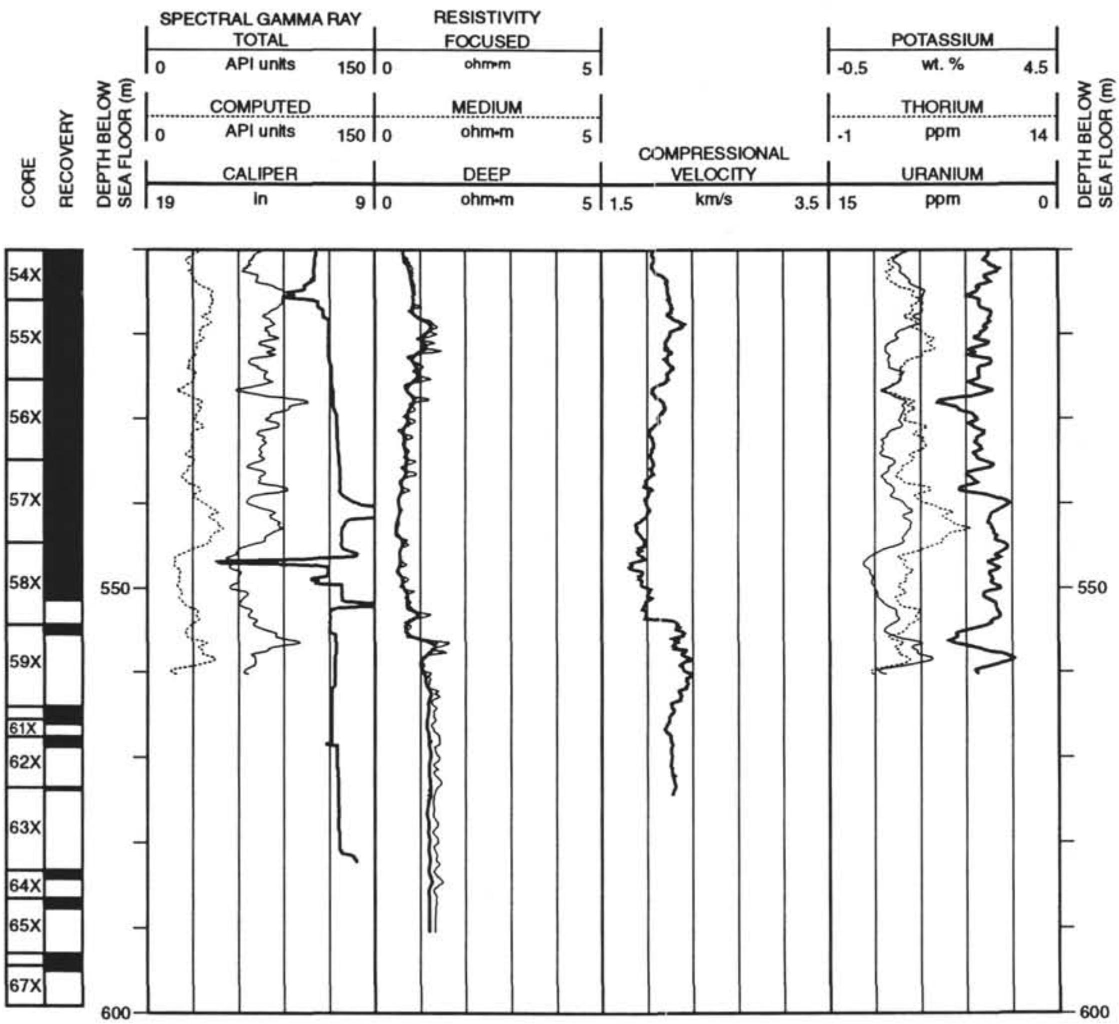

Hole 906A: Density-Porosity-Natural Gamma Ray Log Summary

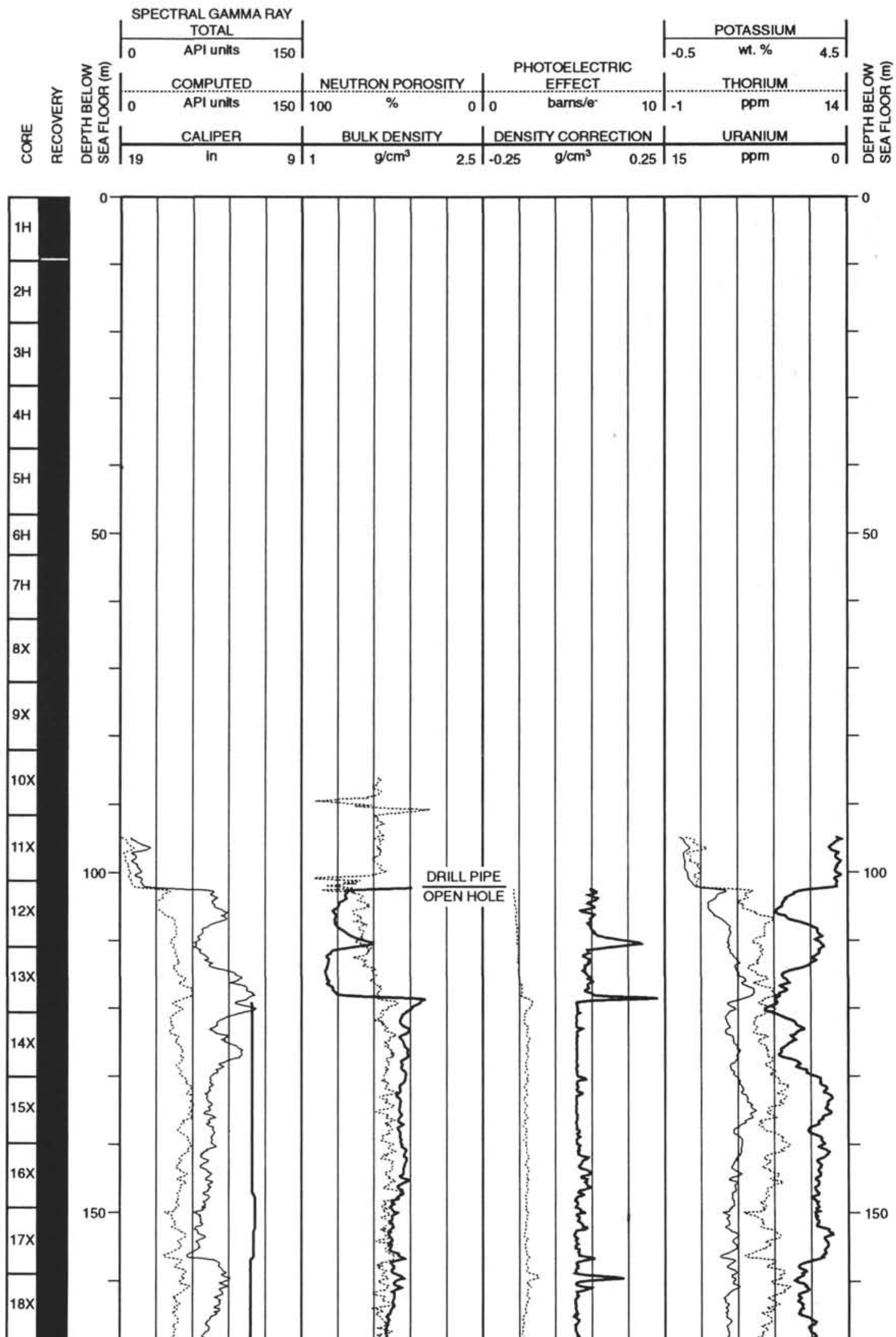

Hole 906A: Density-Porosity-Natural Gamma Ray Log Summary (continued)

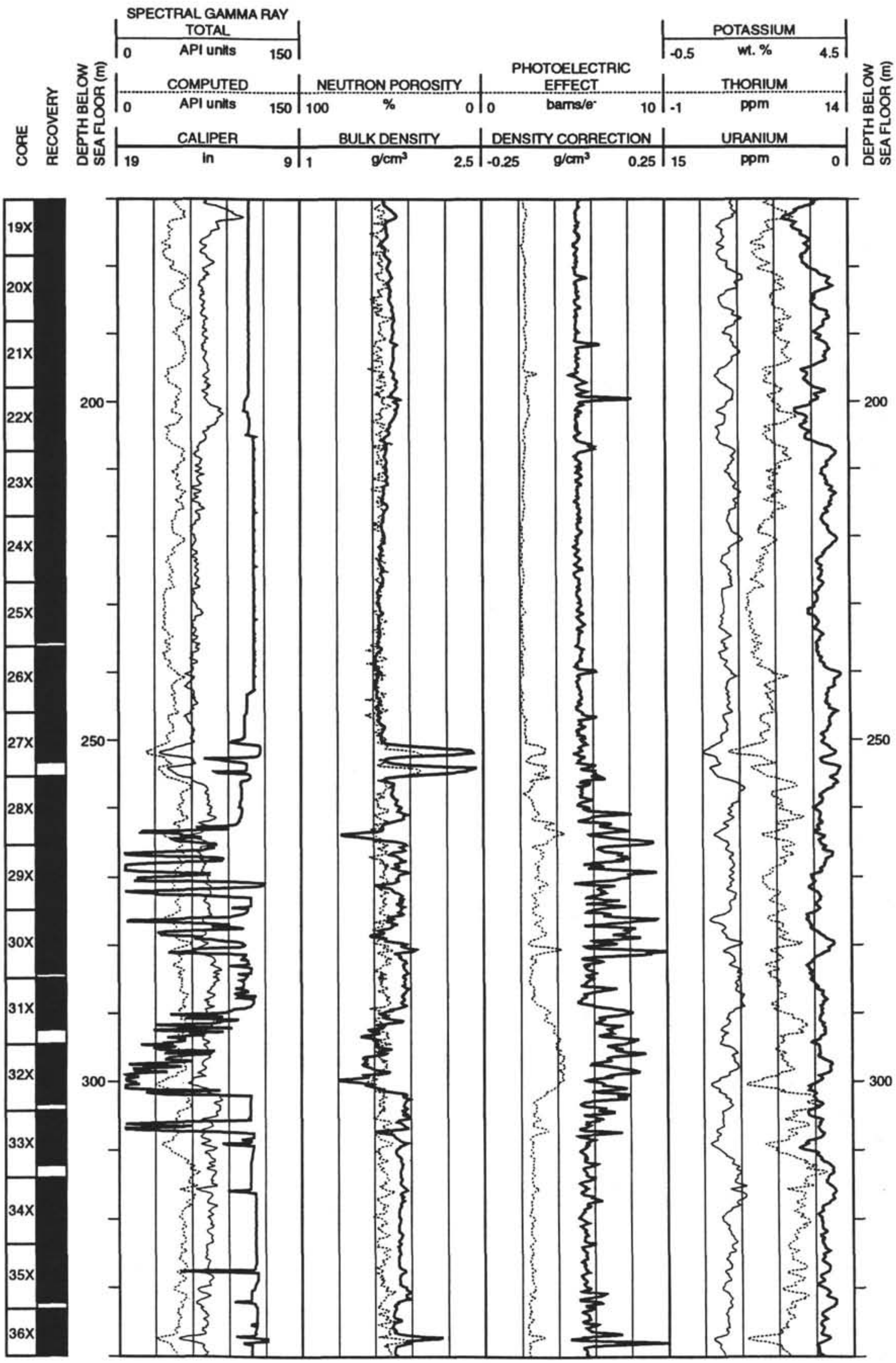

Hole 906A: Density-Porosity-Natural Gamma Ray Log Summary (continued)

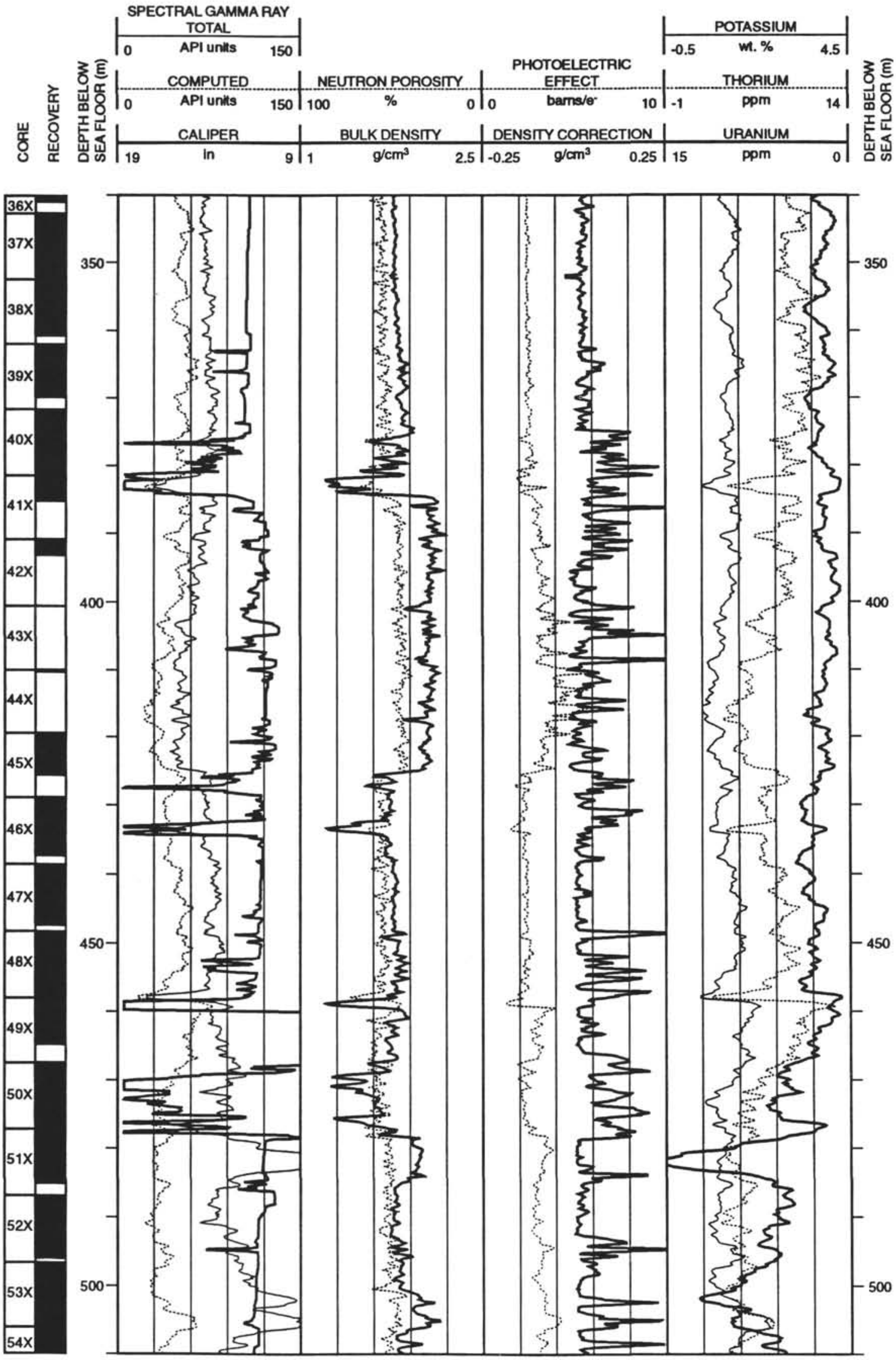

Hole 906A: Density-Porosity-Natural Gamma Ray Log Summary (continued)

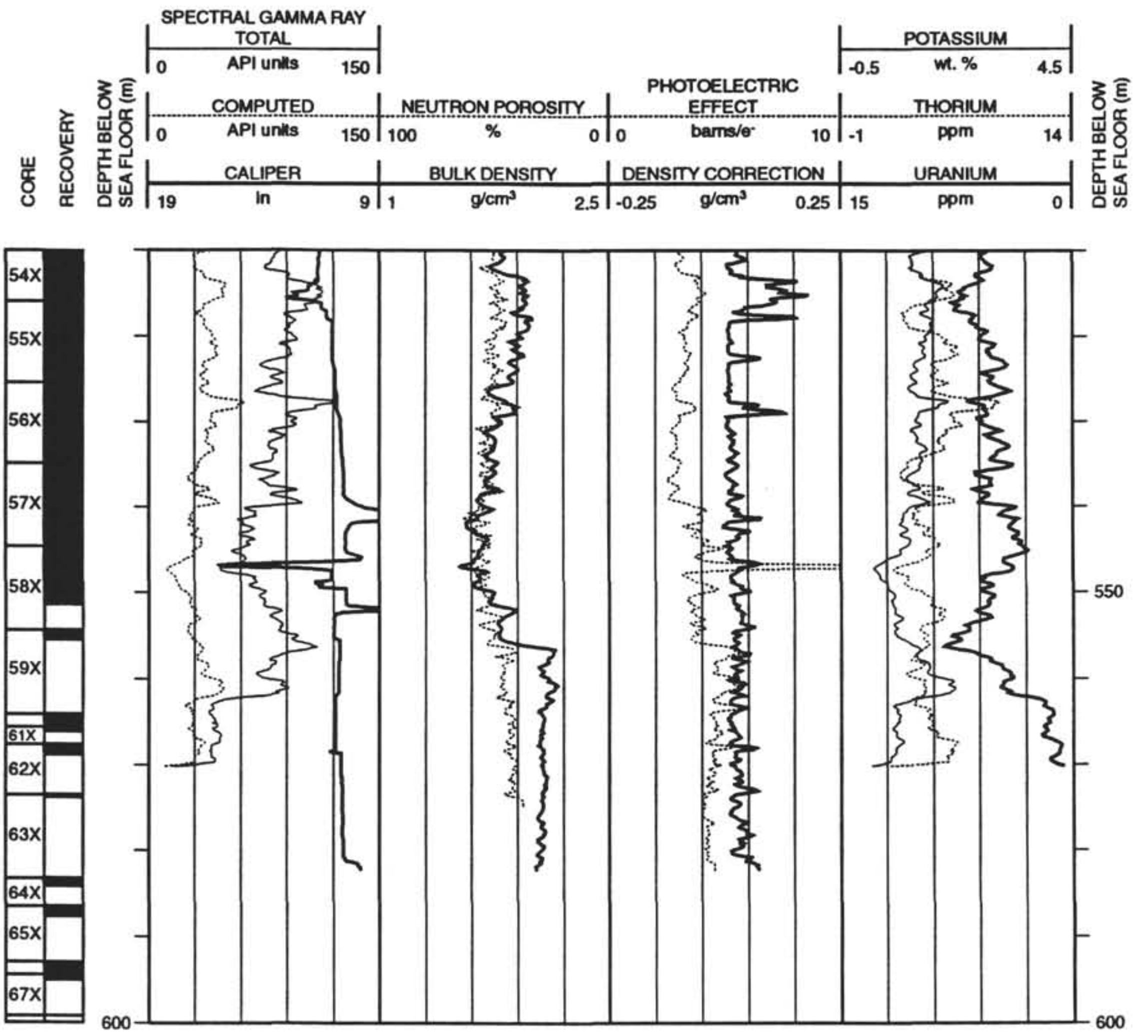

Hole 906A: Processed Geochemical Log Summary

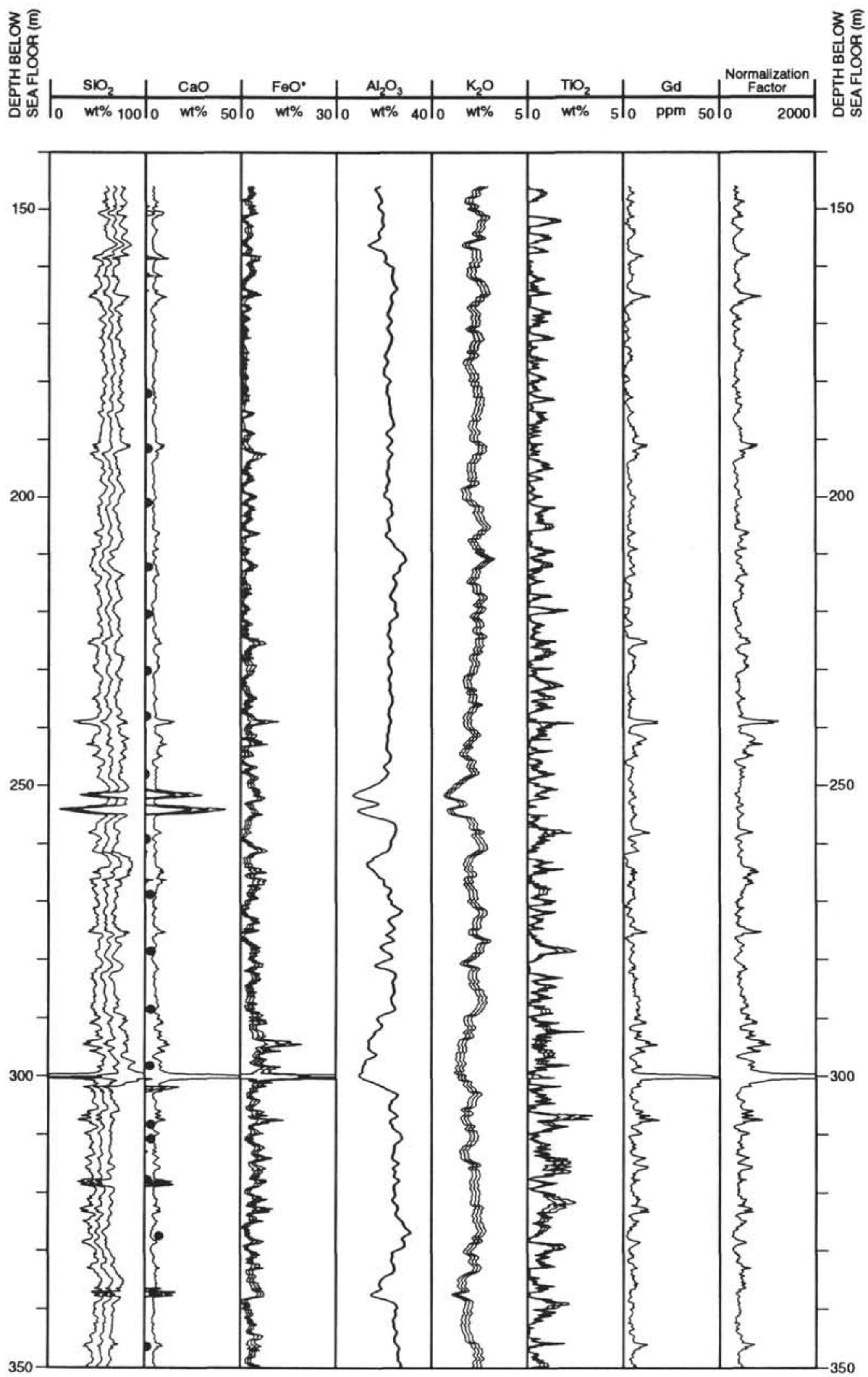

Hole 906A: Processed Geochemical Log Summary (continued)

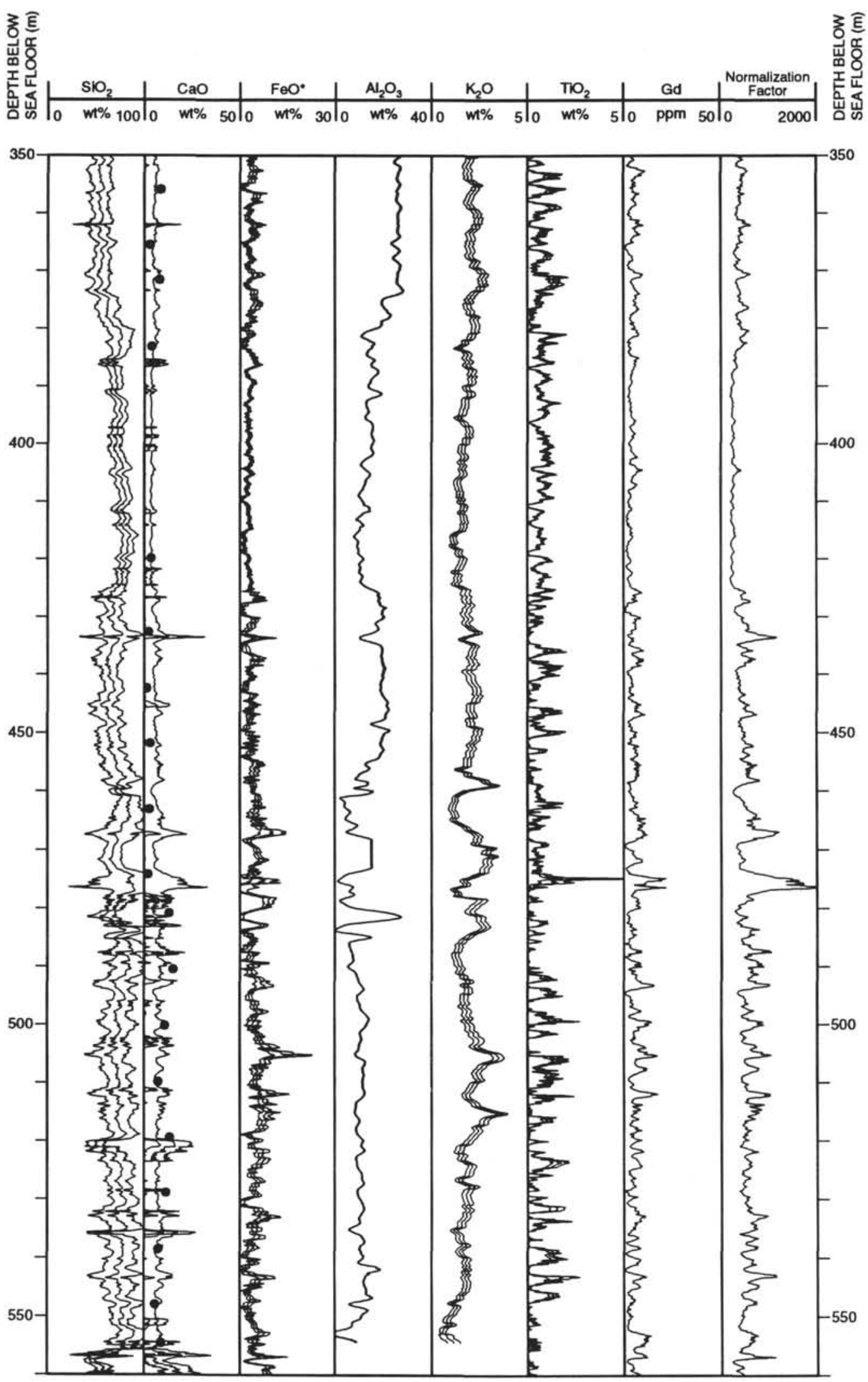

Hole 906A: Natural Gamma Ray Log Summary

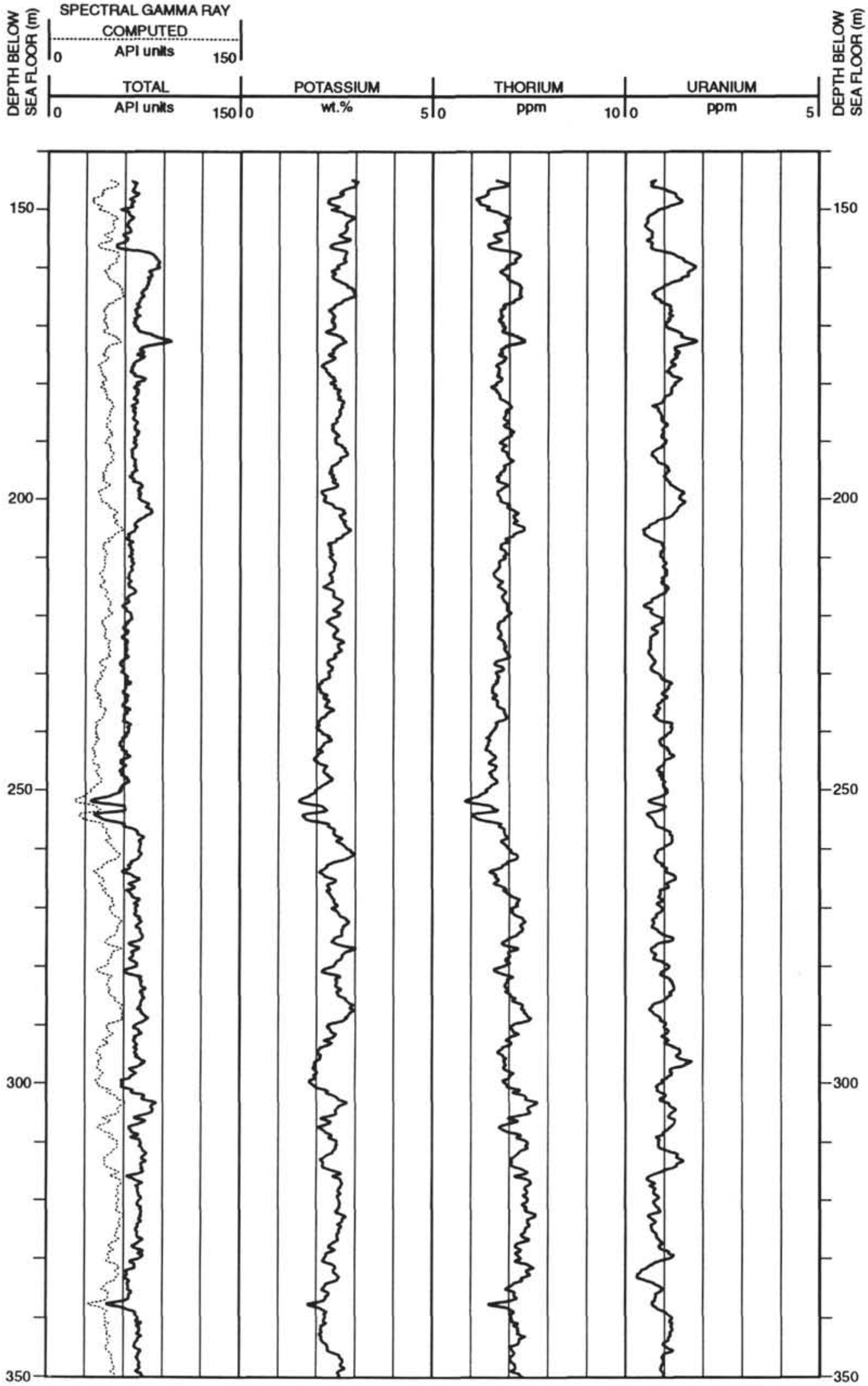

Hole 906A: Natural Gamma Ray Log Summary (continued)